

**UNIwersytet Śląski w Katowicach**

**Wydział Nauk Ścisłych i Technicznych**

**Instytut Fizyki im. Augusta Chelkowskiego**

**Praca doktorska**

**CHELATORY ŻELAZA Z GRUPY TIOSEMIKARBAZONU W TERAPII  
FOTODYNAMICZNEJ – BIOFIZYCZNE I MOLEKULARNE PODSTAWY  
W KONTEKŚCIE TERAPII NOWOTWORÓW**

**Robert Gawecki**

**Promotor: dr hab. Anna Mrozek-Wilczkiewicz, prof. UŚ**

**Chorzów, 2024**

*Pragnę złożyć serdeczne podziękowania mojej Promotor, dr hab. Annie Mrozek-Wilczkiewicz, prof. UŚ, za nieocenione wsparcie oraz nieustające zrozumienie przez cały okres mojej pracy nad doktoratem. Jej cenne wskazówki oraz uwagi nie tylko wzbogaciły tę pracę, ale także znacząco wpłynęły na mój rozwój naukowy. Dziękuję również za ogrom cierpliwości i gotowość do pomocy na każdym etapie powstawania tej pracy.*

*Chciałbym także wyrazić ogromną wdzięczność mojej Rodzinie, której wsparcie i wyrozumiałość były niezastąpione w chwilach wyzwań. Wasza obecność i wiara w moje możliwości motywowały mnie do dalszej pracy.*

*Nie mogę również zapomnieć o koleżankach i kolegach z zespołu Biofizyki Farmaceutycznej oraz wszystkim innym osobom, które wspierały mnie w trakcie tej drogi – zarówno naukowo, jak i osobiście. Dziękuję za każde słowo otuchy, pomocne uwagi i nieustającą inspirację. Wasze wsparcie było dla mnie niezwykle cenne.*

*Dziękuję wszystkim, którzy przyczynili się do powstania tego doktoratu.*

## Spis treści

<b>1. WPROWADZENIE.....</b>	<b>4</b>
<b>1.1. Biofizyczne i molekularne podstawy ALA-PDT .....</b>	<b>4</b>
<b>1.2. Chelatory żelaza w ALA-PDT .....</b>	<b>13</b>
<b>1.3. Cel pracy .....</b>	<b>15</b>
<b>1.4. Materiały i metody .....</b>	<b>16</b>
<b>2. WYNIKI I DYSKUSJA.....</b>	<b>23</b>
<b>2.1. Cytotoksyczność badanych TSC.....</b>	<b>23</b>
<b>2.2. Akumulacja protoporfiryny IX .....</b>	<b>25</b>
<b>2.3. Efekt fototoksyczny .....</b>	<b>26</b>
<b>2.4. Wpływ wybranych TSC na ekspresję genów .....</b>	<b>28</b>
<b>3. PODSUMOWANIE I WNIOSKI.....</b>	<b>32</b>
<b>4. PUBLIKACJE WCHODZĄCE W SKŁAD ROZPRAWY .....</b>	<b>34</b>
<b>4.1. [P1]. Impact of thiosemicarbazones on the accumulation of PpIX and the expression of the associated genes. ....</b>	<b>34</b>
<b>4.2. [P2]. A Thiosemicarbazone Derivative as a Booster in Photodynamic Therapy—A Way to Improve the Therapeutic Effect.....</b>	<b>47</b>
<b>4.3. [P3]. Iron Metabolism in Aminolevulinic Acid-Photodynamic Therapy with Iron Chelators from the Thiosemicarbazone Group.....</b>	<b>58</b>
<b>5. OŚWIADCZENIA WSPÓŁAUTORÓW .....</b>	<b>99</b>
<b>6. LITERATURA.....</b>	<b>106</b>
<b>7. AKTYWNOŚĆ NAUKOWA.....</b>	<b>112</b>

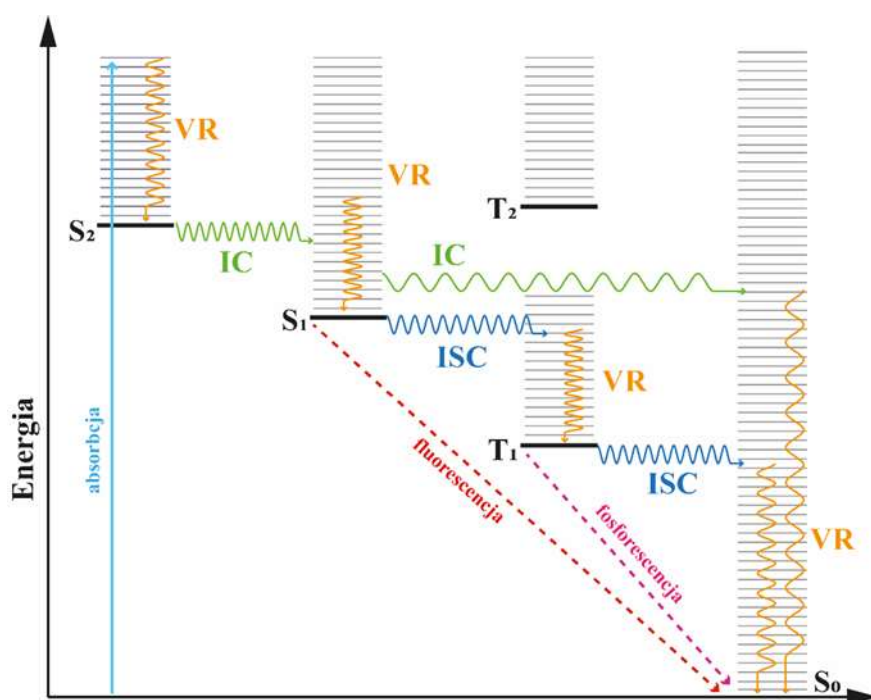
## 1. WPROWADZENIE

Choroby nowotworowe są obecnie jedną z najczęstszych przyczyn zgonów na świecie. Według Global Cancer Observatory (GCO) w 2022 roku nowotwory były odpowiedzialne za prawie 10 miliona zgonów, a także odnotowano 20 milionów nowych przypadków zachorowań [1]. Statystyki te ukazują, jak ważnym i nadal trudnym wyzwaniem dla nauki jest leczenie nowotworów. Obecnie wiele schorzeń tego typu leczy się standardowymi metodami, takimi jak chirurgiczne usunięcie zmienionych chorobowo tkanek w połączeniu z chemioterapią lub radioterapią. W zależności od zastosowanej terapii, jej skutki uboczne mogą wystąpić już w trakcie leczenia lub wiele dni później, prowadząc do tak zwanej toksyczności przewlekłej. Warto zaznaczyć, że wiele chemioterapeutyków charakteryzuje się niską specyficnością wobec tkanek nowotworowych, co dodatkowo nasila efekty uboczne. Często terapia ta ma charakter paliatywny, mający na celu wydłużenie czasu przeżycia pacjenta [2,3]. Dlatego poszukiwanie nowych, bardziej specyficznych i mniej inwazyjnych metod leczenia nowotworów oraz rozwój istniejących terapii stanowi wyzwanie dla współczesnej nauki. W ostatnich latach zaproponowano wiele metod w celu poprawy efektywności i specyficznego leczenia nowotworów oraz pogłębiono wiedzę na temat mechanizmów działania wielu leków. Jednym z obiecujących rozwiązań w leczeniu nowotworów jest terapia fotodynamiczna (PDT; ang. *Photodynamic Therapy*), która charakteryzuje się dużą selektywnością wobec komórek nowotworowych i ma niewielkie efekty uboczne. W ostatnich latach terapia ta cieszy się dużym zainteresowaniem i jest intensywnie rozwijana, aby osiągnąć satysfakcjonujące efekty terapeutyczne.

### 1.1. Biofizyczne i molekularne podstawy ALA-PDT

Terapia fotodynamiczna (PDT) opiera się na interakcji trzech składników: fotouczulacza (PS, ang. *Photosensitizer*), światła o odpowiedniej długości fali oraz tlenu cząsteczkowego. W wyniku tej reakcji powstają reaktywne formy tlenu (RFT), które prowadzą do śmierci komórki. Choć różnego rodzaju PS są obecnie używane w PDT, w niniejszej pracy skupiono się na tak zwanej ALA-PDT, czyli terapii fotodynamicznej opartej na kwasie 5-aminolewulinowym (5-ALA). W przeciwieństwie do innych PS, 5-ALA sam w sobie nie jest fotouczulaczem, a jedynie prekursorem naturalnego fotouczulacza jakim jest protoporfiryna IX (PPIX). Zastosowanie 5-ALA w PDT ma kilka zalet w porównaniu do syntetycznych PS, m. in. jest bardzo dobrze rozpuszczalny w środowisku wodnym, ma bardzo niską toksyczność nawet w dużych dawkach i szybki klirens [4].

Niezależnie od typu PS mechanizm jego wzbudzenia jest uniwersalny. W stanie podstawowym ( $S_0$ ) PS posiada elektrony na najniższych energetycznie orbitalach, po absorpcji fotonu o odpowiedniej energii jeden z elektronów przechodzi na wyższy energetycznie orbital, co nazywamy stanem wzbudzonym ( $S_x$ , gdzie  $x=1,2,3,\dots$  w zależności od zaabsorbowanej energii). Każdy wzbudzony stan  $S_x$  ma dodatkowo poziomy wibracyjne o rosnącej energii. Ze względu na niestabilność energetyczną stanu wzbudzonego, cząsteczka szybko powraca do stanu podstawowego ( $S_0$ ).

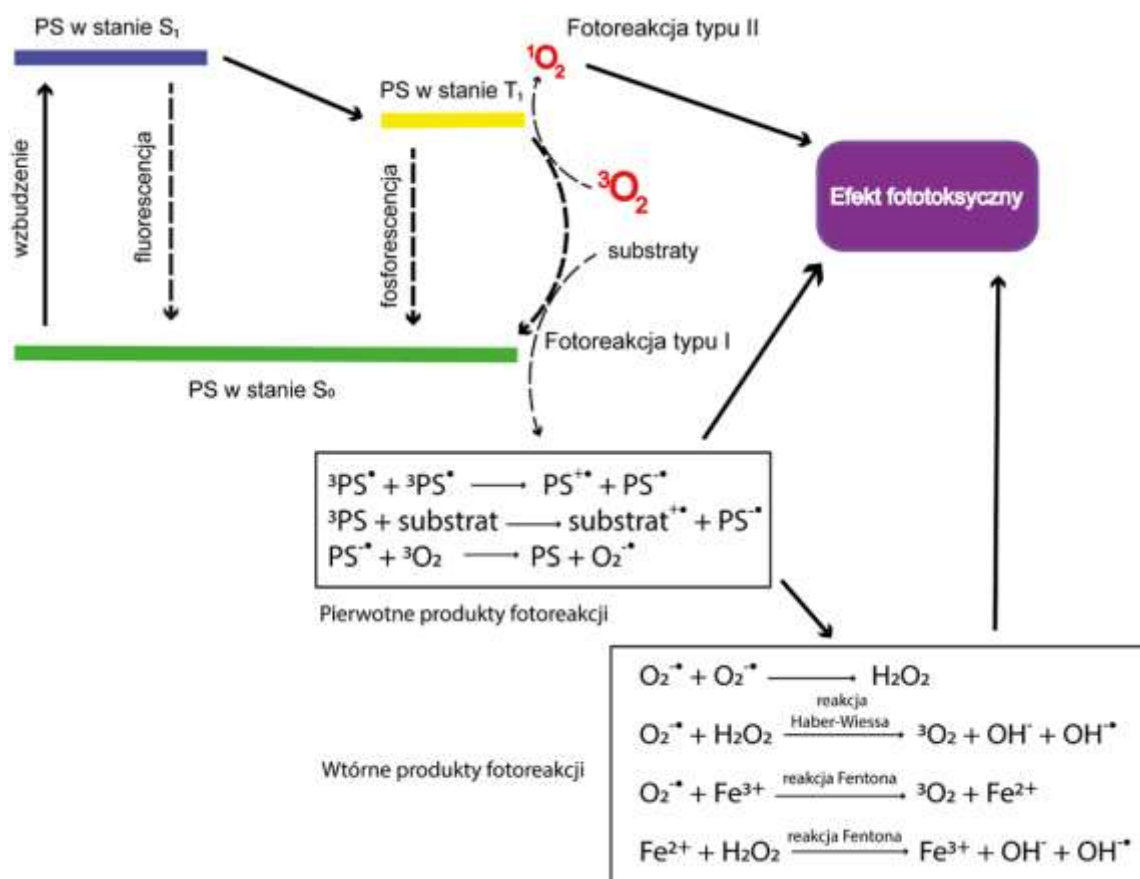


**Rys. 1.** Diagram Jabłońskiego przedstawiający podstawowe procesy fotofizyczne. IC - konwersja wewnętrzna, ISC - przejście międzysystemowe,  $S_x$  - stany singletowe,  $T_x$  - stany trypletowe, VR - relaksacja wibracyjna. Oś y wskazuje rosnące energie stanów elektronowych; na osi x stany elektronowe pogrupowane według krotności spinu (na podstawie [5], zmieniono).

Przejście to może zachodzić kilkoma mechanizmami. Elektron na wysokim poziomie wibracyjnym danego stanu wzbudzonego ( $S_x$ ) szybko przechodzi na najniższy poziom wibracyjny tego stanu w procesie relaksacji wibracyjnej (VR; ang. *Vibrational Relaxation*), rozpraszając energię w postaci ciepła (**Rys. 1**). Jeśli PS zaabsorbuje foton o wyższej energii, przechodzi do wyższych stanów energetycznych ( $S_x$ ), z których poprzez konwersję wewnętrzną (IC; ang. *Internal Conversion*) szybko powracają do stanu  $S_1$ . Relaksacja z  $S_1$  do  $S_0$  może zachodzić dwoma sposobami: promienistym lub bezpromienistym. Przejście promieniste obejmuje emisję wtórnego fotonu (emisja fluorescencji). Wyemitowanie fotonu wtórnego zawsze rozpoczyna się od najniższego poziomu wibracyjnego  $S_1$ .

W przejściu bezpromienistym PS ze stanu  $S_1$  może przejść na izoenergetyczny poziom stanu trypletowego ( $T_1$ ), gdzie dwa elektrony są niesparowane i mają ten sam spin. Proces ten nazywany jest przejściem międzysystemowym (ISC; ang. *Intersystem Crossing*). Większość fotouczulaczy charakteryzuje się wysoką wydajnością kwantową tego przejścia. W stanie  $T_1$  może również wystąpić relaksacja promienista do poziomu  $S_0$  poprzez emisję fosforescencji. Stany trypletowe mają stosunkowo długi czas życia (nawet do kilku sekund), co pozwala na wykorzystanie energii ze stanów trypletowych w reakcjach fotochemicznych [5].

Cząsteczki PS w stanie wzbudzonym trypletowym mogą wywoływać zmiany chemiczne w sąsiednich molekułach poprzez dwie konkurencyjne ścieżki: reakcję fotochemiczną typu I i typu II (**Rys. 2**). Reakcje fotochemiczne typu I często prowadzą do powstania anionów ponadtlenkowych ( $O_2^{\cdot -}$ ) w wyniku przeniesienia elektronu z PS na tlen cząsteczkowy. Aniony ponadtlenkowe mają ograniczoną reaktywność w układach biologicznych, ale mogą reagować ze sobą prowadząc do wytworzenia nadtlenu wodoru ( $H_2O_2$ ), który może łatwo dyfundować przez błony biologiczne. Ponieważ uszkodzenia powodowane przez  $H_2O_2$  nie są ograniczone do jednego przedziału komórkowego, nadtlenek wodoru ma duże znaczenie w powstawaniu uszkodzeń komórkowych podczas PDT. Przy wyższych stężeniach nadtlenek wodoru może reagować z anionami ponadtlenkowymi, tworząc bardzo reaktywny rodnik hydroksylowy ( $HO^{\cdot}$ ) w reakcji Habera-Weissa. Rodnik ten ma wysoki potencjał redoks, przez co może utleniać każdą cząsteczkę w komórce, a dodatkowo energia aktywacji tych reakcji jest bardzo niska. Rodniki hydroksylowe łatwo dyfundują przez błony komórkowe, dlatego podobnie jak w przypadku nadtlenu wodoru, uszkodzenia nie są ograniczone do jednego kompartmentu komórkowego. W obecności jonów metali, takich jak żelazo lub miedź, rodniki hydroksylowe mogą być również wytwarzane w reakcji Fentona [6–8]. Reakcja fotochemiczna typu II zachodzi, gdy energia ze stanu trypletowego PS jest bezpośrednio przekazywana na cząsteczkę tlenu. W stanie podstawowym tlen cząsteczkowy znajduje się w konfiguracji trypletowej ( $^3O_2$ ), mając dwa niesparowane elektrony o równoległych spinach. Pomimo dużego potencjału redoks, w tym stanie jest słabym utleniaczem z powodu zasady zachowania spinu Wignera, która ogranicza oddziaływania między cząsteczkami w różnych stanach spinowych. W stanie wzbudzonym singletowym tlen ( $^1O_2$ ) staje się wysoce reaktywnym utleniaczem. Tlen singletowy, jako cząsteczka obojętna elektrycznie, może z łatwością dyfundować przez cytoplazmę i błony biologiczne. Obszar jego działania jest jednak ograniczony ze względu na niski współczynnik dyfuzji i krótki czas życia. Pomimo tego, tlen singletowy jest bardzo reaktywny i może łatwo reagować z większością molekuł w komórkach, prowadząc do oksydacji lipidów, białek oraz kwasów nukleinowych, co prowadzi komórkę na ścieżkę śmierci [9,10].



**Rys. 2.** Schemat podstawowych reakcji fotochemicznych w trakcie reakcji typu I i II.

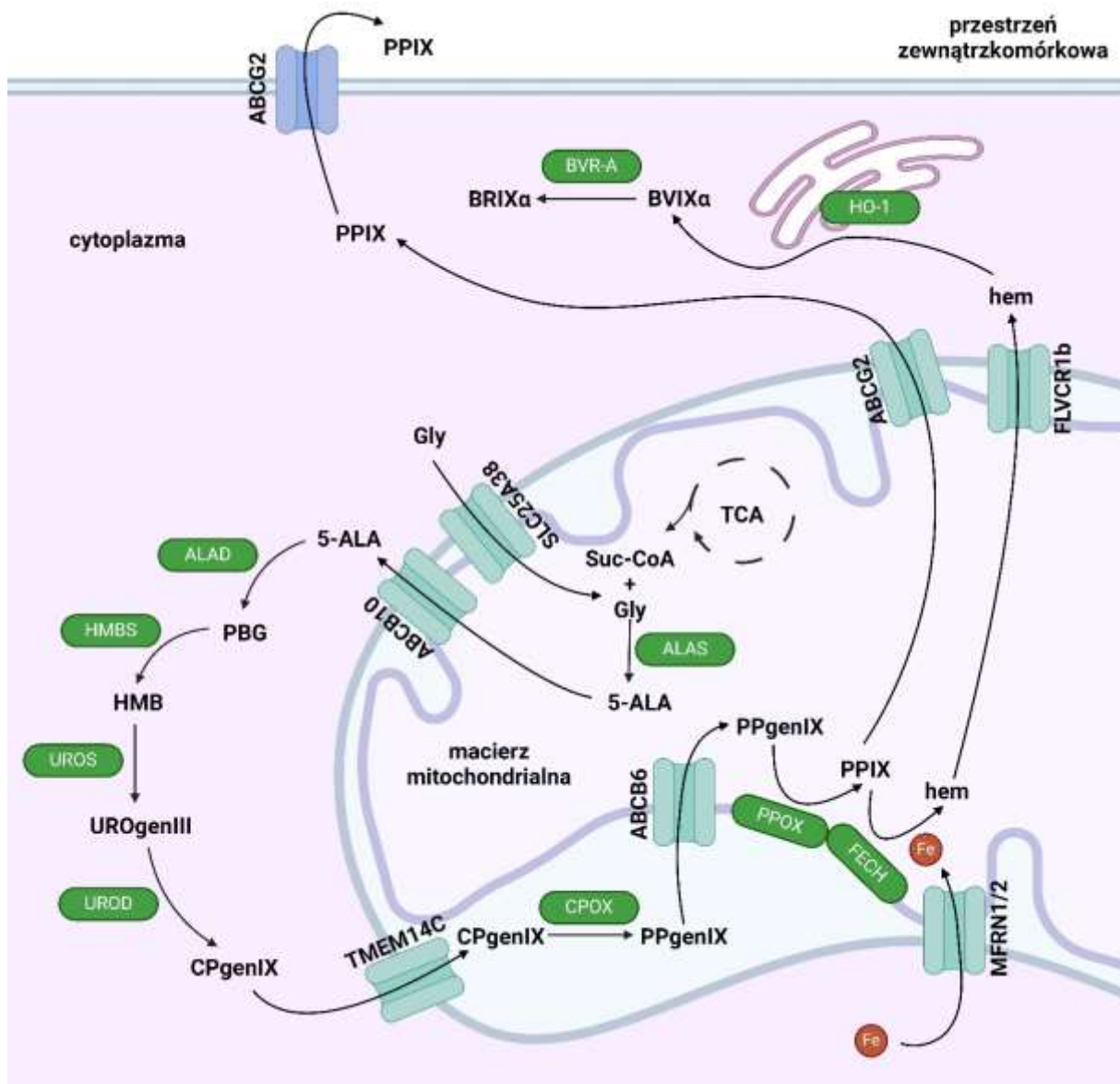
Reakcja fotochemiczna typu II jest procesem dominującym w przypadku większości stosowanych fotouczulaczy, choć oba typy reakcji fotochemicznych (I i II) zachodzą równolegle. Ich stosunek zależy od typu zastosowanego fotouczulacza i stężenia tlenu w środowisku reakcji [6,11].

W odróżnieniu od innych fotouczulaczy, 5-ALA sam w sobie nie jest cząsteczką o cechach fotouczulacza, a jedynie naturalnie występującym aminokwasem niebiałkowym stanowiącym prekursor PPIX – naturalnego, fotouczulacza syntetyzowanego we wszystkich jądrzystych komórkach eukariontów w szlaku biosyntezy hemu. Po pionierskich pracach Malika i Lugaciego (1987) oraz Kennedy’ego i Pottiera (1992), którzy pokazali, że egzogenne podanie 5-ALA prowadzi do zwiększenia wewnątrzkomórkowej akumulacji PPIX, a oświetlenie tych komórek prowadzi do ich śmierci, badania nad molekularnym mechanizmem leżącym u podstaw ALA-PDT zyskały na znaczeniu [12,13].

Biosynteza hemu u ssaków składa się z ośmiu etapów, które zachodzą w cytoplazmie i mitochondriach (**Rys. 3**). Pierwszym etapem jest synteza 5-ALA z glicyny i sukcyńlo-CoA, pochodzącego z cyklu kwasów trójkarboksylowych (TCA). Kondensacja tych substratów odbywa się w macierzy mitochondrialnej, katalizowana przez syntazę kwasu 5-aminolewulinowego (ALAS) oraz fosforan pirydoksalu, będący kofaktorem tego enzymu [14,15]. Drugi etap biosyntezy hemu zachodzi w cytoplazmie, potencjalnym transporterem 5-ALA z mitochondriów do cytoplazmy jest ABCB10 (ang. *ATP-binding cassette sub-family B member 10, mitochondrial*). Choć jego funkcja jako transportera 5-ALA nie została eksperymentalnie udowodniona *in vitro* czy *in vivo*, istnieją badania skłaniające ku wnioskowi, że ABCB10 jest transporterem 5-ALA. Z powodu obniżonej ekspresji ABCB10 kardiomiocyty wykazywały zmniejszony poziom hemu. Pokazano także, że podanie egzogenego 5-ALA przywraca w kardiomiocytach prawidłowy poziom hemu, natomiast podanie glicyny czy nadekspresja ALAS nie powodowała przywrócenia prawidłowego poziomu hemu [16]. W kolejnym etapie, 5-ALA jest przekształcany w porfobilinogen (PBG) przez dehydrogenazę 5-ALA (ALAD), która do swojej prawidłowej funkcji wymaga jonów cynku jako kofaktora. Syntaza hydroksymetylobilanu (HMBS) przekształca PBG w liniową cząsteczkę hydroksymetylobilanu (HMB). Natomiast HMB jest konwertowany do uroporfirynogenu III (UROgen III) przez syntazę uroporfirynogenu (UROS), a następnie UROgen III jest dekarboksylowany przez dekarboksylazę uroporfirynogenu (UROD), prowadząc do powstania koproporfirynogenu III (CPgen III). Kolejny etap biosyntezy hemu zachodzi w obszarze mitochondriów. CPgen III jest prawdopodobnie transportowany do przestrzeni międzybłonowej mitochondriów przez ABCB6 (ang. *ATP-binding cassette sub-family B member 6*). Jak pokazano, ABCB6 nie jest specyficznym transporterem CPgenIII, ponieważ, jak się przypuszcza, może też transportować hem oraz inne porfiryny oraz ich kompleksy z żelazem. Badania przeprowadzone *in vivo* na modelu mysim sugerują, że ABCB6 zlokalizowany w błonie komórkowej może uczestniczyć w eksporcie porfiryn. Natomiast u myszy z nokautem ABCB6 nie stwierdzono znacznych zmian w poziomie hemu, czy innych porfiryn w porównaniu do kontroli [17–19]. W przestrzeni międzybłonowej mitochondriów CPgen III jest przekształcany przez oksydazę koproporfirynogenu (CPOX) do protoporfirynogenu IX (PPgen IX). Ostatnie etapy biosyntezy hemu zachodzą na wewnętrznej błonie mitochondrialnej od strony macierzy mitochondrialnej, gdzie znajduje się wielobiałkowy kompleks metabolizmu hemu, w skład którego wchodzi następujące białka: oksydaza protoporfirynogenu IX (PPOX), ferrochelataza (FECH), ABCB10, ABCB7 (ang. *Iron-sulfur clusters transporter ABCB7, mitochondrial*), mitoferryna 1 (MFRN1), FAM210b, TMEM14C (ang. *Transmembrane protein 14C*) oraz PGRMC1 (ang. *Membrane-associated progesterone receptor component 1*). PPgen IX jest najprawdopodobniej transportowany z przestrzeni międzybłonowej do kompleksu metabolizmu hemu przez TMEM14C do centrum aktywnego



oksydazy protoporfirynogenu IX (PPOX), która jako kofaktor wymaga FAD, gdzie jest konwertowany do protoporfiryny IX (PPIX). Ostatni etap jest katalizowany przez FECH, który do swojego działania potrzebuje klastrów żelazowo-siarkowych typu [2Fe-2S]. FECH wbudowuje jon żelaza ( $\text{Fe}^{2+}$ ) do PPIX, tworząc hem. Żelazo niezbędne do syntezy hemu jest transportowane przez MFRN1. W procesie tym nie do końca poznana rolę pełni też ABCB10. Pozostałe białka kompleksu, takie jak ABCB7, prawdopodobnie uczestniczą w dostarczaniu centrów żelazowo-siarkowych do FECH, a FAM210b i PGRMC1 regulują aktywność FECH [15,20–22]. Powstały hem jest transportowany z mitochondriów do innych przedziałów komórkowych, gdzie jest wykorzystywany do syntezy hemoprotein, prawdopodobnie przez FLVCR1B (ang. *Feline Leukemia Virus subgroup C Receptor 1*) [23]. Ze względu na toksyczność wolnego hemu jego poziom musi być ściśle kontrolowany. Hem jest degradowany przez oksygenazę hemu (HO-1), zlokalizowaną na retikulum endoplazmatycznym. Ekspresja HO-1 jest silnie regulowana przez poziom hemu, ale także przez hipoksję,  $\text{H}_2\text{O}_2$  czy obniżony poziom glutationu. Aktywność HO-1 prowadzi do powstania biliwerdyny IX $\alpha$  (BVIX $\alpha$ ), wolnego jonu żelaza ( $\text{Fe}^{2+}$ ) oraz tlenku węgla (CO). BVIX $\alpha$  ma właściwości antyoksydacyjne i jest szybko przekształcana do bilirubiny IX $\alpha$  (BRIX $\alpha$ ) przez reduktazę biliwerdyny (BVR-A). Bilirubina również ma właściwości antyoksydacyjne, szczególnie skuteczne wobec anionorodnika ponadtlenkowego [24,25]. Pozostałe produkty degradacji hemu także mają cytoprotekcyjne właściwości. Wzrost stężenia wolnego żelaza indukuje ekspresję ferrytyny, która sekwestrując jony żelaza, obniża potencjał oksydacyjno-redukcyjny komórki, zapobiegając tworzeniu się RFT w reakcji Fentona. Natomiast CO zaangażowany jest w regulację wielu procesów komórkowych, m.in. w regulację poziomu interleukin czy pośredniczy w szlakach antyapoptotycznych [26,27].



**Rys. 3.** Schemat metabolizmu hemu. Suc-CoA- sukcyńlo-koenzym A, Gly - glicyna, 5-ALA- kwas 5-aminolewulinowy, PBG - porfobilinogen, HMB - hydroksymetylobilan, UrogenIII – uroporfirynogen III, CPgenIX – koproporfirynogen IX, PPgenIX – protoporfirynogen IX, PPIX – protoporfiryny IX, BVIX $\alpha$  - biliwerdyna IX $\alpha$ , BRIX - bilirubina IX $\alpha$ , ALAS – syntaza kwasu 5-aminolewulinowego, ALAD – dehydrataza kwasu 5-aminolewulinowego, HMBS – syntaza hydroksymetylobilanu, UROS – syntaza uroporfirogenu III, UROD – dekarboksylaza uroporfirynogenu III, CPOX – oksydaza koproporfirynogenu IX, PPOX – oksydaza protoporfirynogenu IX, FECH - ferrochelataza, HO-1 – oksigenaza hemu, BVR-A – reduktaza biliwerdyny SLC25A38 – Solute Carrier Family 25 Member 38, ABCB6 - ATP Binding Cassette Subfamily B Member 6, ABCG2 - Broad substrate specificity ATP-binding cassette transporter

ABCG2, FLVCR1b - Feline Leukemia Virus subgroup C Receptor 1, na podstawie [28,29], zmieniono. Rysunek wykonano za pomocą BioRender.com.

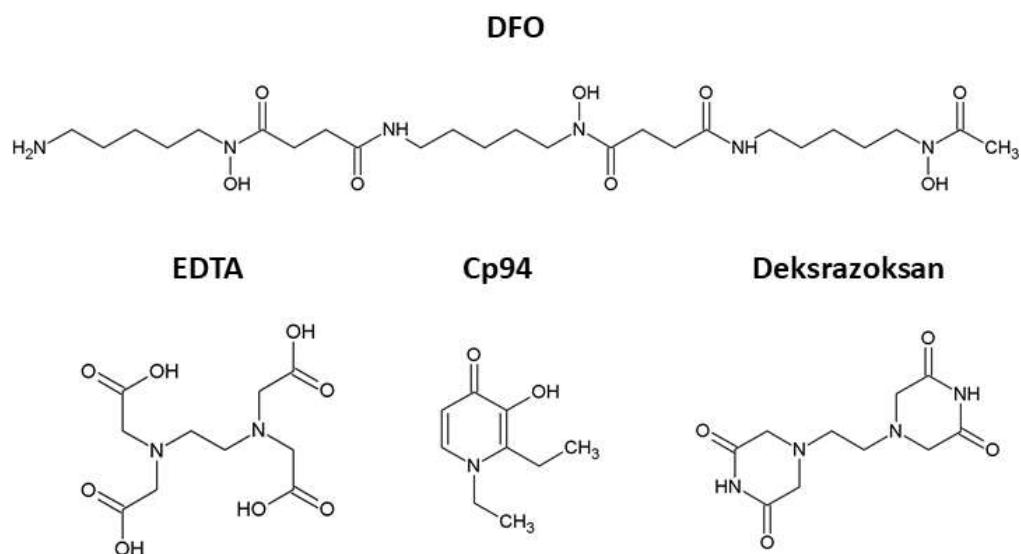
Jedną z największych zalet ALA-PDT jest selektywna akumulacja PPIX w komórkach nowotworowych. Fenomen ten stoi u podstaw tej terapii i pomimo wykorzystania jej w leczeniu i diagnostyce nowotworów, molekularne podstawy tego zjawiska nadal pozostają nie do końca jasne. Choć istnieje wiele czynników wpływających na akumulację PPIX w komórkach nowotworowych takich jak pH, temperatura, stopień unaczynienia, tempo metabolizmu czy ciśnienie tkankowe [30], różnice między metabolizmem hemu komórek nowotworowych, a komórek zdrowych oraz rola transporterów po egzogennym podaniu 5-ALA jest nadal słabo poznana.

Zmiany w ekspresji enzymów szlaku biosyntezy hemu w komórkach nowotworowych w porównaniu do zdrowych były przedmiotem niewielu badań. Pokazano, że ekspresja transkryptu ALAD jest zwiększona w komórkach nowotworu piersi w porównaniu do zdrowych [31]. W przypadku HMBS wykazano jego zwiększoną ekspresję w kilku typach nowotworów jelita grubego [32]. Natomiast zwiększoną ekspresję CPOX i PPOX, obserwowano w nowotworach żołądka i szybko rosnących nowotworach jelita grubego. [33]. Pokazano także, że ekspresja obu tych enzymów może być zależna od ilości żelaza w komórkach. Szczurze hepatocyty o obniżonym stężeniu żelaza wykazywały zwiększoną ekspresję tych enzymów, natomiast przeładowanie żelazem powodowało obniżenie ekspresji CPOX, ale nie PPOX [34]. Różne typy nowotworów jelita grubego mają mniejszy poziom FECH niż komórki niezmiennione nowotworowo [32]. Z racji, że kofaktorem FECH są centra żelazowo-siarkowe sugeruje się, że obserwowana w nowotworach deregulacja biosyntezy hemu może być wywołana zmianami w ich biosyntezie, co wpływa na aktywność FECH. Dodatkowo, potranslacyjne modyfikacje FECH mogą również wpływać na aktywność tego enzymu. Co ciekawe, FECH przy niedoborze żelaza może odłączyć z hemu jon żelaza prowadząc do powstania PPIX. [35–37]. Natomiast, HO-1 ma zwiększoną ekspresję w wielu typach nowotworów [38]. Można by przypuszczać, iż zwiększenie ekspresji HO-1 w komórkach nowotworowych powinno prowadzić do spadku PPIX poprzez katabolizm hemu, jednak taki efekt nie występuje. Przypuszcza się, że HO-1 może wpływać na aktywność pomp eksportujących żelazo (Fe-ATP-azy) poprzez aktywne usuwanie żelaza z komórek i degradację hemu. W związku z powyższym, komórki nowotworowe o zwiększonej ekspresji HO-1 mogą być zdolne do zwiększonej akumulacji PPIX [39,40]. Różnice w poziomie białek HMBS i HO-1 po traktowaniu 5-ALA komórek nowotworowych prostaty wykazały znaczący wzrost ich ekspresji w porównaniu do komórek nietraktowanych [41]. Innym aspektem może być regulacja ekspresji i aktywności poszczególnych enzymów szlaku biosyntezy hemu. Chelakkot i inni pokazali, że aktywacja szlaku Ras/MEK (ang. *Ras/mitogen-activated protein kinase*) zmniejsza akumulację

PPIX w komórkach nowotworowych poprzez dwa niezależne szlaki. Pierwszy z nich, Ras/MEK-HIF-1 $\alpha$ -FECH ma wpływ na aktywność FECH, przez co może wpływać na konwersję PPIX do hemu. Aktywacja Ras/MEK wpływa na zwiększenie ekspresji HIF-1 $\alpha$  (ang. *Hypoxia-inducible factor 1-alpha*), który z kolei działa jako aktywator transkrypcji FECH. Drugi szlak obejmuje ścieżkę Ras/MEK-RSK-ABCB1, w którym aktywacja Ras/MEK prowadzi do zwiększonej ekspresji RSK (ang. *Ribosomal protein S6 kinases*), zaangażowanych w aktywację wielu czynników transkrypcyjnych. Jak pokazano RSK zwiększa ekspresję transportera ABCB1 (ang. *ATP-binding cassette sub-family B member 1*), który z kolei jest częściowo odpowiedzialny za wyrzut PPIX z komórek. Zastosowanie inhibitora MEK powodowało zwiększoną akumulację PPIX w komórkach nowotworowych. Zaobserwowano także, że komórki zdrowe traktowane tym inhibitorem nie wykazywały zwiększonej akumulacji [42]. Rola innych transporterów w selektywnej akumulacji PPIX nie jest dobrze poznana. Jednym z najczęściej badanych transporterów jest ABCG2 (ang. *Broad substrate specificity ATP-binding cassette transporter ABCG2*). Choć jego rola w efektywności ALA-PDT jest stosunkowo dobrze poznana, nie wiadomo, czy jest zaangażowany w preferencyjną akumulację PPIX. Transporter ten jest odpowiedzialny za wyrzut PPIX z mitochondriów i poza komórkę (**Rys. 3**), a jego ekspresja jest zróżnicowana w różnych typach komórek nowotworowych [43]. Komórki nowotworu pęcherza moczowego [44] i żołądka [45] traktowane 5-ALA wykazywały zwiększoną ekspresję ABCG2, w porównaniu do zdrowych komórek. Z kolei badania z zastosowaniem inhibitora ABCG2 wskazywały na jego rolę w zwiększaniu poziomu PPIX w komórkach nowotworów piersi, w porównaniu do komórek prawidłowych. Jednakże, w pracy tej nie pokazano, czy są istotne różnice pomiędzy komórkami traktowanymi 5-ALA, a 5-ALA w kombinacji z inhibitorem oraz czy traktowanie komórek normalnych inhibitorem ABCG2 wpływa znacząco na poziom PPIX [46]. Transportery PEPT1 i 2 (ang. *Peptide transporter 1/2*), których naturalnym substratem są di- lub tripeptydy mają też zdolność do transportu 5-ALA do wnętrza komórek [47,48]. Wyciszenie ekspresji PEPT1/2 w komórkach nowotworowych powoduje znaczne zmniejszenie akumulacji PPIX, natomiast nadekspresja powoduje efekt odwrotny [45,49]. Kolejnym transporterem 5-ALA jest PAT1 (ang. *Proton-coupled amino acid transporter 1*), dla którego naturalnymi substratami są obojętne aminokwasy jak prolina oraz GABA (kwas  $\gamma$ -aminomasłowy) [50]. Jego rola jako transportera 5-ALA została pokazana na kilku typach normalnych komórek jelita cienkiego [51,52]. Inhibicja PAT1 powodowała zmniejszoną akumulację PPIX w nowotworach o wysokiej złośliwości raka prostaty po taktowaniu 5-ALA. Co ciekawe istnieją przesłanki, że PAT1 ma niewielką ekspresję w komórkach nie zmienionych nowotworowo, co sugeruje jego rolę w selektywnej akumulacji PPIX [50].

## 1.2. Chelatory żelaza w ALA-PDT

Jak zostało już wspomniane, komórki nowotworowe mają różną zdolność do akumulacji PPIX. Niestety często bywa, że ilość PPIX w komórkach nie jest wystarczająca do osiągnięcia zadawalającego efektu terapeutycznego. Zastosowanie chelatorów żelaza ma na celu zmniejszenie dostępności tego pierwiastka, a przez to zahamowanie ostatniego etapu biosyntezy hemu, czyli włączenie jonu żelaza do PPIX, wpływając tym samym na wzrost akumulacji PPIX w komórkach. Do dnia dzisiejszego w celu polepszenia efektywności ALA-PDT wykorzystano kilka chelatorów: kwas (etylenodiamino)tetraoctowy (EDTA), deferoksaminę (DFO), 1,2-dietylo-3-hydroksypyridin-4-on (Cp94) oraz deksrazoksan (**Rys. 4**). Pierwszym chelatorem zastosowanym w ALA-PDT był EDTA. Należy do grupy chelatorów nieselektywnych tj. wiążących nie tylko jony żelaza, ale także inne ważne biologicznie jony jak  $\text{Cu}^{2+}$  czy  $\text{Zn}^{2+}$ , a jego powinowactwo do jonów żelaza jest mniejsze niż innych chelatorów stosowanych w ALA-PDT [53]. Pomimo tego pokazano, że zastosowanie EDTA na komórkach bydlęcych fibroblastów znacząco podnosi poziom PPIX, w stosunku do komórek traktowanych wyłącznie 5-ALA [54]. Malik i inni wykazali natomiast, że zastosowanie EDTA w kombinacji z 5-ALA bezpośrednio na skórze myszy powoduje wzrost poziomu PPIX, zarówno w zdrowych tkankach, jak i zmienionych chorobowo. Dodatkowo zwrócono uwagę na słabą penetrację EDTA i 5-ALA w głąb tkanek skóry [55]. DFO, w przeciwieństwie do EDTA, jest bardziej specyficznym chelatorem w stosunku do jonów żelaza. Charakteryzuje się również niską liofilowością i dużą masą molekularną, co utrudnia jego administrację do komórek [56], a wydłużona ekspozycja na DFO może prowadzić do śmierci komórki poprzez znaczne zmniejszenie biodostępności żelaza [57], z racji tego ma on nikłe zastosowanie w ALA-PDT [58,59]. Innym związkiem zastosowanym w ALA-PDT był deksrazoksan, który sam w sobie nie jest chelatorem żelaza, natomiast produkty jego metabolizmu już tak [60]. Jak pokazano, podnosi on poziom PPIX w komórkach linii nowotworu płaskonabłonkowego i glejaka [61]. Obiecującym chelatorem żelaza nie posiadającym wad EDTA i DFO jest Cp94. Jest to związek o niskiej masie cząsteczkowej, dobrej lipofilowości i silnym powinowactwie do jonów  $\text{Fe}^{3+}$ . Pomimo, iż CP94 wiąże jony  $\text{Fe}^{3+}$ , w obecności tlenu cząsteczkowego utlenia jony  $\text{Fe}^{2+}$  do  $\text{Fe}^{3+}$ , nie dyskwalifikuje go to jako potencjalnego chelatora zwiększającego akumulację PPIX [62]. Skuteczność terapii ALA-PDT w kombinacji z CP94 wykazano w wielu badaniach *in vitro* i *in vivo*, zarówno pod względem akumulacji PPIX, jak i jego działania fototoksycznego [61,63–65].



**Rys. 4.** Struktury chelatorów żelaza wykorzystywanych w celu zwiększenia efektywności ALA-PDT.

Innym podejściem było wykorzystanie chelatorów żelaza z grupy tiosemikarbazonu (TSC). Związki te mają szerokie spektrum aktywności biologicznej m.in. działanie przeciwbakteryjne, przeciwrzybicze, przeciwwirusowe, przeciwnowotworowe czy przeciw pasożytnicze [66,67]. Ponadto są dobrymi chelatorami żelaza, co jest szczególnie istotne z punktu widzenia terapii ALA-PDT [68]. W pracy Mrozek-Wilczkiewicz i inni zastosowano silnie cytotoksyczne pochodne TSC w kombinacji z ALA-PDT. Jak pokazano, takie pochodne nie powodowały wzrostu PPIX w badanych liniach komórkowych, natomiast dla niektórych pochodnych zaobserwowano silny efekt synergistyczny [69] oparty na wzmożonej produkcji RFT. Jest to podejście odmienne od prezentowanego w niniejszej pracy, gdyż opiera się na wykorzystaniu silnie cytotoksycznych pochodnych TSC, których mechanizm działania jest związany z bezpośrednim wywołaniem stresu oksydacyjnego. Jednakże fakt ten dowodzi wielocelowości tej klasy związków i podkreśla ich atrakcyjność w kontekście badań nad potencjalnymi lekami.

### 1.3. Cel pracy

Pomimo, że ALA-PDT jest obiecującą metodą leczenia nowotworów posiada ona ograniczenia, dlatego też poszukiwanie nowych metod zwiększenia jej efektywności jest kluczowe dla rozwoju tej metody leczenia. Jednym z takich podejść jest zastosowanie chelatorów żelaza w celu zwiększenia akumulacji PPIX. Jednakże stosowane dotychczas związki mają swoje wady, dlatego też celem niniejszej pracy było:

- wyselekcjonowanie chelatorów żelaza z grupy TSC, które nie wykazują efektu antyproliferacyjnego w komórkach nowotworowych (w warunkach bez naświetlania) oraz ocena ich zdolności do zwiększenia akumulacji protoporfiryny IX (PPIX) w tych komórkach,
- ocena efektywności terapii fotodynamicznej opartej na kwasie 5-aminolewulinowym (ALA-PDT) po zastosowaniu wybranych chelatorów TSC oraz porównanie jej skuteczności z związkiem referencyjnym Cp94 na panelu różnych linii komórkowych,
- analiza zmian w ekspresji genów zaangażowanych w biosyntezę hemu oraz transporterów intermediatów tego szlaku metabolicznego w komórkach nowotworowych po zastosowaniu wyselekcjonowanych chelatorów TSC, w kontekście ich wpływu na efektywność ALA-PDT,
- ocena wpływu wyselekcjonowanych TSC oraz Cp94 na ekspresję genów związanych z metabolizmem żelaza, ze szczególnym uwzględnieniem genów mitochondrialnego metabolizmu żelaza, w celu określenia ich roli w terapii ALA-PDT.

Dzięki zastosowaniu metod spektroskopowych oraz analizy genetycznej, udało się wyjaśnić mechanizmy działania TSC oraz opisać zjawiska, które dotychczas nie były poruszane w literaturze naukowej. Wyniki te stanowią istotny wkład w rozwój dziedziny, otwierając nowe możliwości dla dalszych badań i pogłębiając naszą wiedzę na temat chelatorów żelaza w ALA-PDT.

Badania, których wyniki są zawarte w niniejszej pracy doktorskiej były finansowane w ramach projektu Narodowego Centrum Nauki PRELUDIUM 18 (2019/35/N/NZ7/02780), którego byłem kierownikiem.

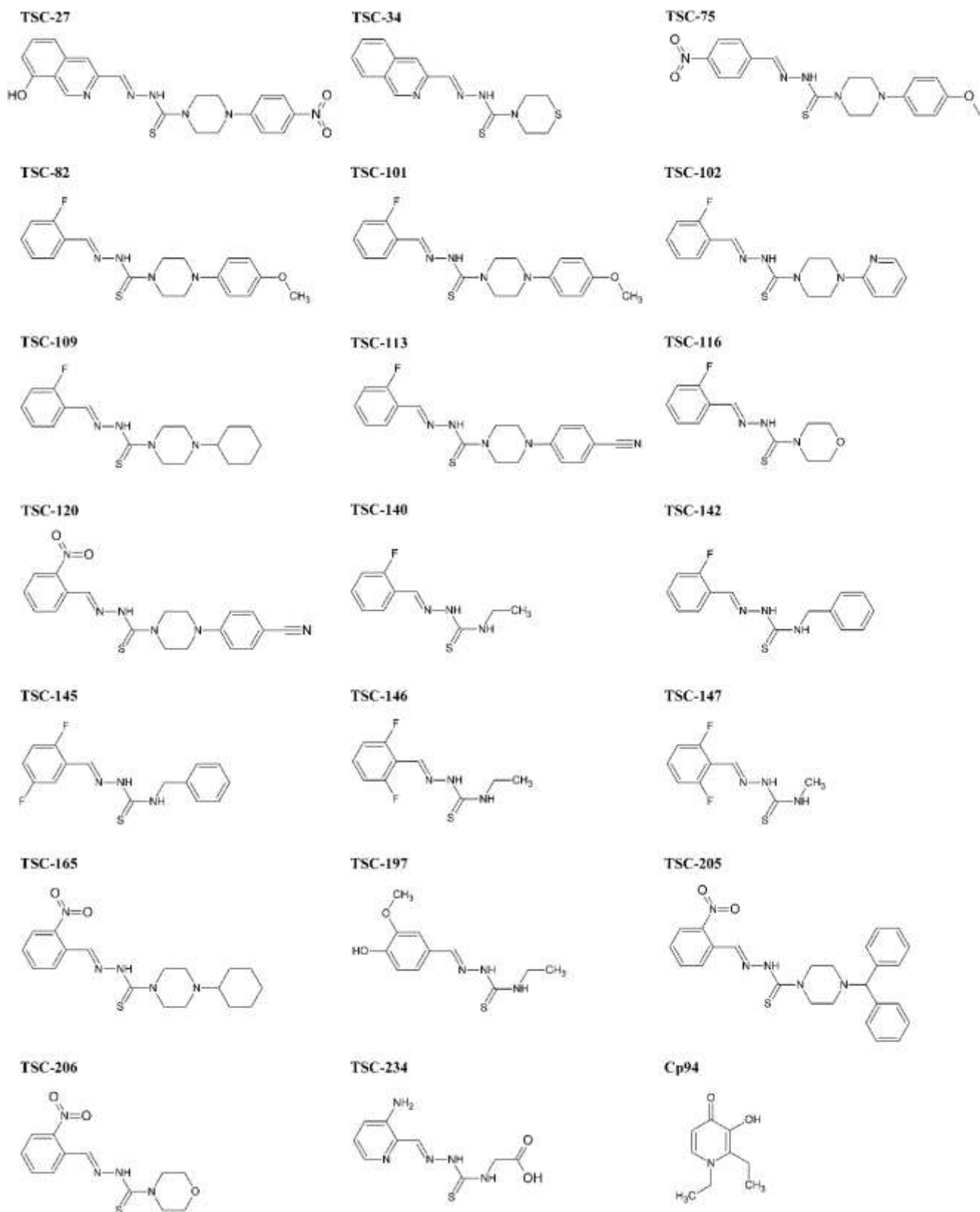
#### ***1.4. Materiały i metody***

Wszystkie badania wchodzące w skład tej pracy zostały wykonane w zespole Biofizyki Farmaceutycznej w Instytucie Fizyki im. Augusta Chełkowskiego Uniwersytetu Śląskiego w Katowicach pod kierownictwem dr hab. Anny Mrozek-Wilczkiewicz, prof. UŚ.

##### *Synteza tiosemikarbazonów*

Badane chelatory z grupy tiosemikarbazonu (**Rys. 5**) zostały zaprojektowane i zsyntezowane przez dr Martę Rogalską (Rejmund) w ramach pracy doktorskiej pod kierownictwem prof. dr hab. inż. Jarosława Polańskiego, Instytut Chemii Uniwersytet Śląski w Katowicach. Udział w syntezie miał również dr hab. inż. Maciej Serda, prof. UŚ z Instytutu Chemii Uniwersytetu Śląskiego w Katowicach.





**Rys. 5.** Struktury badanych tiosemikarbazonów i Cp94.

### ***Linie komórkowe i warunki hodowli***

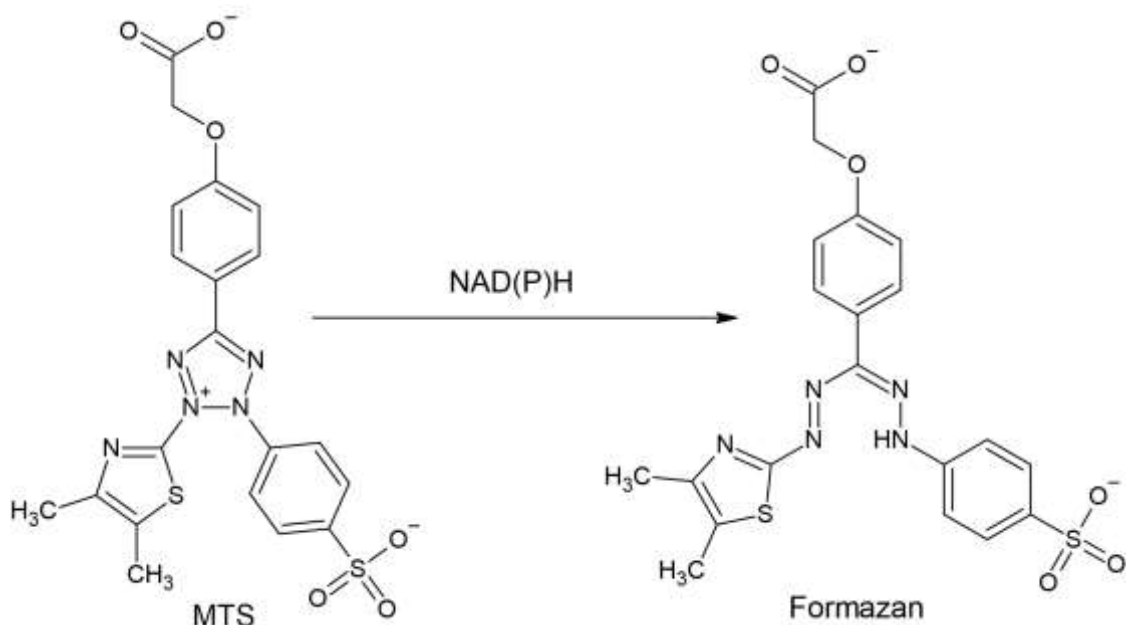
Badania przeprowadzono na panelu ludzkich linii komórkowych: HCT116 (gruczolakorak jelita grubego), MCF-7 (gruczolakorak piersi), A549 (gruczolakorak płuc), Hs683 (glejak), U251 (glejak) oraz linii prawidłowej NHDF (ludzkie fibroblasty). Linie komórkowe U251 i Hs683 zostały uprzejmie udostępnione przez prof. Gabrielę Kramer-Marek z Institute of Cancer Research w Londynie. Linia NHDF została zakupiona w PromoCell, natomiast pozostałe linie w American Type Culture Collection (ATCC).

Wszystkie linie komórkowe hodowano w sterylnych butelkach hodowlanych o objętości 75 cm<sup>3</sup> (Nunc) na pożywce Dulbecco's Modified Eagle's Medium (DMEM) wzbogaconej 12% v/v płodową surowicą bydlęcą (FBS) w przypadku nowotworowych linii komórkowych lub 15% v/v FBS dla linii NHDF. W obu przypadkach pożywka zawierała 1% v/v mieszaninę antybiotyków penicyliny i streptomycyny. Hodowle prowadzono w standardowych warunkach, w 37°C, w atmosferze wysyczonej parą wodną i 5% CO<sub>2</sub>. Wszystkie linie komórkowe były rutynowo badane pod kątem kontaminacji bakteriami z rodzaju *Mycoplasma* za pomocą techniki PCR, stosując startery dla genu kodującego 16S rRNA.

### ***Cytotoksyczność***

W celu oznaczenia cytotoksyczności badanych TSC wykorzystano kolorymetryczny test MTS. Test ten opiera się na redukcji soli tetrazolowej do formazanu przez dehydrogenazy zależne od NAD(P)H. Ilość barwnego formazanu, można oznaczyć ilościowo za pomocą spektrofotometru (**Rys. 6**).

Komórki wysiano na płytkach 96-dołkowych w ilości 5 × 10<sup>3</sup> komórek na dołek w przypadku linii nowotworowych i 4 × 10<sup>3</sup> komórek na dołek w przypadku linii NHDF. Komórki te inkubowano przez 24 godziny w standardowych warunkach, po czym podano badane związki w stężeniu 25 μM lub 50 μM i inkubowano przez następne 72 godziny. Po tym czasie pożywkę zawierającą badane związki usunięto i dodano medium DMEM bez czerwieni fenolowej oraz CellTiter 96® AQueous One Solution (MTS). Po około 1 h inkubacji w 37°C zmierzono absorbancję przy długości fali 490 nm za pomocą czytnika płytek wielodołkowych (Synergy 4, BioTek). Eksperyment powtórzono trzykrotnie w tryplikacie a otrzymane wartości posłużyły do wyliczenia wartości IC<sub>50</sub>, czyli stężenia substancji, przy którym proliferacja 50% populacji komórek zostaje zahamowana. Obliczeń IC<sub>50</sub> dokonano przy użyciu programu GraphPad Prism 8.



**Rys. 6.** Zasada działania testu MTS.

### ***Akumulacja PPIX i efekt fotodynamiczny***

#### ***Akumulacja PPIX***

Oznaczenie akumulacji PPIX dokonano na podstawie intensywności fluorescencji. Komórki wysiano na 96-dółkową czarną płytkę z przezroczystym dnem (Nunc) w ilości  $1,1 \times 10^4$  komórek na dołek i hodowano w standardowych warunkach przez 24 godziny. Po tym czasie, medium usunięto i podano roztwory TSC i Cp94 w stężeniu  $25 \mu\text{M}$ , 5-ALA w stężeniu  $1 \text{ mM}$  oraz ich kombinacje w pożywce bez czerwieni fenolowej. Roztwór 5-ALA był każdorazowo przygotowywany bezpośrednio przed podaniem. Po 24-godzinnej inkubacji ze związkami, fluorescencję PPIX mierzono przy użyciu czytnika płytek wielodołkowych (Synergy 4, BioTek) przy długości fali wzbudzenia  $407 \text{ nm}$  i długości fali emisji  $638 \text{ nm}$ . Uzyskane wartości fluorescencji zostały wykorzystane do obliczenia względnej intensywności fluorescencji PPIX jako tzw. procent 5-ALA. Badania prowadzono w tryplikatach w czterech niezależnych eksperymentach. Wszystkie eksperymenty przeprowadzono przy zredukowanym oświetleniu, aby zapobiec fotowysyblaniu.

### *Efekt fotodynamiczny*

W celu oznaczenia efektu fotodynamicznego wysiano i podano badane związki w identyczny sposób jak opisano przy akumulacji PPIX. Po 24-godzinnej inkubacji ze związkami, medium usunięto, a dołki przepłukano trzykrotnie medium bez czerwieni fenolowej. Komórki naświetlono światłem czerwonym ( $634 \text{ nm} \pm 5 \text{ nm}$ ) w dawce  $12 \text{ J/cm}^2$ . Następnie usunięto medium, w którym naświetlano komórki i zastąpiono świeżym, a komórki poddano dalszej inkubacji w standardowych warunkach przez kolejne 24 godziny. Jednocześnie przeprowadzono identyczny eksperyment z pominięciem etapu naświetlania w celu określenia cytotoksyczności ciemnej. Po inkubacji, żywotność komórek oceniano wykorzystując test MTS, postępując zgodnie z tym samym protokołem, co w przypadku oceny cytotoksyczności. Wszystkie eksperymenty prowadzono w zredukowanym oświetleniu i powtórzono w trzech niezależnych powtórzeniach. Żywotność komórek obliczono za pomocą oprogramowania GraphPad Prism 8.

### *Analiza profilu ekspresji genów*

#### *Projektowanie starterów PCR*

Sekwencje mRNA badanych genów pozyskano z bazy National Center for Biotechnology Information (NCBI). Startery dla poszczególnych sekwencji zostały zaprojektowane w Primer-BLSTA (NCBI), które dodatkowo zweryfikowano w programie Oligo 6.0. Syntezę starterów oraz ich oczyszczanie zlecono firmie Sigma-Aldrich.

#### *Izolacja całkowitego RNA i odwrotna transkrypcja*

Komórki wysiano na szalki Petriego o średnicy 3 cm (Nunc) w ilości  $4 \times 10^5$  komórek, a następnie inkubowano przez 24 godziny w standardowych warunkach. Po tym czasie, dodano świeżo przygotowane roztwory TSC, Cp94 ( $25 \mu\text{M}$ ) i 5-ALA ( $1 \text{ mM}$ ) i inkubowano przez kolejne 24 h. Komórki nietraktowane stanowiły kontrole. Całkowite komórkowe RNA zostało wyizolowane metodą Chomczyńskiego, korzystając z komercyjnego odczynnika TRIzol Reagent (ThermoFisher). Otrzymane lizaty komórkowe zebrano do mikroprobówek i dodano chloroform, a następnie inkubowano 3 minuty w temperaturze pokojowej i zwirowano ( $12\ 000 \times g$  przez 20 min.,  $4 \text{ }^\circ\text{C}$ ). Zebrano warstwę wodną zawierającą RNA, precypitowano RNA dodając 0,5 mL izopropanolu (10 minut w temperaturze pokojowej) i zwirowano ( $12\ 000 \times g$ , 10 min.,  $4 \text{ }^\circ\text{C}$ ). Uzyskane RNA przepłukano trzykrotnie 1 mL 75 % etanolem i zwirowano ( $7\ 500 \times g$ , 5 min.,  $4 \text{ }^\circ\text{C}$ ). Otrzymane pelety RNA suszono na powietrzu przez kilka minut, po czym rozpuszczono w 20  $\mu\text{L}$  ddH<sub>2</sub>O-DEPC. Ocenę

jakości i ilości otrzymanego RNA wykonano przy pomocy spektrofotometru NanoDrop 2000 (ThermoFisher).

Syntezę cDNA przeprowadzono wykorzystując komercyjny zestaw GoScript™ Reverse Transcriptase kit (Promega). W skład mieszaniny reakcyjnej dla pojedynczej próby wchodziły zawsze 2 µg wyizolowanego całkowitego RNA, 0,5 µL startera oligo(dT)<sub>23</sub> oraz ddH<sub>2</sub>O-DEPC, a całkowita objętość mieszaniny wynosiła 5 µL. Tak przygotowaną mieszaninę inkubowano 5 min. w temperaturze 70 °C, po czym natychmiast schłodzono na lodzie przez 5 minut. W kolejnym kroku, dodano przygotowaną mieszaninę odwrotnej transkryptazy GoScript™, buforu reakcyjnego, mieszaniny deoksynukleotydów, jonów magnezu i ddH<sub>2</sub>O-DEPC, do końcowej objętości 20 µL. Reakcję odwrotnej transkrypcji prowadzono w termocyklerze C1000 Touch™ (Bio-Rad) w następujących warunkach: 25 °C, 5 minut; 42 °C, 60 minut; 70 °C, 15 minut, na koniec mieszaninę schłodzono na lodzie i przechowywano w -80 °C (jeśli była taka potrzeba).

#### *Ilościowa reakcja PCR w czasie rzeczywistym*

Ilościową reakcję PCR w czasie rzeczywistym (RT-qPCR) przeprowadzono w termocyklerze CTX96 Touch™ Real-Time PCR Detection System (Bio-Rad). Mieszaninę reakcyjną stanowiło cDNA jako matryca, startery dla poszczególnych genów oraz PowerUp™ SYBR® Green Master Mix (ThermoFisher) i woda. Reakcję prowadzono w warunkach: początkowa denaturacja - 95 °C przez 120 sekund, a następnie 40 cykli: denaturacja - 95 °C, 15 sekund; przyłączanie starterów 60 °C, 30 sekund; wydłużanie - 72 °C, 60 sekund. Ocena temperatury topnienia otrzymanych produktów z dokładnością do 0,1 °C/s. Eksperymenty prowadzono w tryplikatach w 3 niezależnych powtórzeniach. Uzyskane wyniki normalizowano do genu referencyjnego (GAPDH) na podstawie metody Livaka i Schmittgena (metoda  $2^{-\Delta\Delta C_T}$ ) Analizę ekspresji genów przeprowadzono w oprogramowaniu Bio-Rad CFX Manager 3.1.

#### ***Oznaczenie wolnego hemu***

Oznaczenie wolnego hemu prowadzono z wykorzystaniem komercyjnie dostępnego zestawu Hemin Assay Kit (Abcam). W tym celu komórki wysiano na szalki Petriego o średnicy 3 cm w ilości  $1 \times 10^6$  komórek, hodowano przez 24 h w warunkach standardowych. Następnie, komórki traktowano TSC (25 µM) i 5-ALA (1 mM) i inkubowano przez 24 h. Po inkubacji komórki przemyto PBS i poddano lizie 1% v/v roztworem Triton X-100 w PBS. Otrzymane lizaty sonifikowano i odwirowano przy  $10\,000 \times g$  przez 10 minut, po czym zmierzono stężenie wolnego hemu przy użyciu zestawu

Hemin Assay Kit (Abcam; Cambridge, Wielka Brytania) zgodnie z protokołem producenta. Stężenie hemu obliczono na podstawie krzywej kalibracyjnej z trzech niezależnych eksperymentów.

### ***Chelatacja jonów żelaza***

Ocenę chelatacji jonów żelaza (III) przez badane TSC i Cp94 przeprowadzono przygotowując roztwory wyjściowe w DMSO o stężeniu 8,358 mM. Wszystkie próbki rozcieńczono ultraczystą wodą do uzyskania stężenia 100  $\mu$ M. Do każdego dołka 96-dołkowej płytki z przezroczystym dnem (Nunc) dodawano po 200  $\mu$ L roztworu zawierającego badany związek w stężeniu 50  $\mu$ M i rosnące stężenia jonów żelaza od 0 do 50  $\mu$ M. Widma absorpcji rejestrowano po 4-godzinnej inkubacji w temperaturze pokojowej przy użyciu czytnika płytek wielodołkowych Varioskan LUX (ThermoFisher) w zakresie 275-800 nm z krokiem co 5 nm. Wyniki zostały przedstawione na wykresach i przeanalizowane za pomocą oprogramowania OriginPro (OriginLab Corporation).

### ***Analiza statystyczna***

Wszystkie wyniki wyrażono jako średnie arytmetyczne  $\pm$  odchylenie standardowe (SD) z co najmniej trzech niezależnych eksperymentów. Analizę statystyczną przeprowadzono przy użyciu GraphPad Prism 8.0 (GraphPad Software), stosując test ANOVA z testem post-hoc Tukeya. Poziom istotności (p-value) < 0,05 uznano za znamienne statystycznie.

## 2. WYNIKI I DYSKUSJA

### 2.1. Cytotoksyczność badanych TSC

Pierwszym etapem badań nad zastosowaniem pochodnych TSC w ALA-PDT było wyselekcjonowanie związków charakteryzujących się brakiem działania hamującego proliferację komórek bez naświetlania (tzw. toksyczność ciemna). Kryterium to było kluczowe, gdyż TSC o działaniu cytotoksycznym nie prowadzą do wzrostu stężenia PPIX, co eliminuje je z potencjalnych kandydatów na związki wspomagające efektywność ALA-PDT. W związku z tym przeprowadzono badania cytotoksyczności na panelu nowotworowych linii komórkowych o różnym pochodzeniu.

Wyniki badań cytotoksyczności, zestawione w **Tabeli 1**, obejmują analizowane pochodne TSC, opisane w publikacjach [P1] i [P2]. Na podstawie otrzymanych wyników stwierdzono, że większość badanych pochodnych TSC nie wykazuje istotnej cytotoksyczności wobec analizowanych linii komórkowych. W przypadkach, gdzie obserwowano niewielkie efekty cytotoksyczne, nie stanowiły istotnej przeszkody dla dalszych badań. Silny efekt cytotoksyczny stwierdzono tylko dla pochodnej TSC-27 i TSC-101 na linii U251. Dla związku referencyjnego, Cp94, nie zaobserwowano działania cytotoksycznego na badanych liniach komórkowych. Dodatkowo, badania cytotoksyczności przeprowadzono na prawidłowej linii komórkowej NHDF (ludzkie fibroblasty), co było kluczowe dla oceny ich selektywności i bezpieczeństwa terapeutycznego badanych pochodnych TSC wobec niezmiennych nowotworowo komórek. Brak efektu cytotoksycznego wobec NHDF sugeruje, że badane związki mogą mieć potencjał w ALA-PDT, gdzie kluczowym celem jest maksymalizacja selektywności wobec komórek nowotworowych przy minimalizacji efektów ubocznych w zdrowych tkankach.

Na podstawie uzyskanych wyników uznano, że wszystkie testowane pochodne nie wykazują istotnego efektu cytotoksycznego, co kwalifikuje je do dalszych etapów badań i wskazuje na ich potencjalne zastosowanie w terapii ALA-PDT, jako związki mogące zwiększać efektywność tej terapii. W związku z tym podjęto decyzję o zastosowaniu stężenia 25  $\mu$ M w kolejnych badaniach.

**Tabela 1.** Zestawienie wyników cytotoksyczności i kodowanie TSC z publikacji [P1] i [P2].

Lp.	TSC	Atyproliferacyjna aktywność IC <sub>50</sub> [μM]					
		HCT116	MCF-7	Hs683	A549	U251	NHDF
1.	TSC-27 (1 w P1)	11,69±1,77	20,93±0,37	16,11±1,23	>25	2,78±0,25	>25
2.	TSC-34 (2 w P1)	18,31±0,92	>25	>25	>25	>25	13,06±1,90
3.	TSC-75 (3 w P1)	>25	>25	>25	>25	>25	>25
4.	TSC-82	47,56±1,99	>50	>50	nb	nb	>50
5.	TSC-101 (4 w P1)	12,10±1,03	11,30±1,59	>25	18,02±0,77	7,55±0,28	>50
6.	TSC-102	>50	>50	>50	nb	nb	>50
7.	TSC-109	30,87±0,64	42,97±1,33	>50	nb	nb	>50
8.	TSC-113	>50	>50	>50	nb	nb	>50
9.	TSC-116	34,88±0,96	>50	>50	nb	nb	>50
10.	TSC-120 (5 w P1)	>25	>25	>25	>25	>25	>25
11.	TSC-140	>50	>50	>50	nb	nb	>50
12.	TSC-142	>50	>50	>50	nb	nb	>50
13.	TSC-145	>50	>50	>50	nb	nb	>50
14.	TSC-146	>50	>50	>50	nb	nb	>50
15.	TSC-147	>50	>50	>50	nb	nb	>50
16.	TSC-165 (6 w P1)	11,78±3,28	>25	>25	>25	>25	>25
17.	TSC-197	>50	>50	>50	>25	nb	>50
18.	TSC-205 (7 w P1)	>25	>25	>25	>25	>25	>25
19.	TSC-206 (8 w P1)	>25	>25	>25	>25	>25	>25
20.	TSC-236 (9 w P1)	>25	>25	>25	>25	>25	>25
21.	Cp94	>50	>50	>50	nb	nb	>50

nb – nie badano



## 2.2. Akumulacja protoporfiryny IX

W celu zweryfikowania hipotezy dotyczącej wpływu pochodnych TSC na akumulację PPIX w komórkach, przeprowadzono eksperymenty, które polegały na pomiarze fluorescencji PPIX po inkubacji z pochodnymi TSC, 5-ALA oraz ich kombinacją.

Wyniki pokazały, że różne linie komórkowe wykazywały zróżnicowane poziomy fluorescencji PPIX po inkubacji z 5-ALA. Najwyższe poziomy zaobserwowano dla linii komórkowych MCF-7 i A549, natomiast najniższe dla linii HCT116. Co istotne, traktowanie tylko pochodnymi TSC nie prowadziło do znaczących wzrostów poziomu intensywności fluorescencji PPIX (Fig.2 w [P1]). Natomiast po traktowaniu kombinacją TSC i 5-ALA, największe wzrosty intensywności fluorescencji PPIX zaobserwowano dla linii HCT116 (**Tab. 2**), która miała najmniejszy przyrost po traktowaniu tylko 5-ALA. Dla tej linii komórkowej zidentyfikowano najwięcej pochodnych TSC powodujących znaczący przyrost intensywności fluorescencji PPIX. W przypadku linii MCF-7, również stwierdzono dość duże przyrosty PPIX po traktowaniu TSC. W pozostałych liniach komórkowych przyrosty PPIX nie były tak duże i o wiele mniej pochodnych TSC powodowało znaczące wzrosty. W przypadku linii U251 żadna pochodna TSC nie powodowała wzrostu PPIX, dlatego linia ta nie była uwzględniona w dalszych badaniach. Ponadto nie stwierdzono wzrostu poziomu PPIX w żadnej z linii komórkowych traktowanych kombinacją Cp94 i 5-ALA (Fig. 3 w [P3]). Może to wynikać z faktu, że zastosowane stężenie Cp94 wynosiło 25  $\mu\text{M}$ , podczas gdy w wielu wcześniejszych badaniach odnotowujących wyraźny wzrost poziomu PPIX stosowano stężenia powyżej 100  $\mu\text{M}$ . Brak znaczącego wzrostu PPIX po traktowaniu Cp94 i 5-ALA wskazuje na znacznie większą efektywność niektórych TSC w porównaniu do tego chelatora.

Traktowanie linii prawidłowej NHDF, tylko TSC lub kombinacją TSC i 5-ALA nie powodowało wzrostu intensywności fluorescencji PPIX. W kontekście terapii ALA-PDT jest to istotne, ponieważ zmniejsza ryzyko uszkodzenia zdrowych tkanek podczas terapii, co przekłada się na wyższą selektywność i bezpieczeństwo, przy jednoczesnym maksymalnym działaniu terapeutycznym ukierunkowanym na komórki nowotworowe.

Do dalszych badań na podstawie wyników z [P1] wybrano TSC-34 z racji, że pochodna ta podnosiła poziom PPIX w większości badanych linii komórkowych. Natomiast, z pracy [P3] do dalszych badań wzięto wszystkie pochodne TSC podnoszące poziom PPIX. Dla wybranych pochodnych TSC, pomimo znanego faktu, że są one dobrymi chelatorami żelaza, postanowiono

określić ich zdolność do chelatacji. Uzyskane wyniki wskazują, że wszystkie pochodne TSC chelatuja jony żelaza (III) w środowisku wodnym (Fig. 4 w [P3]).

**Tabela 2.** Podsumowanie wyników akumulacji PPIX z publikacji [P1] i [P2].

TSC-	Wzrost RFU PPIX względem 5-ALA			
	HCT116	MCF-7	Hs683	A549
<b>TSC-27</b>	4,0	-	-	2,4
<b>TSC-34</b>	4,2 w [P1]	1,6 w [P1]	1,7 w [P1]	-
	4,14 w [P2]	1,66 w [P2]	1,68 w [P2]	-
<b>TSC-101</b>	3,0	-	-	2,2
<b>TSC-109</b>	2,47	1,66	-	-
<b>TSC-113</b>	3,0	1,9	-	-
<b>TSC-116</b>	2,6	1,64	-	-
<b>TSC-206</b>	-	-	1,6	-

### 2.3. Efekt fototoksyczny

Wzrost akumulacji PPIX nie zawsze jest wyznacznikiem efektywności terapii ALA-PDT. W związku z tym, podjęliśmy badania, mające na celu identyfikację pochodnych TSC o znacznym wpływie na efekt fototoksyczny. W publikacji [P2] wykazaliśmy, że zastosowanie samego TSC-34 nie wywołuje efektu fototoksycznego, co jest korzystne z punktu widzenia ALA-PDT. Nie stwierdzono także istotnego statystycznie spadku żywotności komórek we wszystkich układach eksperymentalnych na komórkach nienaświetlanych (Fig. 3 w [P2]), co sugeruje brak niepożądanych efektów ubocznych w przypadku braku naświetlania. Identyczne obserwacje uzyskano dla badanych pochodnych TSC i Cp94 w publikacji [P3] (Fig. 5).

W przypadku naświetlania komórek traktowanych samym TSC-34, nie stwierdziliśmy znaczącego spadku żywotności komórek. Co ciekawe, zarówno w publikacji [P2], jak i [P3], nie zaobserwowaliśmy efektu fototoksycznego po naświetlaniu komórek traktowanych wyłącznie 5-ALA na wszystkich badanych liniach komórkowych (**Tab. 3**). Wynik ten jest sprzeczny z doniesieniami literaturowymi, w których obserwowano znaczący lub średni efekt fototoksyczny po traktowaniu 5-ALA. Brak efektu fotocytotoksycznego był raportowany w kilku pracach. Badania sugerują, że w komórkach traktowanych wyłącznie 5-ALA nadal dochodziło do biosyntezy hemu, co oznacza,

że stężenie PPIX mogło być niewystarczające do osiągnięcia znacznego efektu terapeutycznego. Wyniki pokazały, że stężenie wolnego hemu znacząco wzrastało w komórkach traktowanych wyłącznie 5-ALA w porównaniu do kontroli. Z kolei zastosowanie kombinacji TSC-2 z 5-ALA powodowało obniżenie stężenia wolnego hemu do poziomu jak w komórkach kontrolnych na liniach HCT116, MCF-7 i Hs683 (Fig.4 w [P2]). W linii A549 poziom wolnego hemu nie uległ statystycznie istotnym zmianom po traktowaniu TSC-34 w kombinacji z 5-ALA.

**Tabela 3.** Podsumowanie wyników badań dotyczących cytotoksyczności (ciemnej i jasnej) na podstawie [P2] i [P3].

Lp.	TSC + 5-ALA	Frakcja przeżywająca [% kontroli]							
		Nienaświetlane				Naświetlane [12 J/cm <sup>2</sup> ]			
		HCT116	MCF-7	Hs683	A549	HCT116	MCF-7	Hs683	A549
1.	5-ALA	98,36 ±4,44	100,50 ±4,92	99,02 ±5,69	99,75 ±6,90	97,69 ±9,36	95,95 ±8,54	95,95 ±8,54	95,68 ±8,33
2.	TSC-34	88,65 ±3,69	92,69 ±3,69	95,65 ±3,69	92,24 ±3,33	<b>33,56</b> <b>±3,84</b>	<b>45,56</b> <b>±2,85</b>	<b>39,54</b> <b>±6,54</b>	76,53 ±1,91
3.	TSC- 109	90,56 ±2,35	96,65 ±4,65	94,92 ±4,65	nb	95,92 ±2,86	94,05 ±3,58	94,05 ±3,58	nb
4.	TSC- 113	97,69 ±6,54	96,86 ±7,59	97,65 ±7,59	nb	<b>40,87</b> <b>±6,89</b>	<b>31,50</b> <b>±7,65</b>	87,36 ±7,65	nb
5.	TSC- 116	98,56 ±8,25	98,56 ±6,59	98,52 ±6,59	nb	85,98 ±6,6584	87,98 ±6,65	87,98 ±6,65	nb
6.	Cp94	101,32 ±5,32	98,69 ±3,98	98,69 ±3,98	nb	97,56 ±5,68	86,56 ±7,68	86,56 ±7,68	nb

nb- nie badano

Te obserwacje można wytłumaczyć tym, że egzogenne podanie 5-ALA omija system regulacji biosyntezy hemu poprzez mechanizm ujemnego sprzężenia zwrotnego. Dodatkowo, brak zmian

w dostępności żelaza umożliwia konwersję PPIX w hem, co może tłumaczyć niską efektywność terapeutyczną samego 5-ALA na badanych liniach komórkowych.

Jak pokazaliśmy w [P2] i [P3] komórki naświetlane wykazywały znaczące spadki żywotności komórek po zastosowaniu TSC-34 i TSC-113 w połączeniu z 5-ALA na liniach HCT116 i MCF-7, i Hs683 (tylko pochodna TSC-34), natomiast dla linii komórkowej A549 efekt fototoksyczny był niewielki w porównaniu do innych linii komórkowych (**Tab. 3**). Warto podkreślić, że, nie zaobserwowano spadku żywotności komórek w żadnej z testowanych linii po traktowaniu Cp94 w połączeniu z 5-ALA. Wyniki te jednoznacznie demonstrowują skuteczność TSC-34 i TSC-113 w zwalczaniu komórek nowotworowych podczas ALA-PDT. Mimo stosunkowo niskiego stężenia TSC (25  $\mu$ M), uzyskano wyraźny efekt terapeutyczny, co wyróżnia te związki w porównaniu z referencyjnym Cp94, który nie wykazał porównywalnej skuteczności.

#### **2.4. Wpływ wybranych TSC na ekspresję genów**

Mechanizm działania wybranych pochodnych TSC nie może być wyjaśniony jedynie na podstawie wyników dotyczących akumulacji PPIX lub naświetlania, dlatego podjęliśmy badania na poziomie molekularnym w celu wyjaśnienia otrzymanych wyników. W pierwszym etapie określiliśmy ekspresje poszczególnych genów szlaku biosyntezy hemu w komórkach nie traktowanych względem linii komórkowej NHDF (Fig. 3 w [P1]). Ekspresja niektórych genów tego szlaku była podniesiona, szczególnie HMBS we wszystkich badanych liniach komórkowych. W linii HCT116 stwierdzono także podniesiony poziom CPOX i PPOX. W większości linii komórkowych zarejestrowano stosunkowo niski poziom HO-1, choć z doniesień literaturowych wynika, że większość nowotworów ma zwiększoną ekspresję tego genu. Na podstawie tych danych nie można jednoznacznie określić, która linia komórkowa będzie bardziej podatna na ALA-PDT w kombinacji z pochodnymi TSC. W związku z tym w kolejnym etapie badań było sprawdzenie ekspresji tych genów po traktowaniu TSC w kombinacji z 5-ALA. W publikacji [P1] pokazaliśmy, że ekspresja większości genów szlaku biosyntezy hemu nie ulega zmianie po traktowaniu 5-ALA i kombinacji 5-ALA z TSC-34 (Fig. 4 i Fig. S1 w [P1]). Jedynie ekspresja FECH oraz HO-1 została zmieniona. Jednak traktowanie kombinacją 5-ALA i TSC-34, powodowało zmniejszenie ekspresji HO-1 na linii MCF-7 i HCT116, podczas gdy dla Hs683 odnotowano wzrost ekspresji tego genu (Fig. 4 w [P1]). W przypadku linii A549 nie zaobserwowano żadnych znaczących zmian ekspresji badanych genów. Zmiany w ekspresji FECH zostały zauważone dla linii Hs683 i HCT116. Linia Hs683 po traktowaniu TSC-34 i 5-ALA

wykazywała zwiększoną ekspresję tego genu, podczas gdy na linii HCT116 ekspresja ta była zmniejszona. Podobne wyniki otrzymano w pracy [P3] gdzie, komórki linii HCT116 i MCF-7 wykazywały zmniejszoną ekspresję FECH po traktowaniu TSC-34 oraz TSC-113 w kombinacji z 5-ALA, natomiast w linii Hs683 w obu tych przypadkach ekspresja ta była zwiększona. Poziom HO-1 również był analogiczny do wyników z [P1], z wyjątkiem komórek HCT116 traktowanych TSC-113 i 5-ALA, gdzie nie zaobserwowano istotnych zmian w ekspresji tego genu. W przypadku linii Hs683 ekspresja HO-1 była zwiększona po traktowaniu zarówno TSC-34 jak i TSC-113 (Fig. 6 i 7 w [P3]). Traktowanie komórek HCT116 i MCF-7 kombinacją Cp94 i 5-ALA powodowało spadek ekspresji FECH, natomiast w przypadku HO-1 jedynie dla linii MCF-7 został stwierdzony spadek jego ekspresji. Otrzymane wyniki wskazują, że zmniejszona ekspresja FECH prowadzi do zwiększonej akumulacji PPIX, co w połączeniu z obniżoną ekspresją HO-1, a przez to obniżoną ochroną przed RFT, może tłumaczyć silny efekt fototoksyczny na liniach HCT116 i MCF-7 po traktowaniu TSC-34 i TSC-113. W przypadku linii Hs683, mimo że wzrost ekspresji FECH może sugerować słabą efektywność terapii, nie wyjaśnia on silnej odpowiedzi po traktowaniu TSC-34, co sugeruje istnienie innych, niezidentyfikowanych jeszcze mechanizmów.

W pracy [P2] skoncentrowano się na ekspresji transporterów zaangażowanych w przepływ intermediatów szlaku biosyntezy hemu pomiędzy kompartmentami komórkowymi. Spośród badanych transporterów tylko dwa wykazały statystycznie istotne zmiany w ekspresji po traktowaniu kombinacją 5-ALA i TSC-34. Pierwszym z nich był ABCG2 (ang. *broad substrate specificity ATP-binding cassette transporter ABCG2*), jeden z najczęściej badanych transporterów w kontekście efektywności ALA-PDT, który uczestniczy w usuwaniu PPIX z komórki. Jak pokazano jego zwiększona ekspresja koreluje z niską akumulacją PPIX oraz niską efektywnością ALA-PDT. Statystycznie istotne zmiany w ekspresji ABCG2 zaobserwowano we wszystkich badanych liniach komórkowych. Porównując wzrost ekspresji genu ABCG2 pomiędzy komórkami traktowanymi samym 5-ALA, a tymi które były traktowane kombinacją 5-ALA i TSC-34, stwierdzono zależność, że im wyższy stosunek, tym niższa akumulacja PPIX, co potwierdzają nasze wcześniejsze badania (Fig. 2 i Tab. 1 w [P2]). Obserwacja ta jest zgodna z doniesieniami literaturowymi, z wyjątkiem linii komórkowej A549, w której nie zaobserwowano znaczącej akumulacji PPIX, a wzrost ekspresji ABCG2

w porównaniu do komórek traktowanych tylko 5-ALA był najmniejszy spośród badanych linii komórkowych. Drugim transporterem o zmienionej ekspresji była mitoferryina 1 (MFRN1), pełniąca rolę transportera żelaza do mitochondriów. W publikacji [P2] stwierdzono znaczący wzrost ekspresji MFRN1 na liniach komórkowych Hs683 i A549 po traktowaniu kombinacją TSC-34 i 5-ALA (Fig. 2

w [P2]). W publikacji [P3] stwierdzono wzrost ekspresji tej izoformy na linii HCT116 (Fig. 10 w [P3]). Wzrost ekspresji stwierdzono także po traktowaniu Cp94 i 5-ALA na tej linii komórkowej. W przypadku MFRN2 ekspresja była zwiększona w linii HCT116 oraz Hs683. Traktowanie komórek kombinacją TSC-113 i 5-ALA powodowało spadek ekspresji obu izoform MFRN na linii HCT116, a w przypadku linii MCF-7 obniżenie ekspresji izoformy 2. Wzrost ekspresji MFRN1 stwierdzono także dla linii MCF-7 po traktowaniu Cp94 i 5-ALA. Obniżona ekspresja MFRN po traktowaniu TSC-113, może wyjaśniać skuteczność tego związku w ALA-PDT poprzez zmniejszenie transportu żelaza, co hamuje syntezę hemu i promuje akumulację PPIX. Z kolei komórki Hs683, inkubowane ze związkiem TSC-34, wykazały zwiększoną ekspresję MFRN, co teoretycznie mogłoby osłabić skuteczność ALA-PDT, jednakże nie zaobserwowano takiego efektu. Wzrost ekspresji MFRN może odzwierciedlać odpowiedź komórki na zwiększone zapotrzebowanie na żelazo, a nie bezpośrednio wpływać na skuteczność ALA-PDT na tej linii komórkowej.

Wyniki dotyczące ekspresji MFRN oraz zastosowanie chelatorów żelaza z grupy TSC w ALA-PDT skłoniły nas do pogłębienia badań nad genami zaangażowanymi w metabolizm żelaza, ze szczególnym uwzględnieniem jego mitochondrialnego aspektu. W związku z tym podjęliśmy dalsze badania mające na celu zrozumienie wpływu pochodnych TSC na metabolizm żelaza oraz ich wpływu na skuteczność ALA-PDT. Jednym z badanych genów była mitochondrialna ferrytyna (FTMT), która pełni funkcję magazynu żelaza w mitochondriach i wykazuje aktywność ferooksydazy. Zwiększoną ekspresję tego genu zaobserwowano po traktowaniu kombinacją TSC-34 i 5-ALA we wszystkich badanych liniach komórkowych, a także na linii HCT116 po traktowaniu Cp94 i 5-ALA (Fig. 8 w [P3]). Zwiększona ekspresja FTMT może prowadzić do zmian w polaryzacji błony mitochondrialnej, powodując uszkodzenie mitochondriów i zwiększoną produkcję RFT. Te zmiany mogą z kolei zakłócać morfologię mitochondriów. Jednym z głównych czynników utrzymujących architekturę mitochondriów jest kompleks MICOS (ang. *mitochondrial contact site and cristae organizing system*), który fizycznie oddziałuje z FECH. Zaburzenie funkcji MICOS prowadzi do akumulacji PPIX i obniżenia aktywności FECH. Interakcja pomiędzy FTMT a FECH może wyjaśniać skuteczność terapii ALA-PDT po inkubacji z TSC-34 linii komórkowych HCT116 i MCF-7.

Kolejnym badanym genem była frataksyna (FNX), która pełni rolę donora siarki w biosyntezie klastrów żelazowo-siarkowych. Jednak dokładna funkcja tego białka pozostaje w dużej mierze niepoznana. W naszych badaniach wykazano zmniejszenie ekspresji FNX na liniach HCT116 i MCF-7 po traktowaniu kombinacją TSC-113 i Cp94 w połączeniu z 5-ALA (Fig. 9 w [P3]). FXN nie wpływa bezpośrednio na szlak biosyntezy hemu, a zmniejszenie jej ekspresji może wpływać na aktywność FECH, poprzez zmniejszenie biosyntezy klastrów żelazowo-siarkowych, będących kofaktorem

FECH, a przez to prowadzić do zwiększenia stężenia PPIX. W przypadku transportera ABCB8, który uczestniczy w eksporcie żelaza z mitochondriów do cytoplazmy, stwierdzono znaczące wzrosty jej ekspresji na wszystkich badanych liniach komórkowych po traktowaniu Cp94 w kombinacji z 5-ALA, a także na linii Hs683 po traktowaniu TSC-34 i 5-ALA (Fig. 12 w [P3]). Wpływ ekspresji ABCB8 na efektywność ALA-PDT pozostaje niezbadany, ale wcześniejsze badania sugerują, że obniżenie ekspresji tego genu prowadzi do zmniejszonego przeżycia komórek, uszkodzeń mitochondriów i zwiększonego poziomu RFT. Podwyższona ekspresja ABCB8 może prowadzić do odwrotnego efektu, czyli zwiększać przeżywalność komórek, co może wyjaśnić brak efektu fototoksycznego po traktowaniu Cp94 i 5-ALA. Mimo wzrostu ekspresji ABCB8 po zastosowaniu TSC-34, nadal obserwowano efekt fototoksyczny, co potwierdza skuteczność TSC-34 w ALA-PDT. Ostatnim badany genem był DMT1 (ang. *divalent metal transporter 1*), który uczestniczy między innymi w transporcie żelaza do komórki. Ekspresja tego genu była zróżnicowana na badanych liniach komórkowych (Fig. 11 w [P3]). Na linii HCT116 traktowanie zarówno TSC-34 i TSC-113 w kombinacji z 5-ALA powodowały znaczący spadek ekspresji tego genu. W przypadku linii MCF-7, traktowanie TSC-113 oraz Cp94 z 5-ALA również wywoływało znaczny wzrost ekspresji DMT1. Spadek ekspresji był obserwowany jedynie na linii Hs683 po traktowaniu TSC-34 i 5-ALA. Wpływ ekspresji tego genu na efektywność ALA-PDT może polegać na zmniejszeniu poboru żelaza z przestrzeni międzykomórkowej.

### 3. PODSUMOWANIE I WNIOSKI

W niniejszej pracy zidentyfikowano dwie spośród 20 badanych pochodnych tiosemikarbazonu, które wykazały szczególnie obiecujące właściwości w kontekście poprawy efektywności terapii fotodynamicznej opartej na kwasie 5-aminolewulinowym. Te dwie pochodne, TSC-34 i TSC-113, charakteryzowały się brakiem cytotoksyczności ciemnej oraz zdolnością do chelatowania jonów żelaza. Zastosowanie tych pochodnych w połączeniu z 5-ALA prowadziło do znacznego wzrostu akumulacji PPIX oraz wywoływało silny efekt fototoksyczny na różnych liniach komórkowych, co potwierdza ich duży potencjał w poprawie efektywności ALA-PDT.

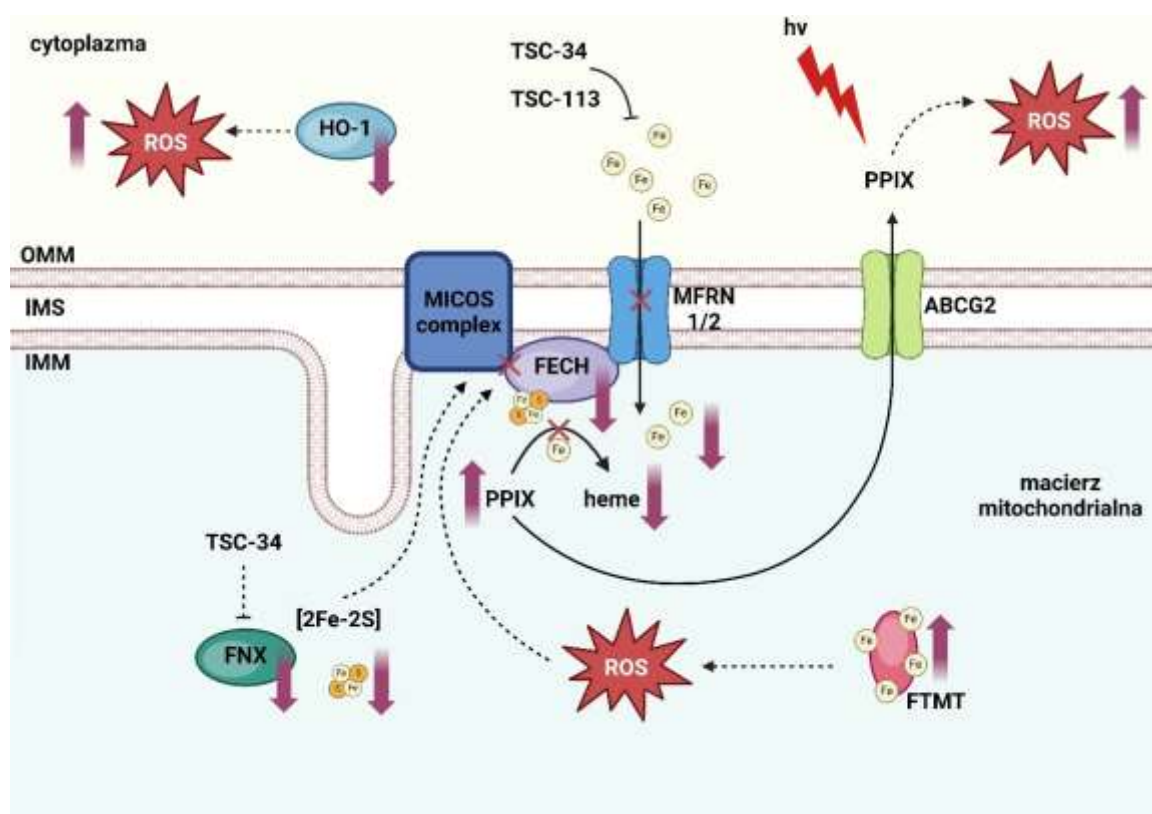
Mechanizm działania tych związków opiera się na modulacji ekspresji genów związanych z metabolizmem żelaza i biosyntezą hemu, co prowadzi do zwiększonej akumulacji PPIX i silnego efektu fototoksycznego. W liniach komórkowych HCT116 i MCF-7 pochodne TSC-34 i TSC-113 powodowały obniżenie ekspresji genów FECH i HO-1, co sprzyjało akumulacji PPIX i zwiększało skuteczność terapii. Obniżenie ekspresji FECH było zależne od dwóch mechanizmów. W przypadku TSC-34 obserwowano spadek ekspresji FNX, co prowadziło do zmniejszenia produkcji centrów żelazowo-siarkowych, będących kofaktorami FECH, oraz wzrost poziomu FTMT, co mogło wpływać na interakcję pomiędzy kompleksem MICOS a FECH, ograniczając aktywność FECH. Z kolei TSC-113 powodowała wyraźny spadek ekspresji MFRN, zmniejszając dostępność żelaza dla FECH, co również skutkowało zwiększoną akumulacją PPIX i silnym efektem fototoksycznym. Dodatkowo, obniżenie ekspresji HO-1 osłabiało mechanizmy ochrony komórek przed reaktywnymi formami tlenu, co potęgowało efekt terapeutyczny.

Nietypową odpowiedź na TSC-34 zaobserwowano dla linii komórkowej Hs683. Pomimo zwiększonej ekspresji genów FECH i HO-1, co zazwyczaj ogranicza efektywność ALA-PDT, TSC-34 w kombinacji z 5-ALA wywołała wzrost poziomu PPIX oraz silny efekt fototoksyczny. To niestandardowe zachowanie sugeruje bardziej złożony mechanizm działania na tej linii komórkowej, który wymaga dalszych badań. Możliwe jednak, że zwiększona ekspresja FTMT odpowiada za zaobserwowany efekt poprzez zaburzenie aktywności FECH, co prowadzi do nasilonego efektu fototoksycznego, mimo wzrostu ekspresji FECH.

W porównaniu z pochodnymi TSC, Cp94, powszechnie stosowany chelator żelaza w ALA-PDT, okazał się mniej skuteczny. Brak wzrostu akumulacji PPIX oraz niska fotocytotoksyczność sugerują, że pochodne TSC są znacznie bardziej efektywne w stosowanych stężeniach niż Cp94, co czyni je obiecującymi kandydatami do dalszych badań nad polepszeniem efektywności ALA-PDT.



Poniżej, na **Rys. 7**, przedstawiono schematyczny mechanizm działania, który ilustruje wpływ pochodnych TSC na metabolizm żelaza, biosyntezę hemu oraz akumulację PPIX, ze szczególnym naciskiem na zmiany w ekspresji genów odpowiedzialnych za te procesy. Schemat ten stanowi podsumowanie najważniejszych wyników przedstawionych w niniejszej pracy, pokazując, w jaki sposób pochodne TSC-34 i TSC-113, poprzez regulację ekspresji kluczowych genów, takich jak FECH, HO-1, FNX, MFRN i FTMT, prowadzą do zwiększonej akumulacji PPIX i silnego efektu fototoksycznego w terapii ALA-PDT.



**Rys. 7.** Schematyczne podsumowanie mechanizmu działania TSC-34 i TSC-113. FECH-ferrochelataza, MFRN1/2 – mitoferryna1/2, FNX – frataksyna, FTMT – mitochondrialna ferrytyna, HO-1 - oksygenaza hemowa, ROS – reaktywne formy tlenu, OMM – zewnętrzna błona mitochondrialna, IMS - przestrzeń międzybłonowa, IMM – wewnętrzna błona mitochondrialna, Rysunek wykonano za pomocą BioRender.com.

#### **4. PUBLIKACJE WCHODZĄCE W SKŁAD ROZPRAWY**

##### **4.1. [P1]. Impact of thiosemicarbazones on the accumulation of PpIX and the expression of the associated genes.**

**Autorzy:** Gawecki R., Malarz K., Rejmund M., Polanski J., Mrozek-Wilczkiewicz A. **Referencja:** Journal of Photochemistry and Photobiology B: Biology, 2019, 199, 111585.

**Numer DOI:** 10.1016/j.jphotobiol.2019.111585

**Impact Factor czasopisma:** 4.383 (2019)

**Liczba punktów MNiSW czasopisma:** 100 (2019)

Mój udział w pracy polegał na wykonaniu i analizie wyników cytotoksyczności, akumulacji PPIX oraz ekspresji genów.



Contents lists available at ScienceDirect

Journal of Photochemistry &amp; Photobiology, B: Biology

journal homepage: [www.elsevier.com/locate/jphotobiol](http://www.elsevier.com/locate/jphotobiol)

## Impact of thiosemicarbazones on the accumulation of PpIX and the expression of the associated genes

Robert Gawecki<sup>a</sup>, Katarzyna Malarz<sup>a</sup>, Marta Rejmund<sup>b</sup>, Jaroslaw Polanski<sup>b</sup>,  
Anna Mrozek-Wilczkiewicz<sup>a,\*</sup>

<sup>a</sup>A. Chelkowski Institute of Physics, Silesian Center for Education and Interdisciplinary Research, University of Silesia, Chorzow, Poland

<sup>b</sup>Institute of Chemistry, University of Silesia, Katowice, Poland



### ARTICLE INFO

#### Keywords:

Thiosemicarbazones  
Accumulation of PpIX  
5-Aminolevulinic acid  
Heme pathway gene expression  
Metal chelator

### ABSTRACT

Thiosemicarbazone derivatives are known for their broad biological activity including their antitumor potency. The aim of the current study was to examine the effect of a novel series of non-toxic iron chelators on the accumulation of protoporphyrin IX after external 5-aminolevulinic acid administration. From this series we selected one the most promising derivative which causes a pronounced increase in the concentration of protoporphyrin IX. The increase of the photosensitizer concentration is necessary for the trigger the efficient therapeutic effect of the photodynamic reaction. For selected compound **2** we performed an examination of a panel of the genes that are involved in the heme biosynthesis and degradation. Results indicated the crucial roles of ferrochelatase and heme oxygenase in the described processes. Surprisingly, there was a strict dependence on the type of the tested cell line. A decrease in the expression of the two aforementioned enzymes after incubation with compound **2** and 5-aminolevulinic acid is a commonly known fact and we detected this trend for the MCF-7 and HCT 116 cell lines. However, we noticed the upregulation of the tested targets for the Hs683 cells. These unconventional results prompted us to do a more in-depth analysis of the described processes. In conclusion, we found that compound **2** is a novel, highly effective booster of photodynamic therapy that has prospective applications.

### 1. Introduction

Nowadays, traditional cancer treatment strategies, including chemotherapy, radiotherapy and the surgical removal of a tumor, are complemented with novel regimens such as gene therapy [1], monoclonal antibodies [2], stem cells [3] and photodynamic therapy (PDT) [4]. The main advantage of the newest therapies is their selectivity towards normal cells [5]. Among the aforementioned methods of treatment, PDT can also be used for diagnosing the cancer [6]. In this therapy, an external or biosynthesized drug, in this case a photosensitizer (PS), must be activated by light at a specific wavelength. In order to trigger the photodynamic reaction, an interaction of the PS with light and oxygen that is dissolved in the tissue is required [7]. During this process reactive oxygen species (ROS) are generated and

disturbing proper redox balance cause cytotoxic effect in the cell [6]. A variant of PDT is 5-ALA-PDT, in which 5-aminolevulinic acid (5-ALA) is used [8]. 5-ALA is a prodrug that is produced naturally in mammalian cells and this is the substrate for the heme biosynthesis (Scheme 1). The external administration of 5-ALA causes the production of intracellular protoporphyrin IX (PpIX), which is an effective photosensitizer that has also good fluorescent properties [9]. The therapeutic and diagnostic properties of 5-ALA-PDT are used in the treatment and diagnosis of many types of cancer including brain [10], skin [11], bladder [12], cervix [13] and colon [14]. As was mentioned above PDT therapy is characterised by its great selectivity towards normal cells. This fact is explained by the differences in the expression of the genes that are involved in the heme biosynthesis in cancer and normal cells [15]. An examination of the literature concerning this issue led to the conclusion

**Abbreviations:** 5-ALA, 5-aminolevulinic acid; 5-ALA-PDT, 5-aminolevulinic acid-based photodynamic therapy; CAT, catalase; CP94, 1,2-diethyl-3-hydroxypyridin-4-one; CPOX, coproporphyrinogen-III oxidase; DFO, deferoxamine; EDTA, ethylenediaminetetraacetic acid; FBCH, ferrochelatase; GAPDH, glyceraldehyde 3-phosphate dehydrogenase; HMBS, hydroxymethylbilane synthase; HO-1, heme oxygenase-1; MnSOD, superoxide dismutase; PDT, photodynamic therapy; PpIX, protoporphyrin IX; PPOX, Protoporphyrinogen oxidase; ROS, reactive oxygen species; TSC, thiosemicarbazone; TSC-PDT, thiosemicarbazone-based photodynamic therapy; UROD, Uroporphyrinogen III decarboxylase; UROS, Uroporphyrinogen III synthase

\* Corresponding author.

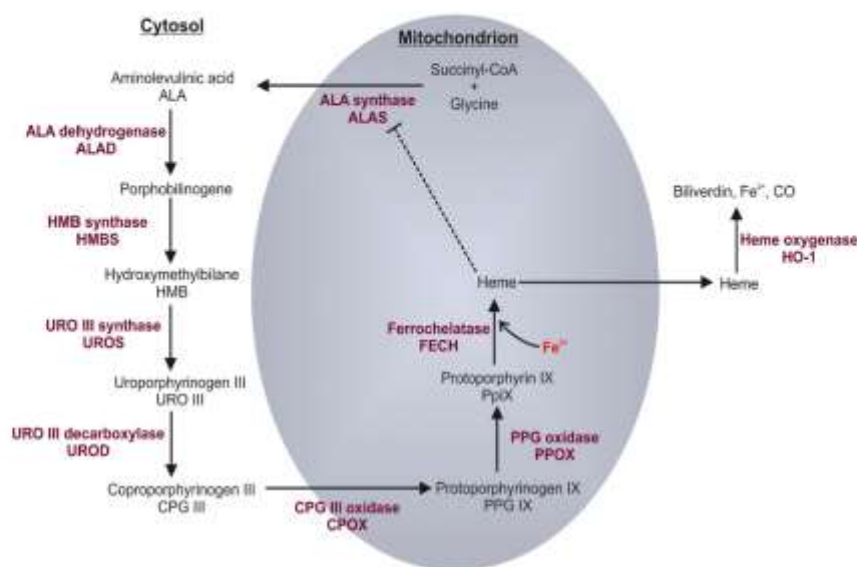
E-mail address: [anna.mrozek-wilczkiewicz@us.edu.pl](mailto:anna.mrozek-wilczkiewicz@us.edu.pl) (A. Mrozek-Wilczkiewicz).

<https://doi.org/10.1016/j.jphotobiol.2019.111585>

Received 5 February 2019; Received in revised form 30 July 2019; Accepted 7 August 2019

Available online 08 August 2019

1011-1344/ © 2019 Elsevier B.V. All rights reserved.



Scheme 1. Heme biosynthesis pathway.

that there are many conflicting results depending on the type of cell line. Beginning from ALAS, which is the first enzyme in the heme pathway, we found an example of it reducing the mRNA level in colon cancer [16], but elevating it in the case of lung cancer [17]. When examining the subsequent enzymes, we had a similar nuanced observation. Krieg et al. indicated that the HMBS (an alternative name for PBGD) differentiated its concentration in the different cell lines that were tested [18]. We also found examples of a discernible discrepancy in the UROD gene expression in a human breast [19], head and neck cancer [20] compared to normal tissues. The conversion of PpIX into heme occurs through the participation of the ferrochelatase (FECH) enzyme. It seems obvious that its activity is crucial with regard to the PpIX accumulation and therefore its therapeutic use. In contrast to the other enzymes in this case, we observed a decreasing trend in the FECH activity or in its gene expression [18,21]. The degradation of the heme is preceded by heme oxygenase (HO-1), which plays an important role in maintaining the correct cell homeostasis and decreasing oxidative stress [22]. The expression of HO-1 is often elevated in colon [23], lung [24], breast [25] and glioma [26] cancer cells compared to normal tissues.

Despite the differences that were observed in the gene expression and enzyme activity of the heme biosynthesis and the degradation that occurred in different types of tumors, we also observed alternations after the administration of 5-ALA. Several examples are described for ALAD and HMBS in [27]. In the case of FECH, its low activity consequently results in an increased PpIX level in colon [16], glioma [28] and breast [29] cancer cells. The complexity of the processes that are involved in heme biosynthesis and 5-ALA-PpIX production prompted us to explore this issue more deeply.

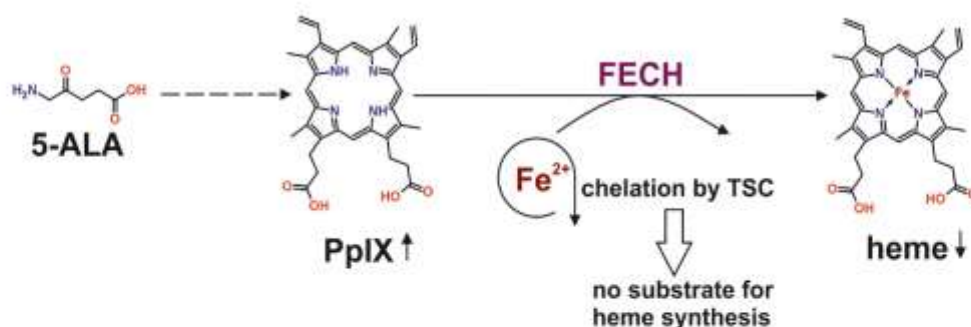
As was mentioned above, the external administration of 5-ALA resulted in an increased production of PpIX and this in turn affected its phototoxic effect in PDT. However, the concentration of the photosensitizer is frequently insufficient to achieve a good therapeutic effect. The use of iron-chelating compounds in 5-ALA-PDT significantly increased the concentration of PpIX [30]. An explanation of this phenomenon could be the fact that chelators affect the PpIX concentration by blocking the transformation of PpIX into heme. This step is catalysed by ferrochelatase and the use of iron chelators inhibits

the production of heme by binding the iron ions. The result of such a strategy is an accumulation of PpIX in the cell/tissue (Scheme 2). One

of the chelators that were used was EDTA (ethylenediaminetetraacetic acid), which has been studied on the leukemia cell line [31], or DFO (deferoxamine), which was tested, *inter alia*, on glioma cells [32]. However, possibly due to the high molecular weight and low lipophilicity of DFO, these results were not repeated on an *in vivo* model [33]. Pye et al. presented a new generation of chelator with boosting photodynamic effect properties – CP94 (1,2-diethyl-3-hydroxypyridin-4-one) [34]. This specific iron chelator is a small molecule that has an optimal lipophilicity and increased the PpIX concentration on *in vitro* [35,36] and *in vivo* [37,38] models.

A new generation of metal chelators that may have potential applications in PDT therapy are thiosemicarbazones (TSC). This group of compounds is known for its excellent anticancer, antiviral, antifungal and antibacterial properties [39–42]. We have presented new applications for several of these TSC derivatives in PDT therapy [43,44]. However, our strategy was different from the commonly known approach of using chelators for blocking the last step of the heme synthesis (Scheme 2). The inhibition of the heme production increases the concentration of the PpIX. Increasing the therapeutic effect by increasing the drug concentration is a standard method of treatment. The combination therapy is a modern way, in which two or more drugs are applied simultaneously. This approach not only increases the effectiveness of the therapy, but also significantly reduces the dose of the drug, thus reducing its toxicity. As mentioned above photosensitizer activated by light generates ROS leading to an oxidative stress [45]. One novelty was the use of TSC derivatives in a synergic approach by boosting the generation of ROS. An increased cytotoxicity was observed after combination of TSC compounds that had a high level of anticancer activity with PpIX [43]. These good antiproliferative properties of TSC are associated with ROS generation [46,47]. To confirm our hypothesis about shared disturbing of redox homeostasis through ROS production, we performed experiments involving genes expression of superoxide dismutase (MnSOD) and catalase (CAT) as well lipid peroxidation. A detailed analysis of the antioxidant systems confirmed, that after incubation with the combination of TSC and exogenous photosensitizer oxidative stress was notably increased [44]. For non-toxic TSC derivatives, we did not observe an enhanced therapeutic effect or increased level of PpIX. This was in contrast to the commonly known fact that iron chelators affect heme synthesis by chelating iron, thereby





**Scheme 2.** The influence of an iron chelator on increasing the production of PpIX in the heme biosynthesis pathway.

increasing the concentration of PpIX. These observations prompted us to explore this subject more deeply by expanding the research to a broader group of TSC derivatives, cell lines and examining the heme biosynthesis genes. In this study, several novel, non-toxic TSC derivatives were investigated for their effect on the accumulation of PpIX after the exogenous application of 5-ALA on a few cell lines of different origins, including brain (U251 and Hs683), lung (A549), breast (MCF-7), colorectal (HCT 116) cancer cells and normal human dermal fibroblasts (NHDF). We also investigated the gene expression of the heme biosynthesis pathway as well as the heme oxygenase gene after treatment with 5-ALA and 5-ALA combined with a compound 2, which increased the PpIX concentration in three of six examined cell lines. Obtained results confirmed some of the commonly known facts, like downregulation of *FECH* and *HO-1* genes in MCF-7 and HCT 116 cell lines. However, some results were surprising and in this work upregulation of aforementioned genes in Hs638 cell line is presented for the first time. Additionally this opposite results were both obtained for derivative 2.

## 2. Materials and Methods

### 2.1. General Procedure for the Synthesis of the Thiosemicarbazides (as Previously Described in [47])

The mixtures of (1,1'-thiocarbonyl) bis-1H-imidazole (5 mM) and suitable derivative of piperazine, glycine, morpholine or thiomorpholine (5 mM) in methylene chloride (25 mL) were stirred for 24 h at room temperature. The solutions were extracted three times with distilled water and organic phases were dried over MgSO<sub>4</sub> and evaporated. The obtained thioketones were refluxed for 2 h with hydrazine hydrate (5 mM). Final thiosemicarbazides were crystallized from dry methanol.

#### 4-(4-nitrophenyl)piperazine-1-carbothiohydrazide (substrate for 1)

Yellow powder; yield 87%; mp: 207–208 °C; <sup>1</sup>H NMR (400 MHz, *d*<sub>6</sub>-DMSO, ppm): δ 3.57 (s, 4H, CH<sub>2</sub>), 3.91 (s, 4H, CH<sub>2</sub>), 4.97 (s, 2H, NH<sub>2</sub>), 6.97 (d, 2H, *J* = 9.3 Hz), 8.08 (m, 2H, Ar-H), 9.15 (s, 1H, NH). <sup>13</sup>C NMR (101 MHz, *d*<sub>6</sub>-DMSO, ppm): δ 45.7; 46.7; 112.5; 126.2; 137.3; 154.6; 182.8.

#### Thiomorpholine-4-carbothiohydrazide (substrate for 2)

White crystal powder; yield 89%; mp: 160–161 °C; <sup>1</sup>H NMR (400 MHz, *d*<sub>6</sub>-DMSO, ppm): δ 4.03 (m, 8H, CH<sub>2</sub>), 4.83 (s, 2H, NH<sub>2</sub>), 9.19 (s, 1H, NH). <sup>13</sup>C NMR (101 MHz, *d*<sub>6</sub>-DMSO, ppm): δ 26.4; 50.8; 182.3.

#### [(hydrazinylcarbonothioyl)amino]acetic acid (substrate for 3)

White powder; yield 85%; mp: 242–243 °C; <sup>1</sup>H NMR (500 MHz, *d*<sub>6</sub>-DMSO, ppm): δ 4.09 (s, 2H, CH<sub>2</sub>), 5.27 (s, 2H, NH<sub>2</sub>), 7.14 (s, 1H, NH), 8.01 (s, 1H, OH), 12.69 (s, 1H, NH). <sup>13</sup>C NMR (126 MHz, *d*<sub>6</sub>-DMSO, ppm): δ 44.8; 164.9; 166.6.

#### 4-(diphenylmethyl)piperazine-1-carbothiohydrazide (substrate for 4)

Light pink powder; yield 79%; mp: 158–159 °C; <sup>1</sup>H NMR (400 MHz, *d*<sub>6</sub>-DMSO, ppm): δ 2.29 (t, 4H, *J* = 4.9 Hz), 3.72 (t, 4H; *J* = 4.9 Hz), 4.33 (s, 1H, CH); 4.75 (s, 2H, NH<sub>2</sub>), 7.20 (t, 2H, *J* = 7.3 Hz), 7.31 (t, 4H, *J* = 7.5 Hz), 7.43 (d, 4H, *J* = 7.1 Hz), 9.04 (s, 1H, NH). <sup>13</sup>C NMR (126 MHz, *d*<sub>6</sub>-DMSO, ppm): δ 19.0; 50.7; 51.9; 56.5; 128.2; 129.1; 137.1; 142.8; 147.8; 181.1.

#### Morpholine-4-carbothiohydrazide (substrate for 5)

White crystal powder; yield 88%; mp: 170–171 °C; <sup>1</sup>H NMR (400 MHz, *d*<sub>6</sub>-DMSO, ppm): δ 3.59 (m, 4H, CH<sub>2</sub>), 3.68 (m, 4H, CH<sub>2</sub>), 4.79 (s, 2H, NH<sub>2</sub>), 9.12 (s, 1H, NH). <sup>13</sup>C NMR (101 MHz, *d*<sub>6</sub>-DMSO, ppm): δ 48.2; 66.2; 183.4.

#### 4-cyclohexylpiperazine-1-carbothiohydrazide (substrate for 6)

White powder; yield 59%; mp: 178–179 °C; <sup>1</sup>H NMR (400 MHz, *d*<sub>6</sub>-DMSO, ppm): δ 1.19 (m, 6H, CH<sub>2</sub>), 1.73 (d, 4H; *J* = 8.4 Hz), 3.36 (m, 4H, CH<sub>2</sub>), 3.66 (s, 4H, CH<sub>2</sub>), 4.73 (s, 2H, NH<sub>2</sub>), 9.02 (s, 1H, NH). <sup>13</sup>C NMR (126 MHz, *d*<sub>6</sub>-DMSO, ppm): δ 25.7; 26.3; 28.7; 48.3; 48.7; 62.9; 182.9.

#### 4-(4-cyanophenyl)piperazine-1-carbothiohydrazide (substrate for 7)

Light orange powder; yield 70%; mp: 169–170 °C; <sup>1</sup>H NMR (400 MHz, *d*<sub>6</sub>-DMSO, ppm): δ 3.42 (m, 4H, CH<sub>2</sub>), 3.89 (m, 4H, CH<sub>2</sub>), 4.78 (s, 2H, NH<sub>2</sub>), 7.05 (s, 2H, Ar-H), 7.60 (m, 2H, Ar-H), 9.15 (s, 1H, NH). <sup>13</sup>C NMR (101 MHz, *d*<sub>6</sub>-DMSO, ppm): δ 45.9; 48.9; 98.6; 114.3; 120.5; 133.8; 153.0; 182.9.

#### 4-(4-methoxyphenyl)piperazine-1-carbothiohydrazide (substrate for 8)

White powder; yield 81%; mp: 194–195 °C; <sup>1</sup>H NMR (400 MHz, *d*<sub>6</sub>-DMSO, ppm): δ 3.00 (s, 3H, CH<sub>3</sub>), 3.86 (m, 4H, CH<sub>2</sub>), 4.11 (m, 4H, CH<sub>2</sub>), 4.77 (s, 2H, NH<sub>2</sub>), 6.83 (d, 2H, *J* = 9.0 Hz), 6.90 (m, 2H, Ar-H), 9.17 (s, 1H, NH). <sup>13</sup>C NMR (101 MHz, *d*<sub>6</sub>-DMSO, ppm): δ 19.0; 49.9; 56.5; 114.8; 118.2; 145.4; 153.7; 183.1.

4-(3,4-dichlorophenyl)piperazine-1-carbothiohydrazide (substrate for 9)

White powder; yield 68%; mp: 186–187 °C;  $^1\text{H}$  NMR (400 MHz,  $d_6$ -DMSO, ppm):  $\delta$  3.08 (s, 4H,  $\text{CH}_2$ ), 3.86 (m, 4H,  $\text{CH}_2$ ), 4.76 (s, 2H,  $\text{NH}_2$ ), 6.93 (m, 1H, Ar-H), 7.14 (s, 1H, Ar-H), 7.40 (d, 1H,  $J = 9.0$  Hz), 9.19 (s, 1H, NH).  $^{13}\text{C}$  NMR (101 MHz,  $d_6$ -DMSO, ppm):  $\delta$  47.1; 47.3; 115.6; 116.6; 120.1; 130.9; 132.0; 150.7; 183.0.

2.2. General Procedure for the Synthesis of the Thiosemicarbazones (as Previously Described in [47])

To a mixture of thiosemicarbazides (0.5 mM) and appropriate derivative of 2-quinolinecarboxaldehyde, benzaldehyde or 2-pyridinecarboxaldehyde (0.5 mM) in ethanol (5 mL) were added two drops of glacial acetic acid as a catalyst. The glass tubes were sealed and placed into a microwave reactor at 83 °C for 20 min (the reactor power doesn't exceed 50 W). Final products were crystallized from dry methanol.

$N'$ -(8-hydroxyquinolin-2-yl)methylidene]-4-(4-nitrophenyl)piperazine-1-carbothiohydrazide (1) (as previously described in [47])

Yellow powder; yield 78%; mp: 204–205 °C;  $^1\text{H}$  NMR (400 MHz,  $d_6$ -DMSO, ppm):  $\delta$  3.74 (m, 4H,  $\text{CH}_2$ ), 4.14 (m, 4H,  $\text{CH}_2$ ), 6.98 (t, 2H,  $J = 10.2$  Hz), 7.12 (m, 2H, Ar-H), 7.42 (m, 2H, Ar-H), 8.08 (m, 2H, Ar-H), 8.29 (d, 1H,  $J = 8.7$  Hz), 8.38 (s, 1H, CH), 9.84 (s, 1H, OH), 11.74 (s, 1H, NH).  $^{13}\text{C}$  NMR (126 MHz,  $d_6$ -DMSO, ppm):  $\delta$  45.8; 49.6; 112.4; 112.6; 117.8; 118.6; 126.3; 128.6; 129.2; 137.0; 137.3; 138.6; 144.3; 152.2; 153.6; 154.5; 181.0. HRMS (ESI):  $m/z$  calculated for  $\text{C}_{21}\text{H}_{22}\text{N}_6\text{O}_5\text{S}$ : 437.1396, found: 437.1387 [M + H] $^+$ .

$N'$ -(quinolin-2-yl)methylidene]-4-thiomorpholine-1-carbothiohydrazide (2) (as previously described in [47])

Yellow powder; yield 34%; mp: 198–199 °C;  $^1\text{H}$  NMR (400 MHz,  $d_6$ -DMSO, ppm):  $\delta$  2.71 (s, 4H,  $\text{CH}_2$ ), 3.71 (s, 4H,  $\text{CH}_2$ ), 7.61 (d, 1H,  $J = 6.5$  Hz), 7.76 (d, 1H,  $J = 7.1$  Hz), 7.97 (dd, 3H,  $J = 15.1$ ; 7.9 Hz), 8.14 (s, 1H, Ar-H), 8.35 (s, 1H, CH), 12.32 (s, 1H, NH).  $^{13}\text{C}$  NMR (126 MHz,  $d_6$ -DMSO, ppm):  $\delta$  25.7; 52.1; 117.4; 127.3; 128.0; 128.4; 129.2; 130.5; 136.9; 142.4; 147.9; 154.2; 163.2. HRMS (ESI):  $m/z$  calculated for  $\text{C}_{15}\text{H}_{17}\text{N}_5\text{S}_2$ : 317.0895, found: 317.0969 [M + H] $^+$ .

4-(4-methoxyphenyl)- $N'$ -(4-nitrophenyl)methylidene]piperazine-1-carbothiohydrazide (3)

Orange powder; yield 85%; mp: 180–181 °C;  $^1\text{H}$  NMR (400 MHz,  $d_6$ -DMSO, ppm):  $\delta$  3.17 (m, 4H,  $\text{CH}_2$ ), 3.70 (s, 3H,  $\text{CH}_3$ ), 4.08 (s, 4H,  $\text{CH}_2$ ), 6.85 (d, 2H,  $J = 9.0$  Hz), 6.96 (d, 2H,  $J = 8.9$  Hz), 7.90 (d, 2H,  $J = 8.7$  Hz), 8.27 (s, 2H, Ar-H), 8.29 (s, 1H, CH), 11.55 (s, 1H, NH).  $^{13}\text{C}$  NMR (101 MHz,  $d_6$ -DMSO, ppm):  $\delta$  50.2; 50.4; 55.7; 114.8; 118.2; 124.6; 128.1; 141.3; 141.7; 145.3; 148.0; 153.7; 181.2. HRMS (ESI):  $m/z$  calculated for  $\text{C}_{19}\text{H}_{22}\text{N}_6\text{O}_5\text{S}$ : 400.1443, found: 400.1448 [M + H] $^+$ .

4-(3,4-dichlorophenyl)- $N'$ -(4-hydroxy-3-methoxyphenyl)methylidene]piperazine-1-carbothiohydrazide (4)

Yellow powder; yield 64%; mp: 164–165 °C;  $^1\text{H}$  NMR (400 MHz,  $d_6$ -DMSO, ppm):  $\delta$  3.36 (s, 4H,  $\text{CH}_2$ ), 3.82 (s, 3H,  $\text{CH}_3$ ), 4.04 (s, 4H,  $\text{CH}_2$ ), 6.82 (d, 1H,  $J = 7.8$  Hz), 6.96 (d, 1H,  $J = 8.8$  Hz), 7.03 (d, 1H,  $J = 7.9$  Hz), 7.16 (s, 1H, Ar-H), 7.22 (s, 1H, Ar-H), 7.43 (d, 1H,  $J = 8.8$  Hz), 8.03 (s, 1H, CH), 9.51 (s, 1H, OH), 11.15 (s, 1H, NH).  $^{13}\text{C}$  NMR (126 MHz,  $d_6$ -DMSO, ppm):  $\delta$  47.7; 50.0; 55.9; 109.3; 115.5; 116.0; 116.5; 120.1; 122.0; 126.1; 131.0; 132.0; 144.6; 148.5; 149.2; 150.7; 180.8. HRMS (ESI):  $m/z$  calculated for  $\text{C}_{23}\text{H}_{22}\text{Cl}_2\text{N}_6\text{O}_5\text{S}$ : 439.07662, found: 439.0775 [M + H] $^+$ .

4-(4-cyanophenyl)- $N'$ -[(2-nitrophenyl)methylidene]piperazine-1-carbothiohydrazide (5)

Light orange powder; yield 63%; mp: 199–200 °C;  $^1\text{H}$  NMR (400 MHz,  $d_6$ -DMSO, ppm):  $\delta$  3.53 (s, 4H,  $\text{CH}_2$ ), 4.09 (s, 4H,  $\text{CH}_2$ ), 7.01 (d, 2H,  $J = 8.7$  Hz), 7.63 (m, 3H, Ar-H), 7.79 (t, 1H,  $J = 7.6$  Hz), 8.06 (t, 2H,  $J = 7.8$  Hz), 8.61 (s, 1H, CH), 11.61 (s, 1H, NH).  $^{13}\text{C}$  NMR (101 MHz,  $d_6$ -DMSO, ppm):  $\delta$  46.0; 49.3; 98.6; 114.0; 120.5; 125.1; 128.3; 129.2; 130.7; 133.8; 134.1; 139.7; 148.5; 152.9; 181.1. HRMS (ESI):  $m/z$  calculated for  $\text{C}_{19}\text{H}_{19}\text{N}_6\text{O}_2\text{S}$ : 395.1290, found: 395.1296 [M + H] $^+$ .

4-cyclohexyl- $N'$ -[(2-nitrophenyl)methylidene]piperazine-1-carbothiohydrazide (6)

Yellow powder; yield 59%; mp: 173–174 °C;  $^1\text{H}$  NMR (400 MHz,  $d_6$ -DMSO, ppm):  $\delta$  1.21 (m, 5H,  $\text{CH}_2$ ), 1.76 (m, 5H,  $\text{CH}_2$ ), 2.57 (s, 4H,  $\text{CH}_2$ ), 3.89 (s, 4H,  $\text{CH}_2$ ), 7.64 (m, 1H, Ar-H), 7.79 (t, 1H,  $J = 7.7$  Hz), 8.04 (m, 2H, Ar-H), 8.57 (s, 1H, CH), 11.45 (s, 1H, NH).  $^{13}\text{C}$  NMR (126 MHz,  $d_6$ -DMSO, ppm):  $\delta$  25.7; 26.3; 28.8; 31.2; 48.9; 50.7; 125.1; 128.2; 129.2; 130.6; 134.1; 139.3; 148.4; 180.1. HRMS (ESI):  $m/z$  calculated for  $\text{C}_{18}\text{H}_{22}\text{N}_6\text{O}_2\text{S}$ : 376.1807, found: 376.1799 [M + H] $^+$ .

4-(diphenylmethyl)- $N'$ -[(2-nitrophenyl)methylidene]piperazine-1-carbothiohydrazide (7)

Dark orange powder; yield 75%; mp: 111–112 °C;  $^1\text{H}$  NMR (400 MHz,  $d_6$ -DMSO, ppm):  $\delta$  1.06 (t, 1H,  $J = 7.0$  Hz), 2.40 (s, 4H,  $\text{CH}_2$ ), 3.94 (s, 4H,  $\text{CH}_2$ ), 7.32 (t, 5H,  $J = 7.5$  Hz), 7.46 (m, 5H, Ar-H), 7.62 (t, 1H,  $J = 8.5$  Hz), 7.76 (t, 1H,  $J = 7.7$  Hz), 8.02 (m, 2H, Ar-H), 8.53 (s, 1H, CH), 11.45 (s, 1H, NH).  $^{13}\text{C}$  NMR (126 MHz,  $d_6$ -DMSO, ppm):  $\delta$  49.1; 50.3; 51.8; 74.9; 125.1; 127.5; 128.1; 128.3; 129.0; 130.7; 134.0; 139.3; 142.8; 148.4; 181.0. HRMS (ESI):  $m/z$  calculated for  $\text{C}_{28}\text{H}_{22}\text{N}_6\text{O}_2\text{S}$ : 459.1729, found: 460.1818 [M + H] $^+$ .

$N'$ -[(2-nitrophenyl)methylidene]morpholine-1-carbothiohydrazide (8)

Yellow powder; yield 46%; mp: 192–193 °C;  $^1\text{H}$  NMR (400 MHz,  $d_6$ -DMSO, ppm):  $\delta$  3.67 (m, 4H,  $\text{CH}_2$ ), 3.92 (m, 4H,  $\text{CH}_2$ ), 7.64 (m, 1H, Ar-H), 7.79 (t, 1H,  $J = 7.8$  Hz), 8.04 (m, 2H, Ar-H), 8.58 (s, 1H, CH), 11.53 (s, 1H, NH).  $^{13}\text{C}$  NMR (101 MHz,  $d_6$ -DMSO, ppm):  $\delta$  50.8; 66.4; 125.1; 128.3; 129.1; 130.8; 134.1; 139.7; 148.5; 181.4. HRMS (ESI):  $m/z$  calculated for  $\text{C}_{12}\text{H}_{12}\text{N}_6\text{O}_2\text{S}$ : 295.0865, found: 295.0876 [M + H] $^+$ .

[[[(2-(3-aminopyridin-2-yl)methylidene)hydrazinyl]carbonothioyl]amino]acetic acid (9) (as previously described in [48])

Yellow powder; yield 51%; mp: 245–246 °C;  $^1\text{H}$  NMR (500 MHz,  $d_6$ -DMSO, ppm):  $\delta$  1.24 (s, 2H,  $\text{CH}_2$ ), 6.83 (s, 2H, Ar-H), 7.07 (m, 2H,  $\text{NH}_2$ ), 7.83 (dd, 1H,  $J = 4.2$ ; 1.5 Hz), 8.01 (s, 1H, NH), 8.48 (s, 1H, CH), 10.92 (s, 1H, OH), 12.96 (s, 1H, NH).  $^{13}\text{C}$  NMR (126 MHz,  $d_6$ -DMSO, ppm):  $\delta$  44.8; 123.9; 124.2; 125.6; 131.4; 135.6; 144.2; 150.2; 166.6. HRMS (ESI):  $m/z$  calculated for  $\text{C}_9\text{H}_{12}\text{N}_6\text{O}_2\text{S}$ : 254.0712, found: 254.0712 [M + H] $^+$ .

2.3. Cell Culture

The HCT 116, MCF-7 and A549 cell lines were purchased from ATCC. The Hs683 and U251 cell lines were kindly provided by Dr. Gabriela Kramer-Marek from Institute of Cancer Research (London, UK). The normal human dermal fibroblasts (NHDF) were obtained from PromoCell. All of these adherent cell lines were cultured in Dulbecco's Modified Eagle's Medium (DMEM) containing 12% (for the cancer cell lines) or 15% (for the NHDF) of fetal bovine serum (Sigma) and a blend of standard antibiotics - 1% v/v of penicillin and streptomycin (Gibco) in 75 cm<sup>2</sup> flasks (Nunc). For all of the cancer cell lines heat-inactivated FBS was used. The cells were grown under standard conditions at 37 °C



in a humidified atmosphere at 5% CO<sub>2</sub>. All of the cell lines were subjected to routine mycoplasma testing using the PCR technique with specific *Mycoplasma* primers in order to ensure that there was no contamination.

#### 2.4. Cytotoxicity Studies

The cells were seeded in 96-well plates (Nunc) at a density of 5,000 cells/well (for the cancer cell lines) and 4,000 cells/well (for the NHDF) and incubated at 37 °C for 24 h. The next day, freshly prepared solutions of the tested thiosemicarbazone derivatives at varying concentrations (0.5–25 μM) were added to the plate and incubated for the next 72 h, after which, the medium containing the tested compounds was replaced with 100 μL DMEM without phenol red, to which 20 μL of CellTiter 96<sup>®</sup>AQ<sub>One</sub> Solution-MTS (Promega) was added and incubated for 1 h at 37 °C. The absorbance of the samples was measured at 490 nm using a multi-plate reader (Synergy 4, Bio Tek). The obtained results are expressed as a percentage of the untreated control. The inhibitory concentration (IC<sub>50</sub>) values were determined using GraphPad Prism 7. Each individual compound was tested in triplicate in a single experiment with each experiment being repeated three or four times.

#### 2.5. PpIX Fluorescence Intensity in Cells After Incubation With TSC

All of the cell lines were seeded into 96-well plates (Black Clear Bottom, Corning) at a density of 15,000 cells/well for 24 h before the experiment. On the next day the medium was removed and the cells were washed with PBS (Sigma-Aldrich). Then, freshly prepared solutions of 5-ALA (1 mM) and TSC (25 μM) in DMEM without phenol red and FBS were applied to black plate. The cells were incubated in the dark at 37 °C for 24 h. After the incubation period, the fluorescence of the PpIX was measured using a multi-plate reader (Synergy 4, Bio Tek) at a 407 nm excitation and a 638 nm emission wavelength. Untreated cells were used as controls to compare the autofluorescence from the cells with the fluorescence of the PpIX. The experiment were performed in reduced light conditions (to 50 lx) in order to avoid photobleaching the PpIX. The experiments were repeated four times on different days. The PpIX concentration was calculated as a percentage of the control and the results are expressed as the relative fluorescence units (RFU).

#### 2.6. Changes in the Gene Expression After Incubation With TSC

All of the cell lines were seeded in 3 cm Petri dishes (Nunc) at a minimum density of 500,000 cells and incubated at 37 °C for 24 h. The next day, the medium was removed and solutions of 5-ALA (1 mM) and TSC (25 μM) were added. After 24 h, the total RNA was isolated from the cells using TRIzol Reagent (Ambion) according to the manufacturer's instructions. cDNA synthesis was performed with 5 μg of the total RNA using a GoScript<sup>™</sup> Reverse Transcriptase kit (Promega) and Oligo(dT)<sub>20</sub> Primers (Sigma). Quantitative Real-Time PCR was performed using a CFX96 Touch<sup>™</sup> Real-Time PCR Detection System (Biorad) at a reaction volume of 20 μL. The PCR reaction mix included SYBR Green Mix (Biorad) reagent, the appropriate primer pair mixture (0.5 μM each) for each target and 1 μL cDNA. All of the primer pair sequences were designed in Primer 3 and were purchased from Sigma-Aldrich (Table S1). The experiment was set up under the following conditions: initial denaturation at 95 °C for 20 s; followed by 40 denaturation cycles at 95 °C, 10 s; annealing (primer-specific temperature for 20 s) and extension at 72 °C for 30 s. The data from PCR experiments were analysed by comparing of the expression of the target genes to a reference housekeeping gene such as *GAPDH*. For this purpose, the of 2<sup>-ΔΔCT</sup> (Livak and Schmittgen) method were used. The experiments was performed at least five times.

#### 2.7. Statistical Analysis

The results are expressed as the mean ± standard deviation (SD) from at least three independent experiments. Statistical differences in the PpIX accumulation assays were calculated using the one-way ANOVA with a Bonferroni post-hoc test. In turn, statistical analysis for gene expression was performed by two-way ANOVA with a Bonferroni post-hoc test. A *p*-value of 0.05 or less was considered to be statistically significant. GraphPad Prism v.7.0 software (GraphPad Software, USA) was used for the analysis.

### 3. Results and Discussion

#### 3.1. Chemistry

The synthesis of TSC was performed according to the known procedures [46–48]. The structures of the investigated compounds are shown in Fig. 1.

The final TSC compounds were synthesised using a Schiff-based condensation of the appropriate thiosemicarbazide with 2-quinoline-carboxaldehyde (1–2), benzaldehydes (3–8) or 2-pyridinecarboxaldehyde (9).

#### 3.2. Cytotoxicity Studies

In order to characterise the antiproliferative activity of all of the newly synthesised compounds 1–9, we selected five cell lines that represent different human tumors and one normal fibroblast line. As is presented in Table 1, all of the compounds that were synthesised showed either no activity or a weak activity against all of the cancer cell lines and normal fibroblasts. Our previous experience proved that toxic compounds are not suitable for increasing the accumulation of PpIX in cells. After incubation with the cytotoxic compounds no fluorescence (or a very weak fluorescence) was observed due to cell damage. Non-toxic TSC derivatives can affect the accumulation of PpIX without such effects. In the light of these observations, the presented cytotoxic results are satisfactory and enabled us to conduct subsequent experiments.

#### 3.3. PpIX Fluorescence Intensity in Cells After Incubation With a TSC Derivatives

In order to verify the hypothesis concerning the effect of TSC derivatives on the accumulation of PpIX in a cell, the following experiments were performed. We measured the fluorescence of PpIX in a cell after incubation with TSC, 5-ALA or a combination of TSC and 5-ALA. The results are presented in Fig. 2.

The first observation was that the tested cell lines varied the intensity of the PpIX fluorescence after incubation with 5-ALA. Fluorescence level of PpIX was within the range from 718 for MCF-7 to 44 for HCT 116. This was in accordance with the results in [49,50]. The highest PpIX level was observed in the MCF-7 and A549 cell lines (Fig. 2A, B). The intensity decreased for Hs683 and U251 (Fig. 2C, D) and the weakest signal was observed for HCT 116 and NHDF (Fig. 2E, F). It was interesting that for HCT 116 we detected the lowest PpIX signal. The main goal of these experiments was to select the compound that could affect the accumulation of PpIX. Regardless of the PpIX level in each of the following cell lines, compound 2 in combination with 5-ALA caused a significant increase in the PpIX fluorescence in the HCT 116 (4.2 times), Hs638 (1.7 times) and MCF-7 (1.6 times) cells compared to the 5-ALA alone. In general for HCT 116 cell line we detected the largest PpIX increase triggered by the combination of TSC and 5-ALA compared to the 5-ALA alone. For compound 2 and 1 we detected around fourfold enhancement of the PpIX fluorescence signal in comparison to 5-ALA alone (5-ALA alone RFU = 44, 5-ALA + 2 RFU = 183, 5-ALA + 1 RFU = 174), and for compound 4 threefold increase (5-ALA + 4 RFU = 148). This is quite interesting considering the fact that

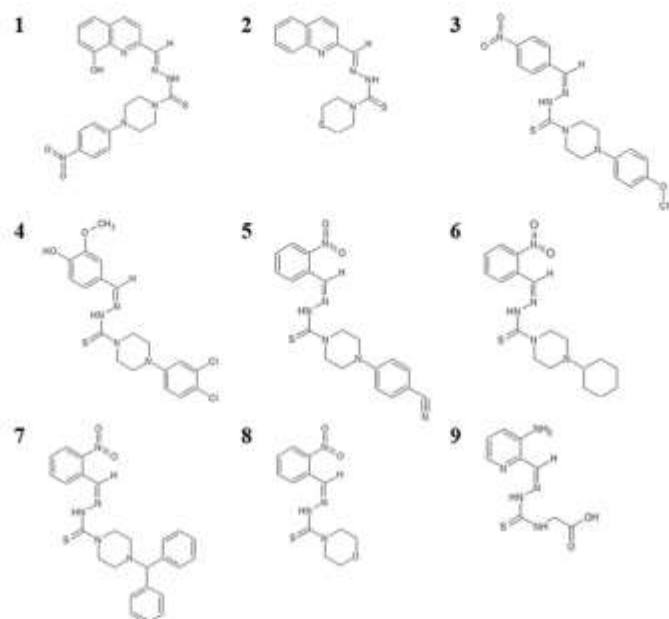


Fig. 1. Structures of the thiosemicarbazones.

**Table 1**  
Antiproliferative activity of the studied compounds expressed as  $IC_{50}$  values.

Comp.	Activity - $IC_{50}$ [ $\mu$ M]					
	HCT 116	MCF-7	U251	Hs683	A549	NIH3T1
1.	11.69 $\pm$ 1.77	20.93 $\pm$ 0.37	2.78 $\pm$ 0.25	16.11 $\pm$ 1.23	> 25	> 25
2.	18.31 $\pm$ 0.92	> 25	> 25	> 25	> 25	13.06 $\pm$ 1.90
3.	> 25	> 25	> 25	> 25	> 25	> 25
4.	12.10 $\pm$ 1.03	11.30 $\pm$ 1.59	7.55 $\pm$ 0.28	> 25	18.02 $\pm$ 0.77	> 25
5.	> 25	> 25	> 25	> 25	> 25	> 25
6.	11.78 $\pm$ 3.28	> 25	> 25	> 25	> 25	> 25
7.	> 25	> 25	> 25	> 25	> 25	> 25
8.	> 25	> 25	> 25	> 25	> 25	> 25
9.	> 25	> 25	> 25	> 25	> 25	> 25

these cell lines had the weakest PpIX fluorescence level. We believe that this may be connected with the fact that in the case of the cell lines that produced a large amount of PpIX itself, the addition of TSC was not as effective as in the case of the lines in which the production of PpIX was inefficient. A similar conclusion was reached in the work [51]. Another cell line, for which we observed an increase in PpIX fluorescence was A549. In this cell line compound 1 with combination with 5-ALA caused 2.4 times enhancement of the PpIX fluorescence. For compound 4 we observed similar result (2.2 times). An increased level of PpIX (1.6 times) was also registered for compound 8, but only in the Hs683 cell line. These results showed that there is not one universal chelator, but that there is a specificity towards the cell type. However, the results indicated that even for cell lines that had an extensive PpIX synthesis, the selected compounds (2 for MCF-7 and 1, 4 for A549) were successful in increasing the concentration of PpIX.

### 3.4. Changes in the Gene Expression After Incubation With a TSC Derivatives

In the following step, we tried to explain the results that were observed. In our opinion, we should look for an answer based on the expression of the genes and the level of proteins that participated in the PpIX biosynthesis pathway. As is shown in the Scheme 1, there are several enzymes that are crucial in heme biosynthesis. We hypothesized that a tested compound could affect these molecules and thereby have an impact on the accumulation of PpIX. In order to verify this hypothesis, we determined the basal level of the seven genes that are involved in heme production and degradation (*HO-1*) in the six tested cell lines (Fig. 3). The expression of all of the tested genes was compared to their expression in the normal fibroblasts.

For the HCT 116 cells, we observed high levels in the expression of



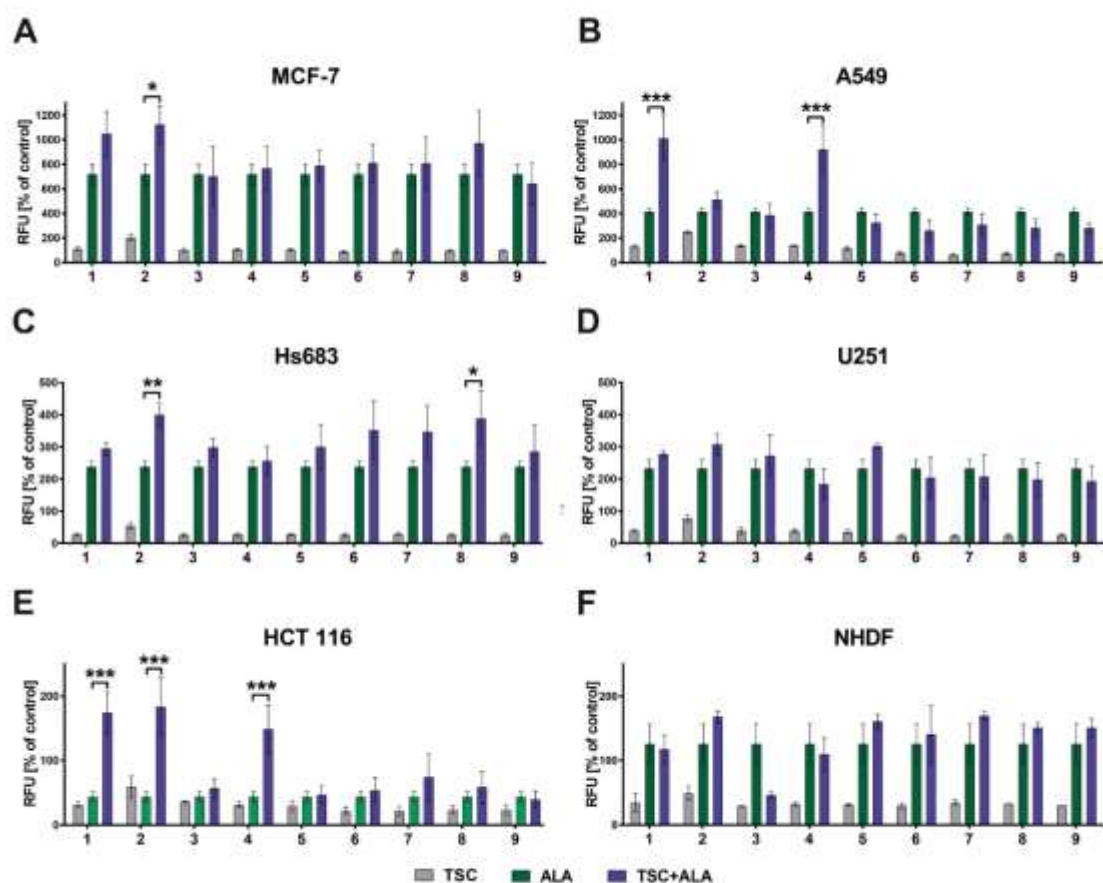


Fig. 2. The fluorescence intensity of the PpIX after incubation with the tested TSC derivatives (25  $\mu$ M), 5-aminolevulinic acid (1 mM) and a combination of TSC with 5-aminolevulinic acid (25  $\mu$ M and 1 mM final concentration, respectively) following cancer cell lines - MCF-7 (A), A549 (B), Hs683 (C), U251 (D), HCT 116 (E) and normal cells NHDF (F). The results are shown as the mean  $\pm$  SD of four independent measurements, each performed in triplicate. The data were analysed using the one-way ANOVA with Bonferroni's post-hoc test: \* $p$  < .05, \*\* $p$  < .01, \*\*\* $p$  < .001.

*HMBS*, *CPOX* and *FECH*. In MCF-7, we detected an increased level of *HMBS* and *FECH*, and also *ALAD*. In general, the level of *HMBS* was elevated in all of the tested cell lines compared to NHDF. This is consistent with the results [18,21,52]. Surprisingly, the level of *HO-1* was low for all of the tested cell lines, which is different than the usual increase in many type of cancers [23–25,53]. Based on the previous results concerning the accumulation of PpIX, we selected compound 2 for further research because of its effect on increasing the concentration of PpIX in the MCF-7, Hs683 and HCT 116 cell lines, but not in A549. For this reason, we decided to trace the impact of this derivative on the genes expression involved in PpIX biosynthesis and degradation in these four cell lines in detail. The data that is presented in Fig. 4 proves that combination of TSC with 5-ALA had an effect on *HO-1* for all of the tested cell lines except A549.

The presented results illustrate the tested genes alterations after incubation with 5-ALA-TSC combination in comparison to the results that were obtained for 5-ALA alone. The statistical analysis of the results for 5-ALA alone compared to the untreated cells is presented in

Fig. S1 in the S1. In general, after incubation with 5-ALA, we observed a significant increase in the *HO-1* level for all of the tested cell lines except A549. Additionally, an increased *FECH* level was detected for MCF-7 and HCT 116 (Fig. S1A, D). We did not observe any changes in the other genes expression as has been suggested in many publications. However, the combination of 5-ALA and compound 2 yielded the following results. In the case of MCF-7 (Fig. 4A) and HCT 116 (Fig. 4D), the level of *HO-1* was decreased after incubation with compound 2, while for Hs683 (Fig. 4C), there was an increase. In general, there was no effect on the tested genes in A549 (Fig. 4B). We also recorded the changes of *FECH* expression in Hs683 and HCT 116 after incubation with combination of 5-ALA and compound 2. For Hs683, there was an increased level of *FECH*, while we observed the opposite situation for HCT 116, namely, the level of *FECH* decreased. A possible explanation of the observed *FECH* and *HO-1* decrease is the fact, that according to Scheme 2,  $Fe^{2+}$  chelation caused a decrease in the activity of *FECH* due to a lack of substrates for heme synthesis. In turn, the lack of the product (heme) caused a decrease in the activity of *HO-1*. A reversed

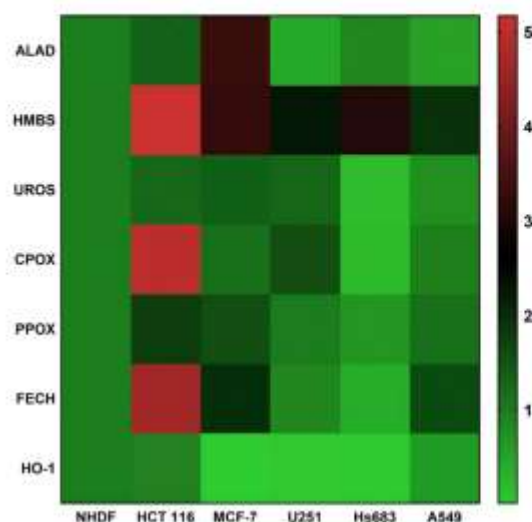


Fig. 3. Heat map displaying the differential expression patterns of the genes that are involved in heme biosynthesis and degradation (y axis) in the cancer cells and normal cells (x axis).

situation was detected for Hs683. The increase in the expression of the *FECH* and *HO-1* genes is a new fact that has yet not been published in the literature. This phenomenon is surprising and has prompted us to perform further studies.

#### 4. Conclusion

The overall goal of these studies was to evaluate the effect of the thiosemicarbazone derivatives on the accumulation of PpIX in cancer cells. It is commonly known that iron chelators can increase the concentration of PpIX after the application of 5-ALA thereby increasing therapeutic efficacy. This is connected with the chelation of the iron ions and the blocking of the last step of heme biosynthesis. However, there are still many gaps in understanding this process. Therefore, in these studies, we explored new TSC derivatives and selected the most promising candidate from among them. We researched several cancer cell lines that had different origins and genetic landscapes. This studies proved that the tested cell lines differed in the production of PpIX after 5-ALA administration. In this work, we present seven TSC derivatives, of which compound 2 turned out to be the most interesting. The most surprising fact was its effect on expression of genes that are involved in the heme biosynthesis and degradation. On the one hand, we observed the typical behaviour for the MCF-7 and HCT 116 cell lines, namely, the downregulation of the *FECH* and *HO-1* genes. However, after incubation with combination of 5-ALA and compound 2, the Hs683 cell line showed a completely opposite trend. This phenomenon is novel and is undoubtedly worth performing an in-depth analysis. To the best of our knowledge, this result is the first to demonstrate the effect of iron

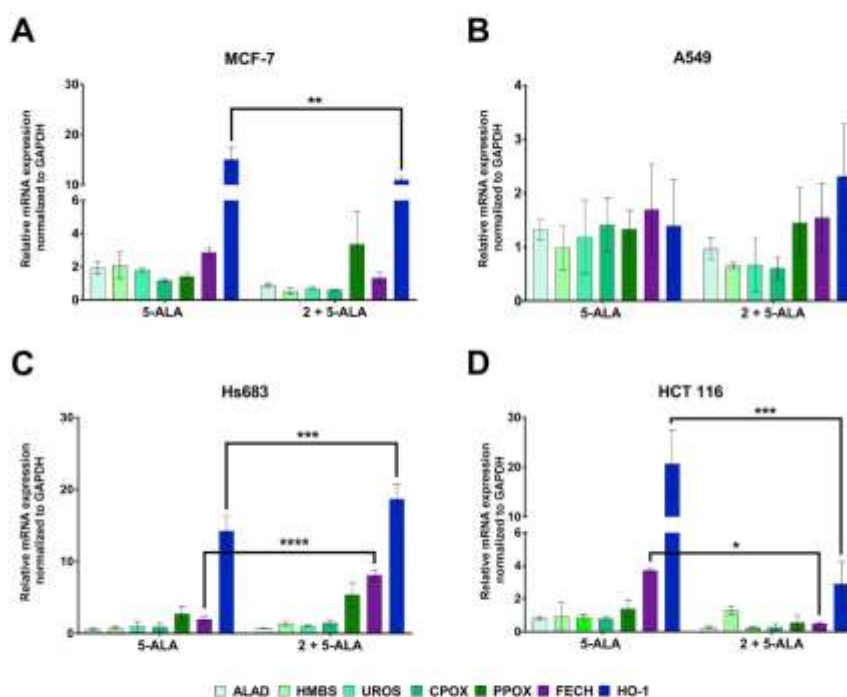


Fig. 4. The effect of 5-ALA (1 mM) alone and in combination with thiosemicarbazone 2 (25  $\mu$ M) on the heme genes expression in the MCF-7 (A), A549 (B), Hs683 (C) and HCT 116 (D) cancer cells. Data were normalised to the control (untreated cells, one value on the y axis). The results are shown as the mean  $\pm$  SD of three independent measurements, each in quadruplicate. The data were analysed using the two-way ANOVA test: \* $p$  < .05, \*\* $p$  < .01, \*\*\* $p$  < .001 compared to the 5-ALA-treated cells.



chelators on the gene expression involved in the heme biosynthesis pathway and degradation. Our further research plans will focus studies that involve the transporters on the cell surface, which are responsive to the PpIX efflux from the cells.

#### Authors' Contributions

AMW created the research hypothesis, designed the biological tests and wrote the manuscript; RG performed and analysed the biological tests; KM and RG performed the PCR experiment; MR carried out the chemical syntheses, which was supervised by JP.

#### Declaration of Competing Interest

None.

#### Acknowledgements

The financial support of the National Science Centre grants 2014/13/D/NZ7/00322 (AMW) and 2016/23/N/NZ7/00351 (KM) was greatly appreciated.

#### Appendix A. Supplementary Data

Supplementary data to this article can be found online at <https://doi.org/10.1016/j.jphotobiol.2019.111585>.

#### References

- [1] M. Boyd, R.S. Spermbg, R.J. Mair, Radiation and gene therapy: rays of hope for the new millennium? *Curr. Gene Ther.* 3 (2003) 319–339 <http://www.ncbi.nlm.nih.gov/pubmed/12871020>.
- [2] L.A. Wheeler, A.G. Manzanares, S.D. Bell, R. Cavaliere, J.M. McGregor, J.C. Greer, H.B. Newton, S.S. Le, B. Badie, J. Portnow, B.S. Teh, T.W. Trask, D.S. Baskin, P.Z. New, L.K. Aguilera, E. Aguilar-Cordova, E.A. Chioica, Phase II multicenter study of gene-mediated cytotoxic immunotherapy as adjuvant to surgical resection for newly diagnosed malignant glioma, *Neuro-Oncology* 18 (2016) 1137–1145, <https://doi.org/10.1093/neuonc/nov002>.
- [3] D. Heitel, M.A. Rahmonov, A. AKhida, M. Nasr, M. Elserafy, S.F. El-Khamisy, Recent advances in stem cells therapy: a focus on cancer, Parkinson's and Alzheimer's, *J. Genet. Eng. Biotechnol.* 16 (2018) 427–432, <https://doi.org/10.1016/j.jgeb.2018.09.002>.
- [4] J. Xu, J. Gao, Q. Wei, Combination of photodynamic therapy with radiotherapy for cancer treatment, *J. Nanshan* 2016 (2016) 1–7, <https://doi.org/10.1155/2016/8507924>.
- [5] S. Kwiatkowski, B. Knap, D. Przystupski, J. Szczko, E. Kędzierska, K. Knap-Czap, J. Kotlińska, O. Mielch, K. Kotowski, J. Kulaćka, Photodynamic therapy – mechanisms, photosensitizers and combinations, *Biomed. Pharmacother.* 106 (2018) 1098–1107, <https://doi.org/10.1016/j.biopha.2018.07.040>.
- [6] M.Q. Almerie, G. Gossedge, K.E. Wright, D.G. Jayne, Photodynamic diagnosis for detection of peritoneal carcinomatosis, *J. Surg. Res.* 195 (2015) 175–187, <https://doi.org/10.1016/j.jss.2015.01.009>.
- [7] T.J. Dougherty, C.J. Gomez, B.W. Henderson, G. Jori, D. Kessel, M. Korbelik, J. Moan, Q. Peng, Photodynamic therapy, *JNCI J. Natl. Cancer Inst.* 90 (1998) 889–905, <https://doi.org/10.1093/jnci/90.12.889>.
- [8] B. Nokes, M. Apel, C. Jones, G. Brown, J.E. Lang, Aminolevulinic acid (ALA): photodynamic detection and potential therapeutic applications, *J. Surg. Res.* 181 (2013) 262–271, <https://doi.org/10.1016/j.jss.2013.02.002>.
- [9] Q. Peng, Y. Warloe, K. Berg, J. Moan, M. Kongsbak, K.E. Gierczyk, J.M. Nesland, 5-Aminolevulinic acid based photodynamic therapy. Clinical research and future challenges, *Cancer* 79 (1997) 2282–2308, [https://doi.org/10.1002/\(sici\)1097-0142\(19970615\)79:12<2282::aid-cncr79>3.0.co;2-6](https://doi.org/10.1002/(sici)1097-0142(19970615)79:12<2282::aid-cncr79>3.0.co;2-6).
- [10] W. Stummer, U. Pichlmeier, T. Meinel, O.D. Westler, F. Zornella, H.-J. Reulen, Fluorescence-guided surgery with 5-aminolevulinic acid for resection of malignant glioma: a randomised controlled multicentre phase III trial, *Lancet Oncol.* 7 (2006) 392–401, [https://doi.org/10.1016/S1473-3045\(06\)70665-9](https://doi.org/10.1016/S1473-3045(06)70665-9).
- [11] G. Smith, B. Clothier, J.E. Francis, H. Gibbs, F. De Matteis, R.C. Hider, Protoporphyrin IX induced by the orally active iron chelator 1,2-dithy-3-hydroxypropyl-4-one in C57BL/10ScSn mice, *Blood* 89 (1997) 1645–1651 <http://www.ncbi.nlm.nih.gov/pubmed/9028337>.
- [12] D. Jochims, F. Wäjes, S. Wagner, B. Zeylenkovic, J. van Moerselaar, M.-O. Grimm, R. Mascher, G. Popken, F. König, R. Eitel, K.-H. Kuehn, Improved detection and treatment of bladder cancer using hexaminolevulinic imaging: a prospective, phase III multicenter study, *J. Urol.* 174 (2005) 862–866 discussion 866 <https://doi.org/10.1097/01.ju.0000169257.19841.2a>.
- [13] A.A. Barnett, J.C. Haller, F. Catndorf, G. Lane, S.B. Brown, D.J.H. Roberts, A randomised, double-blind, placebo-controlled trial of photodynamic therapy using

- 5-aminolevulinic acid for the treatment of cervical intraepithelial neoplasia, *Int. J. Cancer* 103 (2003) 829–832, <https://doi.org/10.1002/ijc.10888>.
- [14] S. Kato, J. Kawamura, K. Kawada, S. Hasegawa, Y. Sakai, Fluorescence diagnosis of metastatic lymph nodes using 5-aminolevulinic acid (5-ALA) in a mouse model of colon cancer, *J. Surg. Res.* 176 (2012) 430–436, <https://doi.org/10.1016/j.jss.2011.10.031>.
- [15] A. Gupta, R.J. Munger, Elevated copper and oxidative stress in cancer cells as a target for cancer treatment, *Cancer Treat. Rev.* 35 (2009) 32–46, <https://doi.org/10.1016/j.ctrv.2008.07.004>.
- [16] W. Kemmer, K. Wan, S. Rattinger, B. Ebert, R. Madenwald, U. Klamm, K.T. Moens, Silencing of human ferrochelatase causes abundant protoporphyrin IX accumulation in colon cancer, *FASEB J.* 22 (2007) 500–509, <https://doi.org/10.1096/fj.07.8888com>.
- [17] J. Hoods, D. Collins, M.M. Aher, A. Shih, T.M. Cao, L.A. Sullivan, R. Bekken, L. Zhang, Enhanced heme function and mitochondrial respiration promote the progression of lung cancer cells, *PLoS One* 8 (2013), <https://doi.org/10.1371/journal.pone.0063402>.
- [18] R.C. Kriegl, H. Messmann, J. Rauch, S. Seeger, R. Knaechel, Metabolic characterization of tumor cell-specific protoporphyrin IX accumulation after exposure to 5-aminolevulinic acid in human colonic cells, *Photochem. Photobiol.* 76 (2007) 518–525, [https://doi.org/10.1562/0021-0655\(2007\)076\[0518MOCOTCS\]2.0.CO;2](https://doi.org/10.1562/0021-0655(2007)076[0518MOCOTCS]2.0.CO;2).
- [19] N.M. Navone, C.F. Polo, A.L. Frisanti, N.E. Andrade, A. Alcira, M. del C. Baillo, Heme biosynthesis in human breast cancer—“in vitro” studies and some heme enzymic activity levels, *Int. J. BioChem* 22 (1990) 1407–1411, [https://doi.org/10.1016/0020-711X\(90\)90230-7](https://doi.org/10.1016/0020-711X(90)90230-7).
- [20] E. Ito, S. Yae, E.H. Moriyama, A.B. Hui, I. Kim, W. Shi, N.M. Alajez, N. Bhogal, G. Li, A. Dutt, A.D. Schimmer, B.C. Wilson, P.P. Liu, D. Durocher, B.G. Neel, B. O'Sullivan, B. Cummings, R. Britzow, J. Wana, F.F. Liu, Uroporphyrinogen decarboxylase is a radiosensitizing target for head and neck cancer, *Sci. Transl. Med.* 3 (2011) 67m7, <https://doi.org/10.1126/scitranslmed.3001922>.
- [21] R.C. Kriegl, S. Fickweiler, D.S. Wolfels, R. Knaechel, Cell-type specific protoporphyrin IX metabolism in human bladder cancer in vitro, *Photochem. Photobiol.* 72 (2000) 226, [https://doi.org/10.1562/0021-0655\(2000\)072<0226:CTSPHM>2.0.CO;2](https://doi.org/10.1562/0021-0655(2000)072<0226:CTSPHM>2.0.CO;2).
- [22] R. Gazzelino, V. Jeney, M.P. Soares, Mechanisms of cell protection by heme oxygenase-1, *Annu. Rev. Pharmacol. Toxicol.* 50 (2010) 323–354, <https://doi.org/10.1146/annurev.pharmtox.010909.105600>.
- [23] H. Yin, J. Fang, L. Liao, H. Maeda, Q. Su, Upregulation of heme oxygenase-1 in colorectal cancer patients with increased circulation carbon monoxide levels, potentially affects chemotherapeutic sensitivity, *BMC Cancer* 14 (2014) 436, <https://doi.org/10.1186/1471-2407-14-436>.
- [24] M.S. Degese, J.E. Mendizabal, N.A. Gaudini, J.S. Gutkind, A. Molino, S.M. Hewitt, A.C. Curcio, O.A. Coso, M.M. Facchinetti, Expression of heme oxygenase-1 in non-small cell lung cancer (NSCLC) and its correlation with clinical data, *Lung Cancer* 77 (2012) 168–175, <https://doi.org/10.1016/j.lungcan.2012.02.036>.
- [25] S.J. Noh, J.S. Bae, U. Janyalindae, H.S. Paek, K.S. Kwon, S.H. Jung, H.J. Youn, H. Lee, B.-H. Park, M.J. Chung, W.S. Moon, M.J. Kang, K.Y. Jung, Expression of nerve growth factor and heme oxygenase-1 predicts poor survival of breast carcinoma patients, *BMC Cancer* 13 (2013) 516, <https://doi.org/10.1186/1471-2407-13-516>.
- [26] N.A. Gaudini, M.E. Fermento, D.G. Salomón, D.J. Obiol, N.C. Andrés, J.C. Zenkisen, J. Azevalo, J. Blasco, A. López Romero, M.M. Facchinetti, A.C. Curcio, Heme oxygenase-1 expression in human gliomas and its correlation with poor prognosis in patients with astrocytoma, *Tumor Biol.* 35 (2014) 2803–2815, <https://doi.org/10.1007/s12277-013-1373-z>.
- [27] S.I. Gibson, D.J. Capriks, J.J. Havens, M.L. Nguyen, R. Hill, A regulatory role for porphobilinogen desaminase (PBGD) in delta-aminolevulinic acid (delta-ALA)-induced photosensitization? *Br. J. Cancer* 77 (1998) 235–242 <http://www.ncbi.nlm.nih.gov/pubmed/9460994>.
- [28] L. Teng, M. Nakada, S.-G. Zhao, Y. Endo, N. Furuyama, E. Naraba, I.V. Pyko, Y. Hayashi, J.-I. Hamada, Silencing of ferrochelatase enhances 5-aminolevulinic acid-based fluorescence and photodynamic therapy efficacy, *Br. J. Cancer* 104 (2011) 798–807, <https://doi.org/10.1038/bjc.2011.12>.
- [29] X. Yang, W. Li, P. Palanichandran, K.A. Myers, C. Wang, B. Chen, Effects of silencing heme biosynthesis enzymes on 5-aminolevulinic acid-mediated protoporphyrin IX fluorescence and photodynamic therapy, *Photochem. Photobiol.* 91 (2015) 923–930, <https://doi.org/10.1111/php.12454>.
- [30] A. Juzeniene, Q. Peng, J. Moan, Topical applications of iron chelates in photosensitization, *Photochem. Photobiol. Sci.* 6 (2007) 1268–1274, <https://doi.org/10.1039/b670546j>.
- [31] J. Hanania, Z. Malik, The effect of EDTA and serum on endogenous porphyrin accumulation and photodynamic sensitization of human K562 leukemic cells, *Cancer Lett.* 65 (1992) 127–131, [https://doi.org/10.1016/0304-3835\(92\)90156-P](https://doi.org/10.1016/0304-3835(92)90156-P).
- [32] P.A. Vakkés, K. Sankoe, J.A. O'Hara, D.W. Roberts, K.D. Paulsen, B.W. Pogge, Deferoxamine iron chelation increases 8-aminolevulinic acid induced protoporphyrin IX in xenograft glioma model, *Photochem. Photobiol.* 86 (2010) 471–475, <https://doi.org/10.1111/j.1751-1097.2009.00664.x>.
- [33] K. Choudry, R.C.C. Brooke, W. Fumar, L.E. Rhodes, The effect of an iron chelating agent on protoporphyrin IX levels and phototoxicity in topical 5-aminolevulinic acid photodynamic therapy, *Br. J. Dermatol.* 149 (2003) 124–130, <https://doi.org/10.1046/j.1365-2133.2003.05351.x>.
- [34] A. Pae, A. Cusnov, Direct comparison of delta-aminolevulinic acid and methyl-aminolevulinic acid-derived protoporphyrin IX accumulations potentiated by desferrioxamine or the novel hydroxypyridinone iron chelator CP94 in cultured human cells, *Photochem. Photobiol.* 83 (2007) 766–773, <https://doi.org/10.1562/0096-0530-07-04-966>.

- [35] E. Blake, A. Cumow, The hydroxypyridinone iron chelator CP94 can enhance FpIX induced PDT of cultured human glioma cells, *Photochem. Photobiol.* 86 (2010) 1154–1160, <https://doi.org/10.1111/j.1751-1097.2010.00770.x>.
- [36] E. Blake, J. Allen, A. Cumow, An in vitro comparison of the effects of the iron-chelating agents, CP94 and dexrazoxane, on protoporphyrin IX accumulation for photodynamic therapy and/or fluorescence guided resection, *Photochem. Photobiol.* 87 (2011) 1419–1426, <https://doi.org/10.1111/j.1751-1097.2011.00985.x>.
- [37] S.-C. Chang, G. Buonaccorsi, A.J. MacRobert, S.G. Bown, 5-aminolevulinic acid (ALA)-induced protoporphyrin IX fluorescence and photodynamic effects in the rat bladder: an in vivo study comparing oral and intravesical ALA administration, *Lasers Surg. Med.* 30 (1997) 254–264, [https://doi.org/10.1002/lsm.1096-9101\(1997\)30:3<254::AID-LSM4>3.0.CO;2-P](https://doi.org/10.1002/lsm.1096-9101(1997)30:3<254::AID-LSM4>3.0.CO;2-P).
- [38] A. Cumow, B. McIlroy, M. Postle-Hacon, J. Porter, A. MacRobert, S. Bown, Enhancement of 5-aminolevulinic acid-induced photodynamic therapy in normal rat colon using hydroxypyridinone iron-chelating agents, *Br. J. Cancer* 78 (1998) 1278–1282, <https://doi.org/10.1038/bjc.1998.671>.
- [39] M. Serda, D.S. Kallinowski, N. Raske, E. Potůčková, A. Mrozek-Wilczkiewicz, R. Musiol, J.G. Malecki, M. Szejewicz, A. Ratuszna, A. Muchowicz, J. Golab, T. Simůnek, D.R. Richardson, J. Polanski, Exploring the anti-cancer activity of novel thiosemicarbazones generated through the combination of retro-fragments: dissection of critical structure-activity relationships, *PLoS One* 9 (2014) e110291, <https://doi.org/10.1371/journal.pone.0110291>.
- [40] R.J. Gibson, M.L. Causton, V.L. Mather, J.R. Cubitts, A.G. Moghissi, A. Scornik, Antiviral activity against the hepatitis C virus (HCV) of 1-indenone thiosemicarbazones and their inclusion complexes with hydroxypropyl- $\beta$ -cyclodextrin, *Eur. J. Pharm. Sci.* 47 (2012) 596–603, <https://doi.org/10.1016/j.ejps.2012.07.019>.
- [41] L.N. de Araújo Neto, M. do Carmo Alves de Lima, J.F. de Oliveira, E.R. de Souza, M.D.S. Buonafina, M.N. Vitor Araújo, F.A. Brayner, L.C. Alves, R.P. Neves, F.J.B. Mendonça-Junior, Synthesis, cytotoxicity and antimutagenic activity of 5-nitrothiophene-thiosemicarbazones derivatives, *Chem. Biol. Interact.* 272 (2017) 172–181, <https://doi.org/10.1016/j.cbi.2017.05.005>.
- [42] N.D. Thanh, N.T.K. Giang, T.H. Quyen, D.T. Huang, V.N. Toan, Synthesis and evaluation of in vivo antioxidants, in vitro antibacterial, MRSA and antifungal activity of novel substituted isatin N-(2,3,4,6-tetra-O-acetyl- $\beta$ -D-glucopyranosyl)thiosemicarbazones, *Eur. J. Med. Chem.* 123 (2016) 532–543, <https://doi.org/10.1016/j.ejmech.2016.07.074>.
- [43] A. Mrozek-Wilczkiewicz, M. Serda, R. Musiol, G. Malecki, A. Saenko, A. Muchowicz, J. Golab, A. Ratuszna, J. Polanski, Iron chelators in photodynamic therapy revisited: synergistic effect by novel highly active thiosemicarbazones, *ACS Med. Chem. Lett.* 5 (2014) 336–339, <https://doi.org/10.1021/ml40422a>.
- [44] A. Mrozek-Wilczkiewicz, E. Malarz, M. Ram-Baron, M. Serda, D. Bauer, F.-P. Montforts, A. Ratuszna, T. Burley, J. Polanski, R. Musiol, Iron chelators and exogenic photosensitizers: synergy through oxidative stress gene expression, *J. Cancer* 8 (2017) 1979–1987, <https://doi.org/10.7150/jca.17959>.
- [45] B.V. Chernyak, D.S. Izyumov, K.G. Lyumzaev, A.A. Pushkovskaya, O.Y. Pletushkina, Y.N. Antonenko, D.V. Sakharov, K.W.A. Wirtz, V.P. Skulachev, Production of reactive oxygen species in mitochondria of HeLa cells under oxidative stress, *Biochim. Biophys. Acta Bioenerg.* 1757 (2006) 525–534, <https://doi.org/10.1016/j.bbabi.2006.02.019>.
- [46] K. Malarz, A. Mrozek-Wilczkiewicz, M. Serda, M. Rejmund, J. Polanski, R. Musiol, The role of oxidative stress in activity of anticancer thiosemicarbazones, *Oncotarget* 9 (2018) 17689–17710, <https://doi.org/10.18632/oncotarget.24844>.
- [47] A. Mrozek-Wilczkiewicz, K. Malarz, M. Rejmund, J. Polanski, R. Musiol, Anticancer activity of the thiosemicarbazones that are based on di-2-pyridine ketone and quinoline moiety, *Eur. J. Med. Chem.* 171 (2019) 180–194, <https://doi.org/10.1016/j.ejmech.2019.03.037>.
- [48] M. Rejmund, A. Mrozek-Wilczkiewicz, K. Malarz, M. Pyrkosz-Bulska, K. Gójski, M. Szejewicz, R. Musiol, J. Polanski, Piperazine fragment improves anticancer activity of Triapine, *PLoS One* 13 (2018) e0188767, <https://doi.org/10.1371/journal.pone.0188767>.
- [49] S.L. Gibbs, B. Chen, J.A. O'Hara, P.J. Hoopes, T. Hasan, B.W. Pogue, Protoporphyrin IX level correlates with number of mitochondria, but increase in production correlates with tumor cell size, *Photochem. Photobiol.* 82 (2006) 1334, <https://doi.org/10.1562/2006-03-11-RA-843>.
- [50] S.L. Gibbs, M.L. Nguyen, J.J. Harens, A. Barbarin, R. Hill, Relationship of 5-aminolevulinic acid-induced protoporphyrin IX levels to mitochondrial content in neoplastic cells in vitro, *Biochem. Biophys. Res. Commun.* 265 (1999) 315–323, <https://doi.org/10.1006/bbrc.1999.1679>.
- [51] S.L. Gibbs, B. Chen, J.A. O'Hara, P.J. Hoopes, T. Hasan, B.W. Pogue, Protoporphyrin IX level correlates with number of mitochondria, but increase in production correlates with tumor cell size, *Photochem. Photobiol.* 82 (2006) 1334, <https://doi.org/10.1562/2006-03-11-RA-843>.
- [52] P. Hilmén, F. de Rooij, M. van Velthuisen, A. Edzhoyan, R. van Hillegenberg, H. Tilanus, J. Wilson, P. Siersema, Biochemical basis of 5-aminolevulinic acid-induced protoporphyrin IX accumulation: a study in patients with (pre)malignant lesions of the oesophagus, *Br. J. Cancer* 78 (1998) 679–682, <https://doi.org/10.1038/bjc.1998.559>.
- [53] Y. Yin, Q. Liu, B. Wang, G. Chen, L. Xu, H. Zhou, Expression and function of heme oxygenase-1 in human gastric cancer, *Exp. Biol. Med.* 237 (2012) 362–371, <https://doi.org/10.1258/ebm.2011.011193>.

## Impact of thiosemicarbazones on the accumulation of PpIX and the expression of the associated genes

Robert Gawecki<sup>1</sup>, Katarzyna Malarz<sup>1</sup>, Marta Rejmund<sup>2</sup>, Jaroslaw Polanski<sup>2</sup>, Anna Mrozek-Wilczkiewicz<sup>1\*</sup>

<sup>1</sup>A. Chelkowski Institute of Physics and Silesian Center for Education and Interdisciplinary Research, University of Silesia, Chorzow, Poland

<sup>2</sup>Institute of Chemistry, University of Silesia, Katowice, Poland

\*anna.mrozek-wilczkiewicz@us.edu.pl

**Keywords:** Thiosemicarbazones, accumulation of PpIX, 5-aminolevulinic acid, heme pathway gene expression, metal chelators

**Table S1.** Primers used to amplify gene fragments for qRT-PCR analysis.

GENE	Forward (F); Reverse (R)	Primers sequence
<i>ALAD</i>	F	5'-GCAGAGTTCCCAAGGACGAG-3'
	R	5'-GGACACAGGCAGACATCACA-3'
<i>HMBS</i>	F	5'-ACCCACACACAGCCTACTTT-3'
	R	5'-TGAACTCCAGATGCGGGAAC-3'
<i>UROS</i>	F	5'-AATTAAGTTTGCAGCCATCGG-3'
	R	5'-CTCAGGTGCTTCCACTCAGG-3'
<i>CPOX</i>	F	5'-TGGCCTCTTCACTCCAGGAT-3'
	R	5'-ACTAAGGCACGGGTAAGTGC-3'
<i>PPOX</i>	F	5'-CTGGGAGGTTCCCTGGTTACA-3'
	R	5'-CAACCTGTGAGCAGTCAGGA-3'
<i>FECH</i>	F	5'-GATGAATTGTCCCCAACAC-3'
	R	5'-GCTTCCGTCCCACTTGATTA-3'
<i>HO-1</i>	F	5'-CATCCCCTACACACCAGCCA-3'
	R	5'-ATGTTGGGGAAGGTGAAGAAGG-3'
<i>GAPDH</i>	F	5'-GAGTCAACGGATTTGGTCGTA-3'
	R	5'GCCCACTTGATTTGGAG-3'

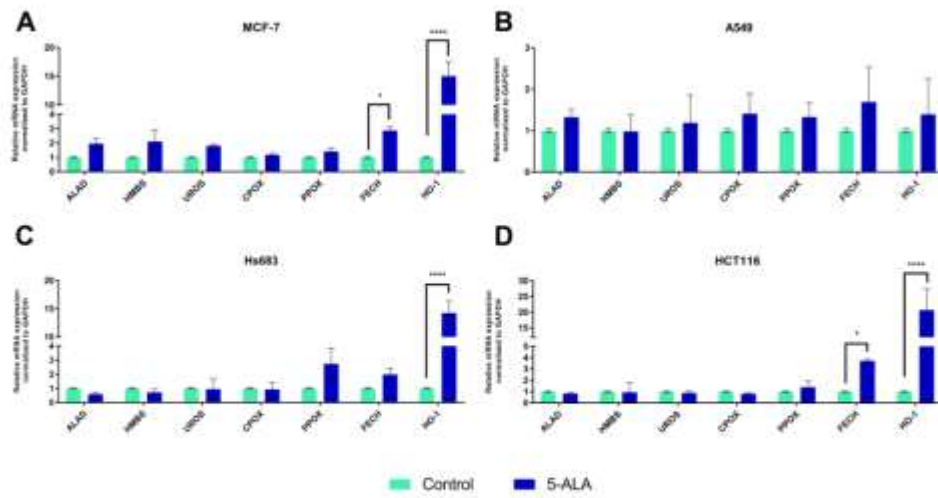


**Figure S1.** The effect of 5-ALA (1mM) alone on the expression of the genes involved in the heme biosynthesis and degradation in the MCF-7 (A), A549 (B), Hs683 (C), HCT 116 (D) cancer cells. Results are shown as the mean  $\pm$  SD of three independent measurements, each in quadruplicate. Data were analyzed using the two-way ANOVA test: \*p < 0.05, \*\*p < 0.01, \*\*\*p < 0.001 compared to the control (untreated cells).

#### **4.2. [P2]. A Thiosemicarbazone Derivative as a Booster in Photodynamic Therapy—A Way to Improve the Therapeutic Effect**

**Autorzy:** Gawecki R., Polanski J., Mrozek-Wilczkiewicz A

**Referencja:** International Journal of Molecular Sciences, 2022, 23(23), 15370

**Numer DOI:** 10.3390/ijms232315370

**Impact Factor czasopisma:** 5,6 (2022)

**Liczba punktów MNiSW czasopisma:** 140 (2022)

Mój udział w pracy polegał na wykonaniu, planowaniu i analizie wszystkich badań biologicznych, pisaniu i redagowaniu manuskryptu.





Article

# A Thiosemicarbazone Derivative as a Booster in Photodynamic Therapy—A Way to Improve the Therapeutic Effect

Robert Gawecki <sup>1</sup>, Jaroslaw Polanski <sup>2</sup> and Anna Mrozek-Wilczkiewicz <sup>1,4</sup>

<sup>1</sup> A. Chełkowski Institute of Physics, University of Silesia in Katowice, 75 Pułku Piechoty 1a, 41-500 Chorzów, Poland

<sup>2</sup> Institute of Chemistry, University of Silesia, 40-007 Katowice, Poland

\* Correspondence: anna.mrozek-wilczkiewicz@us.edu.pl

**Abstract:** Photodynamic therapy is one of the most patient friendly and promising anticancer therapies. The active ingredient is irradiated protoporphyrin IX, which is produced in the body that transfers energy to the oxygen-triggering phototoxic reaction. This effect could be enhanced by using iron chelators, which inhibit the final step of heme biosynthesis, thereby increasing the protoporphyrin IX concentration. In the presented work, we studied thiosemicarbazone derivative, which is a universal enhancer of the phototoxic effect. We examined several genes that are involved in the transport of the heme substrates and heme itself. The results indicate that despite an elevated level of ABCG2, which is responsible for the PpIX efflux, its concentration in a cell is sufficient to trigger a photodynamic reaction. This effect was not observed for 5-ALA alone. The analyzed cell lines differed in the scale of the effect and a correlation with the PpIX accumulation was observed. Additionally, an increased activation of the iron transporter MFNR1 was also detected, which indicated that the regulation of iron transport is essential in PDT.

**Keywords:** thiosemicarbazone; iron chelators; ABC transporters; photodynamic therapy; phototoxic effect; heme



Citation: Gawecki, R.; Polanski, J.; Mrozek-Wilczkiewicz, A. A Thiosemicarbazone Derivative as a Booster in Photodynamic Therapy—A Way to Improve the Therapeutic Effect. *Int. J. Mol. Sci.* **2022**, *23*, 15370. <https://doi.org/10.3390/ijms232315370>

Academic Editor: Michael R. Hamblin

Received: 22 November 2022

Accepted: 4 December 2022

Published: 6 December 2022

**Publisher's Note:** MDPI stays neutral with regard to jurisdictional claims in published maps and institutional affiliations.



Copyright: © 2022 by the authors. Licensee MDPI, Basel, Switzerland. This article is an open access article distributed under the terms and conditions of the Creative Commons Attribution (CC BY) license (<https://creativecommons.org/licenses/by/4.0/>).

## 1. Introduction

Generally, cancer therapies have the most side effects of any of the therapies that are used today. These side effects often create serious psychological and medical problems. Therefore, therapies that are safe for the patient should be developed. One such therapy is photodynamic therapy (PDT), which is one of the few anticancer methods that is relatively safe for the patient [1–3]. The reason for its low toxicity is its selectivity, which is associated with its local effect. In PDT, the photosensitizer, which can be called the active ingredient, accumulates in the tumor and triggers a toxic effect there [4]. The specificity of the therapy itself lies in the interaction of oxygen, the light of the appropriate wavelength and the photosensitizer [5]. An additional advantage of ALA-PDT therapy is that the photosensitizer is produced in the body. As a prodrug, 5-ALA is a substrate for the production of protoporphyrin IX (PpIX), which absorbs the energy from light and then transmits that energy to oxygen, which in turn leads to the production of free radicals and singlet oxygen [6]. The natural synthesis of PpIX has its limitations, however, because PpIX is not the final product. PpIX is the penultimate link in the production of heme, which plays a huge role in our body, but is not a photosensitizer. Therefore, in ALA-PDT therapy, iron chelators that inhibit the incorporation of iron ions into the porphyrin ring are often used [7]. Despite extensive research on ALA-PDT, there are still many unanswered questions, such as the mechanism by which selective PpIX accumulates in cancer cells, and why various cell lines have differing abilities to accumulate PpIX or respond to irradiation. Even less is known about the mechanisms of action of ALA-PDT in combination with iron chelators.

In this work, we continued the study of the use of iron chelators from the TSC group to improve ALA-PDT therapy. In our previous work, we selected a thiosemicarbazone



derivative with quinoline and thiomorpholine fragments; namely, derivative **2** [8]. Because this compound boosts the PpIX concentration in several cell lines, it is the most universal. Therefore, we continued the research with derivative **2** and focused on the transporters that are involved in the heme biosynthesis pathway intermediates: flux and the phototoxic effects (Figure 1). We continued the study on four cancer cell lines (Mcf-7, HCT 116, Hs683 and A549) because we observed interesting differences in the PpIX accumulation and the expression of the genes that are involved in heme biosynthesis and the degradation pathway in untreated cells, and in cells that had been treated with 5-ALA or 5-ALA with TSC. The Hs683 cell lines especially exhibited an atypical behavior that has not yet been described in the literature. In the current work, we extended the study to several targets that are responsible for the transport of the substrates for heme into a cell and its efflux from a cell.

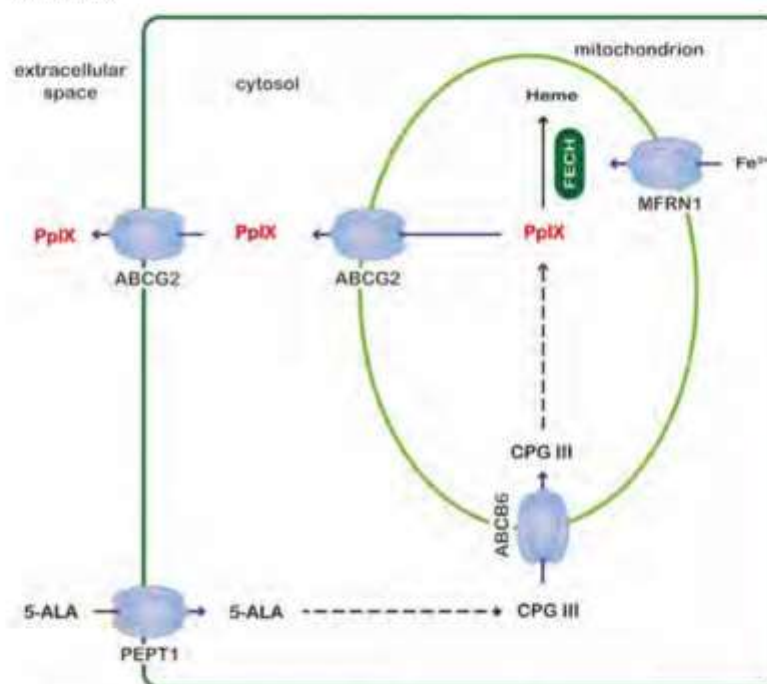


**Figure 1.** Schematic representation of selected transporters involved in the transport of intermediates of the heme biosynthetic pathway. ABCB6—ATP-binding cassette subfamily B member 6; ABCG2—ATP-binding cassette subfamily G member 2, 5-ALA—5-aminolevulinic acid, CPG III—coproporphyrinogen III, FECH—ferrochelatase, MFRN1—mitoferrin 1, PEPT1—peptide transporter 1, PpIX—protoporphyrin IX.

The first analyzed gene was the peptide transporter 1 (PepT1), which plays a crucial role in the delivery of a prodrug (5-ALA) to a cell [9,10]. PepT1 is a prototype transporter of the SLC15 family [11] and its induction is connected with an enhanced therapeutic effect via an increased transport of 5-ALA into a cell [12]. A similar situation was discovered for the ATP-binding cassette (ABC) transporter ABCB6, which transports coproporphyrinogen III into the mitochondria where PpIX is synthesized [13]. Several papers have presented results that indicate the important role of overexpressed ABCB6 in the elevated concentration of PpIX after 5-ALA administration [14,15]. Another type of ATP-binding cassette transporter is ABCB10, which is responsible for the production or efflux of 5-ALA from the mitochondria and plays a crucial role in the heme synthesis pathway [16]. ABCB10 also

forms a complex with mitoferrin1 (MFRN1) and ferrochelatase (FECH), which intensifies the production of heme [17]. Another ATP-binding cassette transporter, which was the subject of the research, was ABCG2. This molecule is responsible for extracting PpIX from the mitochondria [18]. An elevated level of ABCG2 is connected with an insufficient PDT effect after 5-ALA administration. Therefore, many studies have described the inhibition of ABCG2 as a strategy for increasing the PpIX level in a cell [19]. Another important molecule that is involved in heme synthesis is MFRN1, which is responsible for mitochondrial iron delivery [20]. Silencing MFRN1 increased the PpIX levels in healthy mouse fibroblasts.

## 2. Results and Discussion

Using iron chelators in ALA-PDT to increase the efficiency of this therapy is not new. However, the number of chelators that can be used in ALA-PDT is limited and their mechanism of action is poorly understood. In our previous work, we investigated the ability of novel iron chelators from the TSC group to increase the PpIX accumulation on different cell lines with the heterogeneous expression of heme biosynthesis and degradation pathway genes. Of the TSC derivatives that were tested, derivative 2 emerged as the most promising in terms of its applicability in ALA-PDT because it increased the PpIX levels in most of the tested cell lines, did not exhibit any antiproliferative properties [8] and had good iron ion chelating characteristics [21].

In this work, we continued our investigation of using iron chelators from the TSC group as an ALA-PDT enhancer, and focused on selected transporters that are involved in the flux of the heme biosynthesis pathway intermediates as well as on the efficacy of ALA-PDT in combination with TSC. The expression of these transporters is one of the factors that limits the efficacy of ALA-PDT. Of the selected transporters, only two resulted in statistically significant changes in the expression pattern after the 5-ALA treatment in combination with TSC derivative 2. The first of these was ABCG2, which is one of the most studied transporters in this context and is involved in PpIX efflux from the cell, whose increased expression correlated with a low PpIX accumulation as well as a low PDT efficacy [14,22,23]. Statistically significant changes in the ABCG2 expression were observed in all of the tested cell lines after they had been with a combination of 5-ALA and TSC derivative 2 compared to the cells they had been treated with 5-ALA alone (Figure 2). The greatest changes in the expression of this transporter gene were observed for the MCF-7 cell line, in which there was a 5.3-fold increase in its expression after treatment with TSC derivative 2 combined with 5-ALA (Figure 2B), while for the HCT 116 and Hs683 cell lines, there was a 3.6- and 4.16-fold increase in its expression, respectively (Figure 2A,C). For the A549 cell line, the increase was the lowest, namely only 1.8-fold (Figure 2D). When the increase in the ABCG2 gene expression between cells that had been treated with 5-ALA and those that had been treated with the combination of TSC derivative 2 and 5-ALA were compared, it was found that the higher the ratio, the lower the PpIX accumulation, which was shown in our previous work (Table 1 [8]). This observation is consistent with the literature reports. For the exception was the A549 cell line, in which there was no significant accumulation of PpIX, and in which the increase in the ABCG2 expression was the smallest of the studied cell lines.

The second gene whose expression changed significantly for two cell lines after treatment with combination of 5-ALA and TSC derivative 2 compared to cells treated only with 5-ALA was mitoferrin-1 (MFRN1), i.e., Hs683 (3.8-fold increase) and A549 (3.0-fold increase; Figure 2C,D). MFRN1, as was mentioned above, is responsible for the transport of iron ions into the mitochondria. Despite the paucity of literature on iron metabolism and ALA-PDT efficacy, it was shown that breast cancer cell lines that had a down-regulated expression of MFRN1 and MFRN2 had an increased accumulation of PpIX. In contrast, experiments using siRNA showed that silencing the mitoferrin genes resulted in an increased accumulation of PpIX in normal cells [20]. The increase in MFRN1 expression might explain the lack of PpIX accumulation on the A549 cell line after treatment with TSC derivative 2 that was observed in the previous work. In contrast, there was no such correlation for the Hs683 cell line.

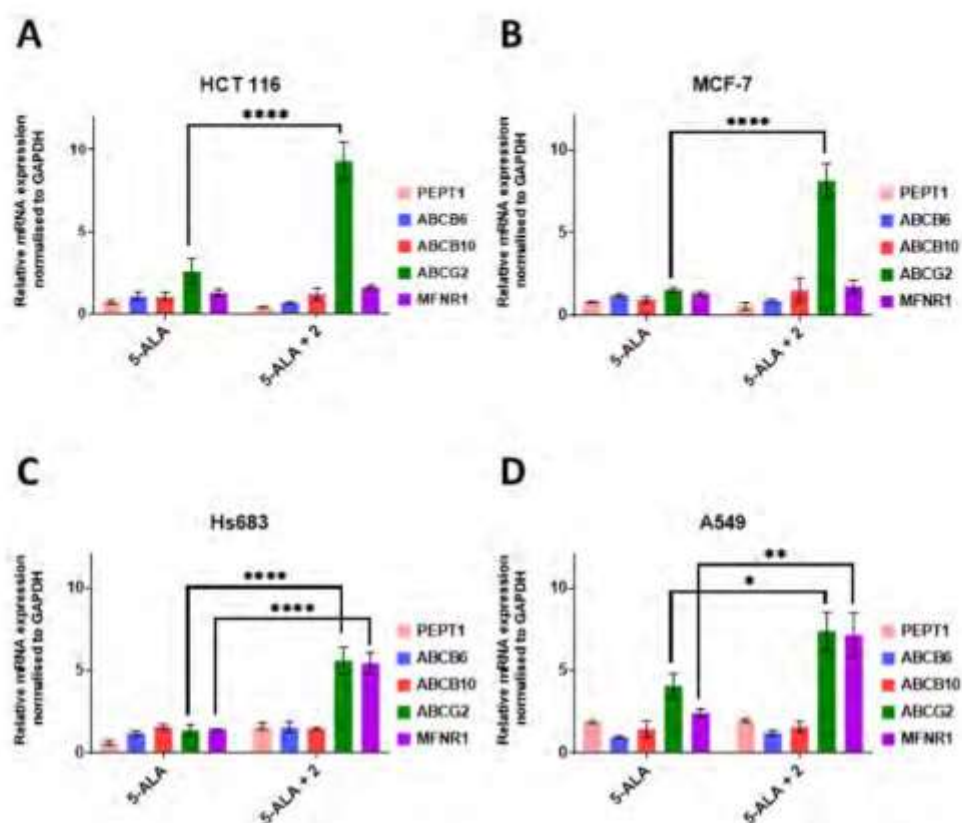


Figure 2. The expression of the genes that are associated with the transport of 5-ALA and heme after treatment with 5-ALA and a combination of 5-ALA with TSC derivative 2. (A)—MCF-7, (B)—HCT 116, (C)—Hs683 and (D)—A549 cell lines. PEPT1—peptide transporter 1; ABCB6—ATP-binding cassette B6; ABCB10—ATP-binding cassette B10; ABCG2—ATP-binding cassette G2; MFRN1—mitoferrin 1. Data analysis was performed using a two-way ANOVA with Tukey's post-hoc test \*  $p < 0.05$ , \*\*  $p < 0.005$ , \*\*\*\*  $p < 0.0001$ .

Table 1. Summary of results from previous work [8].

Cell line	Increase in fluorescence of PpIX relative to 5-ALA after treatment with TSC derivative 2 in combination with 5-ALA.	Expression of mRNA after treatment with TSC derivative 2 in combination with 5-ALA relative to 5-ALA.	
		FECH	HO-1
HCT 116	4.2-fold change	Down-regulated	Down-regulated
MCF-7	1.6-fold change	Non-significant changes	Down-regulated
Hs683	1.7-fold change	Up-regulated	Up-regulated
A549	Non-significant changes	Non-significant changes	Non-significant changes

Based on the results presented above, and the available literature, it can be assumed that the phototoxic effect on the studied cell lines would be minor or that there would be no effect at all. However, the result of the irradiation of cells that had been treated with 5-ALA,



TSC derivative 2 and their combination indicated that the viability decreased statistically significant (Figure 3). The strongest effect was observed for the HCT 116 and Hs683 cell lines (26% and 29% of the surviving fraction, respectively; Figure 3A,C). In the case of the MCF-7 line, the decrease of cell viability was 44% of the surviving fraction (Figure 3B). For the A549 line, the phototoxic effect was the weakest (76% of the surviving fraction; Figure 3D). The observed PDT effect for the HCT 116, MCF-7 and A549 cell lines correlated with the results for the PpIX accumulation because the higher the PpIX accumulation the stronger phototoxicity. Only for Hs683 cell line did the correlation between the PpIX accumulation and cell viability not correlate after irradiation, which is an open question for further research. The lack of a phototoxic effect after treatment with TSC derivative 2 alone is a desirable feature of a booster with potential use in ALA-PDT.

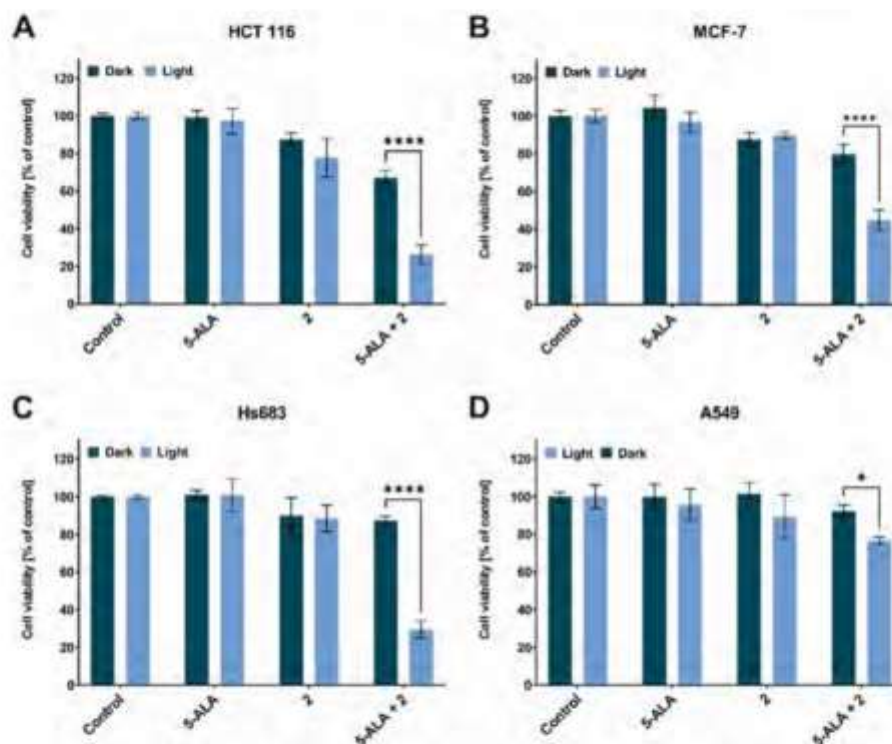


**Figure 3.** Phototoxic effect after red light irradiation at a dose of  $12 \text{ J}/\text{cm}^2$ . (A)—MCF-7, (B)—HCT 116, (C)—Hs683 and (D)—A549 cell lines that had been treated with 5-ALA, TSC derivative 2 and their combination. Data analysis was performed using a two-way ANOVA with Tukey's post-hoc test:  $^+ p < 0.05$ ,  $**** p < 0.0001$ .

Interestingly, there was no phototoxic effect on any of the tested cell lines that had been treated with 5-ALA alone. Most studies have shown that there is a stronger or weaker phototoxic effect during ALA-PDT. However, papers that show no or a weak phototoxic effect in ALA-PDT can also be found [24,25]. The increased expression of ABCG2, as was mentioned earlier, is responsible for the efflux of PpIX from the cell and in our opinion cannot explain the complete absence of a phototoxic effect only on the 5-ALA-treated cells. In order to explain this observation, we assumed that in the cells that had been treated with 5-ALA only, heme was still biosynthesized and thus the concentration of PpIX was insufficient to achieve a satisfactory therapeutic effect. Our results showed that the concentration of free heme significantly increased in the cells that had been treated with

5-ALA alone compared to the control and that when a combination of TSC derivative 2 with 5-ALA was applied, the concentration of heme decreased to a level in the HCT 116, MCF-7 and Hs683 cell lines that was similar to the control (Figure 4A–C). In the case of the A549 cell line, the level of free heme was not statistically significantly different after treatment with the tested compound combinations (Figure 4D). These observations in the 5-ALA-treated cells are not surprising because by exogenously providing 5-ALA, the regulatory system of heme biosynthesis through a negative feedback loop is overcome. In addition, the lack of iron deprivation permits the conversion of PpIX into heme. In the previous work, we showed that on MCF-7 and HCT 116 cell lines, the HO-1 expression levels were significantly elevated after treatment with 5-ALA alone and that they decreased after treatment with TSC derivative 2 in combination with 5-ALA [8]. This enzyme is, among others, responsible for the degradation of heme in cells [26] and its expression pattern correlates with the results that were obtained from the heme concentration study. On the other hand, one of the heme degradation products, i.e., biliverdin, acts as an antioxidant, which may explain the lack of a PDT effect on the 5-ALA-treated cell lines [27,28]. In contrast, for the Hs683 cell line, as was shown in a previous paper, the HO-1 levels increased after treatment with a combination of 5-ALA and TSC derivative 2, which stands in the opposition to the facts that are presented above and yet, this line exhibited a significant decrease in cell viability after irradiation. For the A549 line, no changes were observed in the HO-1 gene expression or in the free heme concentration [8].

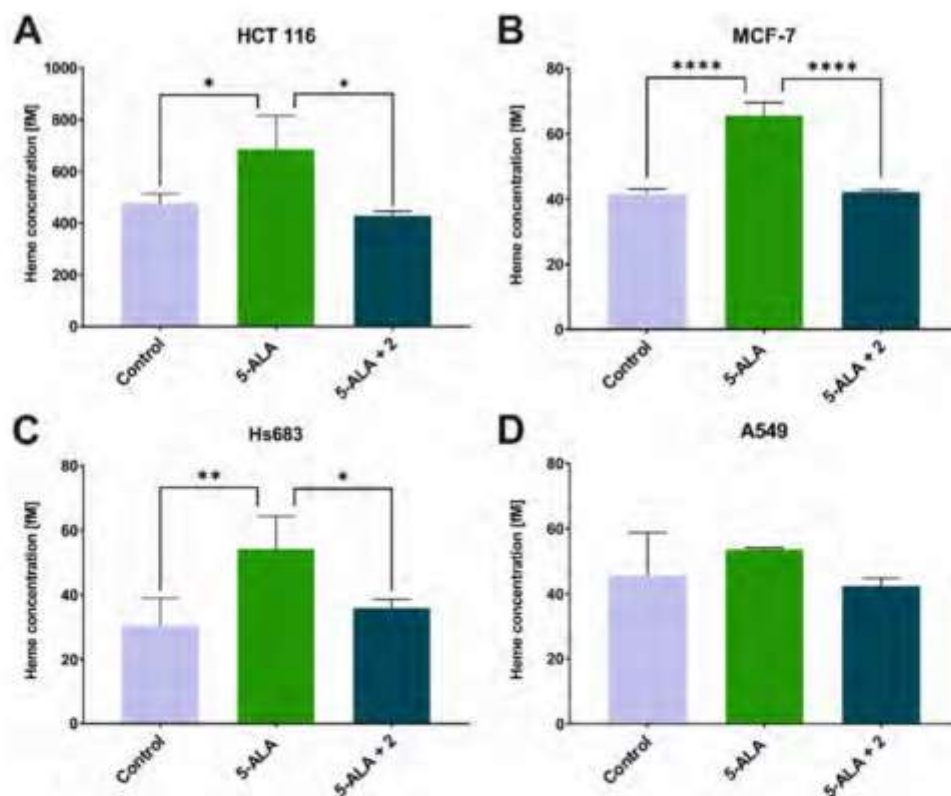


**Figure 4.** Free heme concentration after treatment of 5-ALA and combination of 5-ALA and TSC derivative 2 (A)—MCF-7, (B)—HCT 116, (C)—Hs683 and (D)—A549 cell lines. Data analysis was performed using a one-way ANOVA with Tukey's post-hoc test: \*  $p < 0.05$ , \*\*  $p < 0.005$ , \*\*\*\*  $p < 0.0001$ .

### 3. Materials and Methods

#### 3.1. Cell Lines and Cell Culture

The HCT 116 (colon cancer), MCF-7 (breast cancer) and A549 (lung cancer) cell lines were purchased from the American Type Culture Collection (ATCC; Manassas, VA, USA), while the Hs683 (glioma) cell line was kindly provided by Prof. Gabriela Kramer-Marek from the Institute of Cancer Research (London, UK). All of the cell lines were cultured in Dulbecco's Modified Eagle's Medium (DMEM; Sigma-Aldrich; St. Louis, MO, USA), which had been supplemented with 12% foetal bovine serum (FBS; Sigma-Aldrich; St. Louis, MO, USA) and an antibiotic blend (1% v/v of penicillin and streptomycin; Gibco; Grand Island, NY, USA) in 75 cm<sup>2</sup> flasks (Nunc, Sigma-Aldrich; St. Louis, MO, USA). The cells were cultured in standard conditions of 37 °C in a humidified atmosphere at 5% CO<sub>2</sub>. All of the cell lines were screened for Mycoplasma contamination.

#### 3.2. Transporter Genes Expression

Cells were seeded in 3-cm plastic Petri dishes (Nunc, Sigma-Aldrich; St. Louis, MO, USA) at a density of  $4 \times 10^5$  cells per dish and incubated for 24 h at 37 °C. Then, the old medium was removed and replaced with solutions of 5-ALA (1 mM), derivative 2 (25 µM) and a combination of 5-ALA and derivative 2 in a manner in which their final concentrations matched the concentrations of 5-ALA and derivative 2 alone. After another 24 h of incubation, the total RNA was isolated from the cells with TRIzol Reagent (Invitrogen; Carlsbad, CA, USA) according to the manufacturer's protocol. Reverse transcription was performed on 2 µg total RNA using a GoScript™ Reverse Transcriptase kit (Promega; Madison, WI, USA) and Oligo(dT)<sub>25</sub> Primers (Sigma-Aldrich; St. Louis, MO, USA). Quantitative RT-PCR was performed in a CFX96 Touch™ Real-Time PCR Detection System (Biorad; Hercules, CA, USA) using SYBR® Green Master Mix (Biorad; Hercules, CA, USA), the appropriate primer pairs and a cDNA template. The primers that were used in this study were designed using Primer 3 online software (Table 2) and synthesized by Sigma-Aldrich (Sigma-Aldrich; St. Louis, MO, USA). The data was analyzed based on a comparison of the expression of the target gene to a reference gene, GAPDH, using the  $2^{-\Delta\Delta CT}$  (Livak and Schmittgen) method. The experiments were repeated at least three times in triplicate.

**Table 2.** Primers used in this study.

Gene Name	Sequence 5'-3' (F-Forward, R-Reverse)	
PEPT1	F	AGGCAACAACATATGTCGGGG
	R	CACAGCATCGAAGATCGGGA
ABCB6	F	CTGCGGTATGTGGTCTCTGG
	R	CCAGGTAGACTGTTGGGCTG
ABCB10	F	GTACGGGTGCGACGCA
	R	GTGAACGGCGATAGGGACC
ABCG2	F	GCACAGGAAGTTTACGCACAG
	R	AAGGGGCTAGAAGAAGGGGG
MFRN1	F	ACTCGGTGAAGACACGAATGC
	R	CAGCTATCCCGTTGGCTAGG
GAPDH	F	GAGTCAACGGATTTGGTCGTA
	R	GCCCCACTTGATTTGGGAG

#### 3.3. Heme Concentration Measurement

The cells were seeded at a density  $1 \times 10^6$  cells/dish for 24 h at 37 °C. Next, 5-ALA (1 mM), TSC derivative 2 (25 µM) and a combination of 5-ALA and derivative 2 were added and incubated for 24 h in the dark at 37 °C. After incubation, the cells were washed with PBS and lysed with a 1% Triton X-100 solution in PBS. The lysates were then sonicated and centrifuged at  $10,000 \times g$  for 10 min. The free heme concentration was measured

using a Hemin Assay Kit (Abcam; Cambridge, UK) according to the manufacturer's protocol. The heme concentration was calculated from the calibration curve of three independent experiments.

#### 3.4. Phototoxic Effect

The cells were seeded into a 96-well plate at a density of 11,000 cells/well for 24 h at 37 °C. Then, the medium was removed and 5-ALA (1 mM), derivative 2 (25 µM) and a combination of 5-ALA and derivative 2 were added and incubated for 24 h in the dark at 37 °C. After the incubation, the cells were washed three times with a medium without phenol red and then irradiated or with an LED red light (634 ± 5 nm) at a dose 12 J/cm<sup>2</sup>. The cells were further incubated in the dark under 5% CO<sub>2</sub> at 37 °C for 24 h. After irradiation, the cell viability was determined using an MTS assay. Briefly, the medium was removed and 100 µL of DMEM without phenol red and 20 µL of CellTiter 96<sup>®</sup> AQueous One Solution (Promega; Madison, WI, USA) was added and then incubated for approximately 1 h at 37 °C. Simultaneously, the same experiment was performed with irradiation step being omitted in order to show dark cytotoxicity. The results are presented as the mean ± standard deviation of three independent experiments and the cell viability was calculated using the GraphPad Prism 5 software (GraphPad Software Inc.; San Diego, CA, USA).

#### 3.5. Statistical Analysis

All of the experiments were repeated three times in independent experiments and the results are presented as the mean ± standard deviation. All of the data were analyzed using GraphPad Prism 5 software (GraphPad Software Inc.; San Diego, CA, USA). A two-way ANOVA followed by Tukey's test was used to examine the significance of any differences between more than two groups. A two-tailed *p* value of 0.05 or less was considered significant.

### 4. Conclusions

In conclusion, the use of iron chelators from the thiosemicarbazone group as enhancers is a promising approach for improving the efficiency of ALA-PDT. The TSC derivative 2 is particularly interesting in this case due to its strong photocytotoxic effect, which was obtained on most of the tested cell lines in combination with 5-ALA. Despite the significant increases in ABCG2 gene expression, the observed therapeutic effect on most of the cell lines that were included in this work was substantial. This indicates that TSC derivative 2 is an excellent candidate for increasing the efficiency of ALA-PDT. We also showed that the expression level of the ABCG2 gene correlated with the phototoxic effect for most of the cell lines. The absence of this effect for the A549 lineage may be due to the increased expression of MFNR1. Surprisingly, this study does not explain the strong phototoxic effect that was observed for the Hs683 line and the reasons for this remain an open question. Because of the still insufficient knowledge about the mechanisms of ALA-PDT therapy, the results presented here are a necessary addition to fill in the existing gaps. At the same time, our study still remains an interesting area for further research.

**Author Contributions:** A.M.-W. designed and analyzed the data, wrote the manuscript; R.G. designed, performed the experiments and analyzed the data, wrote the manuscript; J.P. delivered sample 2. All authors have read and agreed to the published version of the manuscript.

**Funding:** The financial support of the National Science Centre grant; 2019/35/N/NZ7/02780 (R.G.).

**Institutional Review Board Statement:** Not applicable.

**Informed Consent Statement:** Not applicable.

**Data Availability Statement:** Not applicable.

**Conflicts of Interest:** The authors declare no conflict of interest.



## References

1. Gunaydin, G.; Gedik, M.E.; Ayan, S. Photodynamic Therapy—Current Limitations and Novel Approaches. *Front. Chem.* **2021**, *9*, 691697. [CrossRef] [PubMed]
2. Benov, L. Photodynamic Therapy: Current Status and Future Directions. *Med. Princ. Pract.* **2015**, *24*, 14–28. [CrossRef] [PubMed]
3. Jori, G. Tumour photosensitizers: Approaches to enhance the selectivity and efficiency of photodynamic therapy. *J. Photochem. Photobiol. B Biol.* **1996**, *36*, 87–93. [CrossRef] [PubMed]
4. Castano, A.P.; Demidova, T.N.; Hamblin, M.R. Mechanisms in photodynamic therapy: Part three—Photosensitizer pharmacokinetics, biodistribution, tumor localization and modes of tumor destruction. *Photodiagnosis Photodyn. Ther.* **2005**, *2*, 91–106. [CrossRef] [PubMed]
5. Shah, N.; Squire, J.; Guirguis, M.; Saha, D.; Hoyt, K.; Wang, K.K.-H.; Agarwal, V.; Obaid, G. Deep-Tissue Activation of Photonanomedicines: An Update and Clinical Perspectives. *Cancers* **2022**, *14*, 2004. [CrossRef]
6. Beik, D.; Eggleston, I.M.; Pourzand, C. Daylight-PDT: Everything under the sun. *Biochem. Soc. Trans.* **2022**, *50*, 975–985. [CrossRef]
7. Curnow, A.; Perry, A.; Wood, M. Improving in vitro photodynamic therapy through the development of a novel iron chelating aminolevulinic acid prod rug. *Photodiagnosis Photodyn. Ther.* **2018**, *25*, 157–165. [CrossRef]
8. Gawęcki, R.; Malarz, K.; Rejmund, M.; Polanski, J.; Mrozek-Wilczkiewicz, A. Impact of thiosemicarbazones on the accumulation of PpIX and the expression of the associated genes. *J. Photochem. Photobiol. B Biol.* **2019**, *199*, 111585. [CrossRef]
9. Anderson, C.M.H.; Jevons, M.; Thangaraju, M.; Edwards, N.; Conlon, N.J.; Woods, S.; Ganapathy, V.; Thwaites, D.T. Transport of the Photodynamic Therapy Agent 5-Aminolevulinic Acid by Distinct H<sup>+</sup>-Coupled Nutrient Carriers Coexpressed in the Small Intestine. *J. Pharmacol. Exp. Ther.* **2010**, *332*, 220–228. [CrossRef]
10. Döring, F.; Walter, J.; Will, J.; Föcking, M.; Boll, M.; Amasheh, S.; Clauss, W.; Daniel, H. Delta-aminolevulinic acid transport by intestinal and renal peptide transporters and its physiological and clinical implications. *J. Clin. Investig.* **1998**, *101*, 2761–2767. [CrossRef]
11. Kottra, G.; Daniel, H. The proton oligopeptide cotransporter family SLC15 in physiology and pharmacology. *Pflugers. Arch.* **2004**, *447*, 610–618. [CrossRef]
12. Hagiya, Y.; Fukuhara, H.; Matsumoto, K.; Endo, Y.; Nakajima, M.; Tanaka, T.; Okura, I.; Kurabayashi, A.; Furihata, M.; Inoue, K.; et al. Expression levels of PEPT1 and ABCG2 play key roles in 5-aminolevulinic acid (ALA)-induced tumor-specific protoporphyrin IX (PpIX) accumulation in bladder cancer. *Photodiagnosis Photodyn. Ther.* **2013**, *10*, 288–295. [CrossRef]
13. Nakayama, T.; Nozawa, N.; Kawada, C.; Yamamoto, S.; Ishii, T.; Ishizuka, M.; Namikawa, T.; Ogura, S.-I.; Hanazaki, K.; Inoue, K.; et al. Mitomycin C-induced cell cycle arrest enhances 5-aminolevulinic acid-based photodynamic therapy for bladder cancer. *Photodiagnosis Photodyn. Ther.* **2020**, *31*, 101893. [CrossRef]
14. Nakayama, T.; Otsuka, S.; Kobayashi, T.; Okajima, H.; Matsumoto, K.; Hagiya, Y.; Inoue, K.; Shuin, T.; Nakajima, M.; Tanaka, T.; et al. Dormant cancer cells accumulate high protoporphyrin IX levels and are sensitive to 5-aminolevulinic acid-based photodynamic therapy. *Sci. Rep.* **2016**, *6*, 36478. [CrossRef]
15. Matsumoto, K.; Hagiya, Y.; Endo, Y.; Nakajima, M.; Ishizuka, M.; Tanaka, T.; Ogura, S.-I. Effects of plasma membrane ABCB6 on 5-aminolevulinic acid (ALA)-induced porphyrin accumulation in vitro: Tumor cell response to hypoxia. *Photodiagnosis Photodyn. Ther.* **2015**, *12*, 45–51. [CrossRef]
16. Bayeva, M.; Khechaduri, A.; Wu, R.; Burke, M.A.; Wasserstrom, J.A.; Singh, N.; Liesa, M.; Shirihai, O.S.; Langer, N.B.; Paw, B.H.; et al. ATP-Binding Cassette B10 Regulates Early Steps of Heme Synthesis. *Circ. Res.* **2013**, *113*, 279–287. [CrossRef]
17. Seguin, A.; Takahashi-Makise, N.; Yien, Y.Y.; Huston, N.C.; Whitman, J.C.; Musso, G.; Wallace, J.A.; Bradley, T.; Bergonia, H.A.; Kafina, M.D.; et al. Reductions in the mitochondrial ABC transporter Abcb10 affect the transcriptional profile of heme biosynthesis genes. *J. Biol. Chem.* **2017**, *292*, 16284–16299. [CrossRef]
18. Hagiya, Y.; Endo, Y.; Yonemura, Y.; Takahashi, K.; Ishizuka, M.; Abe, F.; Tanaka, T.; Okura, I.; Nakajima, M.; Ishikawa, T.; et al. Pivotal roles of peptide transporter PEPT1 and ATP-binding cassette (ABC) transporter ABCG2 in 5-aminolevulinic acid (ALA)-based photocytotoxicity of gastric cancer cells in vitro. *Photodiagnosis Photodyn. Ther.* **2012**, *9*, 204–214. [CrossRef]
19. Kim, J.H.; Park, J.M.; Roh, Y.J.; Kim, I.-W.; Hasan, T.; Choi, M.-G. Enhanced efficacy of photodynamic therapy by inhibiting ABCG2 in colon cancers. *BMC Cancer* **2015**, *15*, 504. [CrossRef]
20. Paradkar, P.N.; Zumbrennen, K.B.; Paw, B.H.; Ward, D.M.; Kaplan, J. Regulation of Mitochondrial Iron Import through Differential Turnover of Mitoferrin 1 and Mitoferrin 2. *Mol. Cell. Biol.* **2009**, *29*, 1007–1016. [CrossRef]
21. Rzycka-Korzec, R.; Malarz, K.; Gawęcki, R.; Mrozek-Wilczkiewicz, A.; Małecki, J.G.; Schab-Balcerzak, E.; Korzec, M.; Polanski, J. Effect of the complex-formation ability of thiosemicarbazones containing (aza)benzene or 3-nitro-1,8-naphthalimide unit towards Cu(II) and Fe(III) ions on their anticancer activity. *J. Photochem. Photobiol. A Chem.* **2021**, *415*, 113314. [CrossRef]
22. Teshigawara, T.; Mizuno, M.; Ishii, T.; Kitajima, Y.; Utsumi, F.; Sakata, J.; Kajiyama, H.; Shubata, K.; Ishizuka, M.; Kikkawa, F. Novel potential photodynamic therapy strategy using 5-Aminolevulinic acid for ovarian clear-cell carcinoma. *Photodiagnosis Photodyn. Ther.* **2017**, *21*, 121–127. [CrossRef] [PubMed]
23. Briel-Pump, A.; Beez, T.; Ebbert, L.; Remke, M.; Weinhold, S.; Sabel, M.C.; Sorg, R.V. Accumulation of protoporphyrin IX in medulloblastoma cell lines and sensitivity to subsequent photodynamic treatment. *J. Photochem. Photobiol. B Biol.* **2018**, *189*, 298–305. [CrossRef] [PubMed]



24. Kim, I.; Johnson, R.; Chung, C.-W.; Jeong, Y.-I.; Kang, D.H.; Suh, H. Poly(L-histidine)-tagged 5-aminolevulinic acid prodrugs: New photosensitizing precursors of protoporphyrin IX for photodynamic colon cancer therapy. *Int. J. Nanomed.* **2012**, *7*, 2497–2512. [[CrossRef](#)]
25. Bourré, L.; Giuntini, F.; Eggleston, I.M.; Wilson, M.; MacRobert, A.J. 5-Aminolaevulinic acid peptide prodrugs enhance photosensitization for photodynamic therapy. *Mol. Cancer Ther.* **2008**, *7*, 1720–1729. [[CrossRef](#)]
26. Ishizuka, M.; Abe, F.; Sano, Y.; Takahashi, K.; Inoue, K.; Nakajima, M.; Kohda, T.; Komatsu, N.; Ogura, S.-I.; Tanaka, T. Novel development of 5-aminolevulinic acid (ALA) in cancer diagnoses and therapy. *Int. Immunopharmacol.* **2011**, *11*, 358–365. [[CrossRef](#)]
27. Frank, J.; Lomejad-Schäfer, M.R.; Schöffl, H.; Flaccus, A.; Lambert, C.; Biesalski, H.K. Inhibition of heme oxygenase-1 increases responsiveness of melanoma cells to ALA-based photodynamic therapy. *Int. J. Oncol.* **2007**, *31*, 1539–1545. [[CrossRef](#)]
28. Nowis, D.; Legat, M.; Grzela, T.; Niderla, J.; Wilczek, E.; Wilczynski, G.M.; Głodkowska, E.; Mrówka, P.; Issat, T.; Dulak, J.; et al. Heme oxygenase-1 protects tumor cells against photodynamic therapy-mediated cytotoxicity. *Oncogene* **2006**, *25*, 3365–3374. [[CrossRef](#)]

#### **4.3. [P3]. Iron Metabolism in Aminolevulinic Acid-Photodynamic Therapy with Iron Chelators from the Thiosemicarbazone Group.**

**Autorzy:** Gawecki R., Rawicka P., Rogalska M., Serda M., Mrozek-Wilczkiewicz A.

**Referencja:** International Journal of Molecular Sciences, 2024, 25(19), 10468

**Numer DOI:** 10.3390/ijms251910468

**Impact Factor czasopisma:** 4,9 (2024)

**Liczba punktów MNiSW czasopisma:** 140 (2024)

Mój udział w pracy polegał na zaplanowaniu, wykonaniu i analizie wszystkich badań biologicznych, współuczestnictwie w badaniach widm absorpcyjnych oraz pisaniu manuskryptu.



Article

# Iron Metabolism in Aminolevulinic Acid-Photodynamic Therapy with Iron Chelators from the Thiosemicarbazone Group

Robert Gawęcki<sup>1,2</sup>, Patrycja Rawicka<sup>1</sup>, Marta Rogalska<sup>3</sup>, Maciej Serda<sup>3</sup> and Anna Mrozek-Wilczkiewicz<sup>1,4,\*</sup>

<sup>1</sup> Institute of Physics, University of Silesia in Katowice, 75 Pułku Piechoty 1A, 41-500 Chorzów, Poland; robert.gawęcki@us.edu.pl (R.G.); patrycja.rawicka@us.edu.pl (P.R.)

<sup>2</sup> SPIN-Lab Centre for Microscopic Research of Matter, University of Silesia in Katowice, 75 Pułku Piechoty 1A, 41-500 Chorzów, Poland

<sup>3</sup> Institute of Chemistry, University of Silesia in Katowice, Szkolna 9, 40-006 Katowice, Poland; rejmund.m@gmail.com (M.R.); maciej.serda@us.edu.pl (M.S.)

<sup>4</sup> Department of Systems Biology and Engineering, Silesian University of Technology, Akademicka 16, 44-100 Gliwice, Poland

\* Correspondence: anna.mrozek-wilczkiewicz@us.edu.pl or anna.mrozek-wilczkiewicz@polsl.pl

**Abstract:** Iron plays a crucial role in various metabolic processes. However, the impact of 5-aminolevulinic acid (ALA) in combination with iron chelators on iron metabolism and the efficacy of ALA-photodynamic therapy (PDT) remain inadequately understood. This study aimed to examine the effect of thiosemicarbazone derivatives during ALA treatment on specific genes related to iron metabolism, with a particular emphasis on mitochondrial iron metabolism genes. In our study, we observed differences depending on the cell line studied. For the HCT116 and MCF-7 cell lines, in most cases, the decrease in the expression of selected targets correlated with the increase in protoporphyrin IX (PPIX) concentration and the observed photodynamic effect, aligning with existing literature data. The Hs683 cell line showed a different gene expression pattern, previously not described in the literature. In this study, we collected an extensive analysis of the gene variation occurring after the application of novel thiosemicarbazone derivatives and presented versatile and effective compounds with great potential for use in ALA-PDT.

**Keywords:** iron metabolism; protoporphyrin IX; 5-aminolevulinic acid; photodynamic therapy; thiosemicarbazone; iron chelators



**Citation:** Gawęcki, R.; Rawicka, P.; Rogalska, M.; Serda, M.; Mrozek-Wilczkiewicz, A. Iron Metabolism in Aminolevulinic Acid-Photodynamic Therapy with Iron Chelators from the Thiosemicarbazone Group. *Int. J. Mol. Sci.* **2024**, *25*, 10468. <https://doi.org/10.3390/ijms251910468>

Academic Editor: Yong Teng

Received: 21 August 2024

Revised: 19 September 2024

Accepted: 26 September 2024

Published: 28 September 2024



**Copyright:** © 2024 by the authors. Licensee MDPI, Basel, Switzerland. This article is an open access article distributed under the terms and conditions of the Creative Commons Attribution (CC BY) license (<https://creativecommons.org/licenses/by/4.0/>).

## 1. Introduction

Photodynamic therapy (PDT), a method characterized by its low invasiveness towards healthy cells, is currently an attractive treatment strategy for various diseases. Despite its great potential against cancer cells, it is mainly used for dermatological treatment and cosmetic procedures. Due to the vast variability within a single cancer type, as well as the individual characteristics of each patient, current treatment methods need to be modified. Therefore, developing non-destructive methods of cancer treatment for the patient is particularly important. In this paper, we present a modification of PDT using 5-aminolevulinic acid (5-ALA) supported by iron chelators from the thiosemicarbazone (TSC) group. Although this strategy is well-known [1,2], there is a paucity of data on the changes in iron metabolism that occur during this therapy. The therapy itself consists of administering 5-ALA, a precursor of the actual drug—the photosensitizer protoporphyrin IX (PPIX), which, when excited with harmless radiation in the red wavelength range, generates reactive oxygen species (ROS) that initiate radical reactions leading to tumor destruction [3]. Using chelators, it is possible to increase the concentration of PPIX by blocking its conversion to heme [4,5]. Despite the use of different classes of chelators such as deferoxamine (DFO) [6], ethylenediaminetetraacetic acid (EDTA) [7], AP2-18 [8], and

Cp94 [9], this therapy has not received much attention. In this work, we present a new group of chelators that effectively increase drug concentration, thereby affecting several cellular pathways. However, as previously mentioned, little is known about the changes that occur in iron metabolism, so in this work, we have performed an extensive analysis of gene variation of iron-management-related targets. In the recent study, we selected molecular targets (Figure 1) related to iron management.

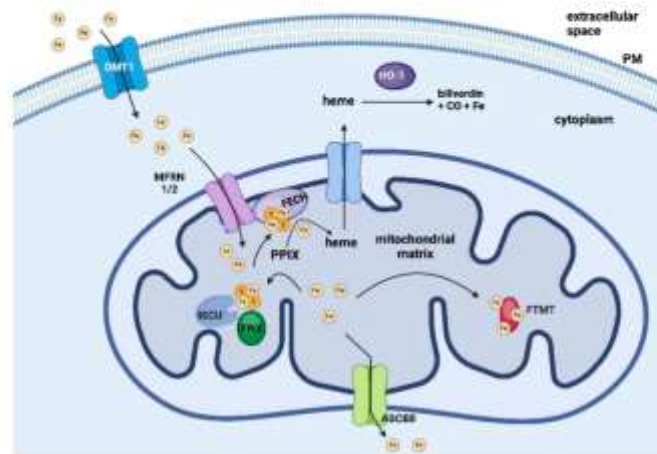


**Figure 1.** Iron metabolism in a cell considering the molecular targets studied in this paper (created in BioRender). PPIX—protoporphyrin IX, FECH—ferrochelatase, HO-1—heme oxygenase, FTMT—ferritin, FXN—frataxin, ICSU—iron-sulfur cluster assembly enzyme, MFRN1/2—mitoferrin 1/2, ABCB8—ATP-binding cassette subfamily B member 8.

Ferrochelatase (FECH) is considered one of the key genes affecting the efficiency of PPIX accumulation and the efficacy of ALA-PDT. This enzyme catalyzes the incorporation of an iron ion into PPIX, leading to the formation of heme. Numerous studies have demonstrated that reduced expression of this gene positively impacts PPIX accumulation and enhances the efficacy of ALA-PDT [10,11]. Another gene frequently studied recently is heme oxygenase (HO-1), an enzyme that degrades heme into biliverdin, carbon monoxide, and iron ions. Downregulation of HO-1 expression has been shown to enhance ALA-PDT efficiency in several cell lines, likely due to its role in protection against ROS [12]. Mitochondrial ferritin (FTMT) is a small protein with structural similarities to cytosolic heavy ferritin (HfT), found within the mitochondrial matrix. Functionally, FTMT serves as a storage site for mitochondrial iron and exhibits ferroxidase activity [13]. Another equally important molecule associated with iron metabolism is frataxin (FXN), which plays a crucial role in the biosynthesis of [2Fe-2S]-type iron centers. FXN is presumed to engage in physical interactions with the iron-sulfur cluster assembly enzyme (ICSU), serving as the primary sulfur donor in the biosynthesis of iron-sulfur clusters. However, the precise role of this protein remains largely unexplored [14,15]. Mitoferrin 1 and 2 (MFRN1 and MFRN2, now SLC25A37 and SLC25A28, respectively) serve as iron transporters, facilitating the transport of iron from the cytoplasm to the mitochondria. These transporters are located in the inner mitochondrial membrane. While both forms of mitoferrin are found in various tissues, MFRN1 exhibits significantly higher expression levels in erythroid tissue cells [16]. Furthermore, it has been demonstrated that MFRN1 forms a complex with ABCB10 and FECH. In this interaction, MFRN1 is directly implicated in transporting iron to the active center of FECH [17]. Another important iron transporter is divalent metal transporter 1 (DMT1, now SLC11A2), which facilitates the cellular uptake of iron ions [18]. While DMT1



is predominantly localized in the cell membrane, reports suggest its potential involvement in the transport of iron ions within the mitochondria as well [19,20]. To comprehensively trace the fate of the iron ion in the cell, we also included the target responsible for its efflux in the analysis. Namely, we focused on the mitochondrial potassium channel ATP-binding subunit (ABC8) gene, which is involved in the mitochondrial-to-cytosolic iron export process and the maturation of cytosolic iron-sulfur cluster-containing enzymes [21].

In our previous work, we have described the TSC-induced changes in the cellular heme biosynthesis and degradation [22]. Interestingly, we observed significant differences depending on the cell line studied, with changes occurring in a manner not previously described in the literature. While the crucial roles of FECH and HO-1 are well-known, their upregulation has not been previously observed. In our subsequent work, we have gone a step further; namely, extending the analysis to other genes related to the transport of the heme substrates and heme itself [23]. These results proved that, despite the upregulation of the ABCG2 transporter involved in the PPIX efflux, our TSCs increased PPIX levels sufficiently to trigger a therapeutic effect. This demonstrates that these compounds have great potential as supportive therapy for ALA-PDT. We also observed interesting changes in the iron transporter MFRN1 behavior; therefore, we have extended the study of its analogs in this paper.

Thiosemicarbazones itself are very interesting compounds known for their unique physicochemical properties, which arise from the presence of the TSC functional group. These properties are influenced by the ability of TSC to form stable complexes with metal ions due to their sulfur and nitrogen donor atoms. They exhibit varied solubility in polar solvents, stability under different pH conditions, and distinct melting points. Additionally, their structural flexibility allows for modifications, which enhances their biological and pharmacological activities, making them of significant interest in medicinal chemistry and material science.

## 2. Results and Discussion

### 2.1. Synthesis

Aromatic TSCs were synthesized according to the methodology previously published by our group and depicted below (Figure 2) [24]. The aliphatic TSC precursors were obtained from commercial resources. However, aromatic TSCs were synthesized in our laboratories. Derivative TSC-34 was described and further investigated by us in [22,23,25]. TSC-146 and TSC-147 were commercially available. TSC-197 was published in [26,27]. The other compounds are newly synthesized.

### 2.2. The Antiproliferative Activity of TSC

As was demonstrated in our previous research, chelators within the TSC group exhibit significant potential for enhancing the efficacy of ALA-PDT [22]. In this study, we selected a set of compounds (Figure 1) from this group to explore their influence on ALA-PDT efficiency and their effects on iron metabolism within malignant cell lines. TSCs are recognized for their diverse range of biological activities. In our studies, the goal was to select compounds that do not inherently possess pro-apoptotic or cell-proliferation-inhibiting effects. This decision stems from the understanding that cytotoxic compounds within the TSC group do not induce an increase in PPIX accumulation [28], which is a fundamental prerequisite for the action of ALA-PDT. In this study, we examined the effects of TSCs and Cp94 on three cell lines of different origins. As illustrated in Table 1, none of these compounds exhibited antiproliferative activity against the tested cancer cell lines. Furthermore, they showed no activity against normal human fibroblasts, which is crucial for the selectivity of this therapy. The utilization of these chelators for PDT is justified by their potential to enhance the photodynamic effect without exhibiting inherent dark toxicity. In the majority of studies involving iron chelators, the chelators are administered at doses that do not adversely affect cell viability [29–31]. In our approach, we chose chelators

from the TSC group at a concentration of 25  $\mu\text{M}$  and Cp94 at the same concentration for comparison.

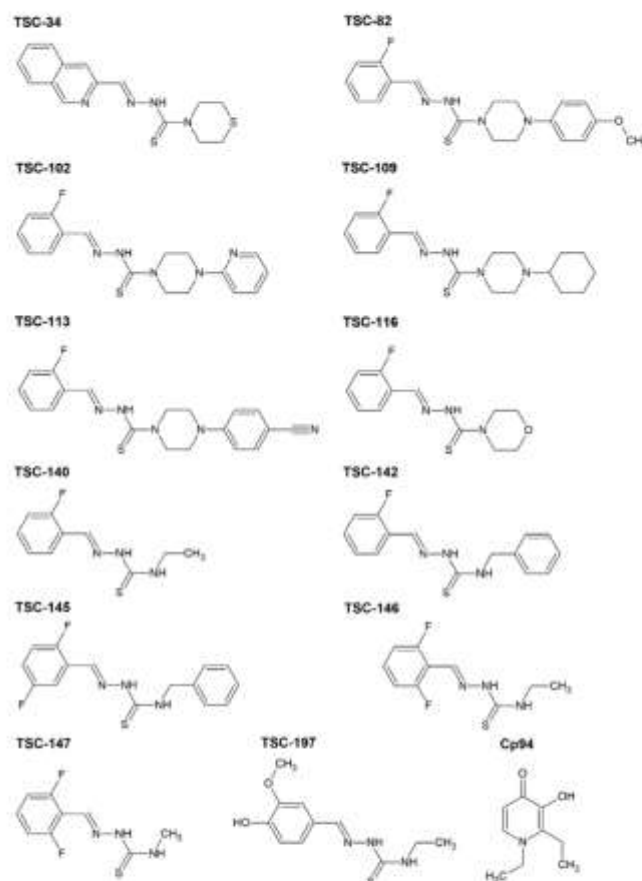


**Figure 2.** The structures of the TSCs and Cp94 examined in this study.

**Table 1.** Antiproliferative properties expressed as  $\text{IC}_{50}$  of the tested TSCs and Cp94 on a panel of tumor cell lines and human normal fibroblasts (NHDFs).

No.	TSC	$\text{IC}_{50}$ [ $\mu\text{M}$ ]			
		HCT116	MCF-7	Hs683	NHDF
1	TSC-34	$18.31 \pm 0.92$	>50	>50	$13.06 \pm 1.90$
2	TSC-82	$47.56 \pm 1.99$	>50	>50	>50
3	TSC-102	>50	>50	>50	>50
4	TSC-109	$30.87 \pm 0.64$	$42.97 \pm 1.33$	>50	>50
5	TSC-113	>50	>50	>50	>50
6	TSC-116	$34.88 \pm 0.96$	>50	>50	>50
7	TSC-140	>50	>50	>50	>50
8	TSC-142	>50	>50	>50	>50
9	TSC-145	>50	>50	>50	>50

Table 1. Cont.

No.	TSC	IC <sub>50</sub> [μM]			
		HCT116	MCF-7	Hs683	NHDF
10	TSC-146	>50	>50	>50	>50
11	TSC-147	>50	>50	>50	>50
12	TSC-197	>50	>50	>50	>50
13	Cp94	>50	>50	>50	>50

### 2.3. An Accumulation of PPIX

To select promising TSC derivatives for improving ALA-PDT efficiency, we examined the fluorescence intensity of PPIX. The results clearly show that only some derivatives significantly increase the fluorescence intensity of PPIX after 5-ALA treatment in combination with TSC. In the HCT116 and MCF-7 cell lines, significantly elevated PPIX levels were observed after treatment with several derivatives (Figure 3A,B). All the data presented in Figure 3 represent statistically significant fold-changes relative to 5-ALA. For the HCT116 line, 4.14, 2.47, 3.0, and 2.26-fold changes were observed with the combination of 5-ALA and TSC-34, TSC-109, TSC-113, and TSC-116, respectively, compared to 5-ALA treatment alone. In the MCF-7 line, the fold increases were lower: 1.66, 1.64, and 1.9-fold increases for TSC-34, TSC-109, TSC-116, and TSC-113, respectively, in combination with 5-ALA. No significant changes were observed after treatment with Cp94 and 5-ALA in both cell lines. For the Hs638 line, a significant increase in PPIX fluorescence intensity was observed only with the combination of TSC-34 and 5-ALA. Similar to the other cell lines, no increase in PPIX intensity was observed for cells treated with Cp94 and 5-ALA (Figure 3C). The use of chelators to increase PPIX accumulation is not a new concept. Early chelators included compounds such as EDTA and DFO, which significantly raised PPIX levels in various cells. However, EDTA binds a variety of biologically important ions and can also raise PPIX levels in healthy tissues. On the other hand, DFO is an iron-selective chelator, but its large, lipophilic structure hinders cellular uptake [4]. Cp94, which lacks these drawbacks, has been shown to significantly raise PPIX levels in various cell lines. However, in our experiments, increased PPIX levels were not observed in any cell line treated with Cp94. This discrepancy can be explained by the concentration of Cp94 used, which was 25 μM. Many studies that reported significant PPIX increases used concentrations above 100 μM [8,31]. Considering this, the use of TSC derivatives is much more effective than Cp94.

### 2.4. An Ability to Chelate Iron Ions

Although TSCs are known for their ability to chelate iron ions, our compounds are novel. Therefore, to test their iron-chelating capabilities, we examined all compounds that caused an increase in PPIX fluorescence intensity. Spectroscopic measurements were conducted in an aqueous environment to closely mimic cellular conditions. The recorded absorption spectra, shown in Figure 4, illustrate the interaction with iron (III) ions, maintaining a constant compound concentration while varying the ion concentration. An isosbestic point was observed for all studied compounds, indicating the existence of at least two forms: free and bound with metal ions. The spectra revealed a decrease in the characteristic absorption band of each compound as the concentration of iron ions increased. Additionally, a new band emerged upon the addition of iron ions, with its absorbance increasing proportionally to the metal ion concentration. This new band likely corresponds to the formation of a complex between the tested compound and the metal ions. The specific positions of absorption maxima for each band and the isosbestic point are detailed in Table 2.

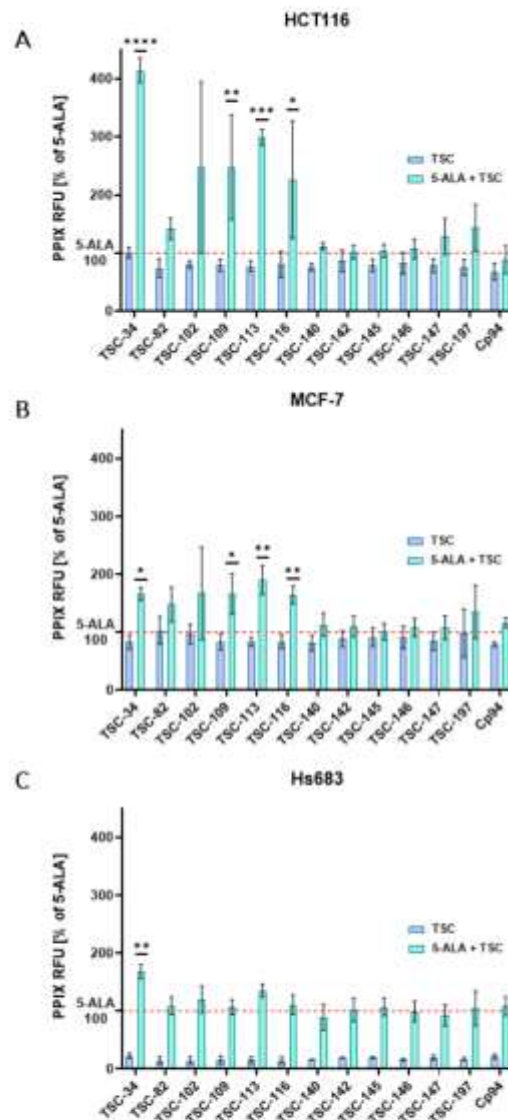


**Figure 3.** Accumulation of PPIX after treatment with 5-ALA, TSCs, Cp94, and their combinations on (A): HCT116, (B): MCF-7, and (C): Hs683 cell lines. The red dotted line on the graph depicts the fluorescence intensity of PPIX following treatment with 5-ALA alone. The data are presented as the means  $\pm$  standard deviation from three independent experiments and analyzed using one-way ANOVA with Tukey's post hoc test, indicating significance levels as follows: \*  $p < 0.05$ , \*\*  $p < 0.01$ , \*\*\*  $p < 0.001$ , \*\*\*\*  $p < 0.0001$ .



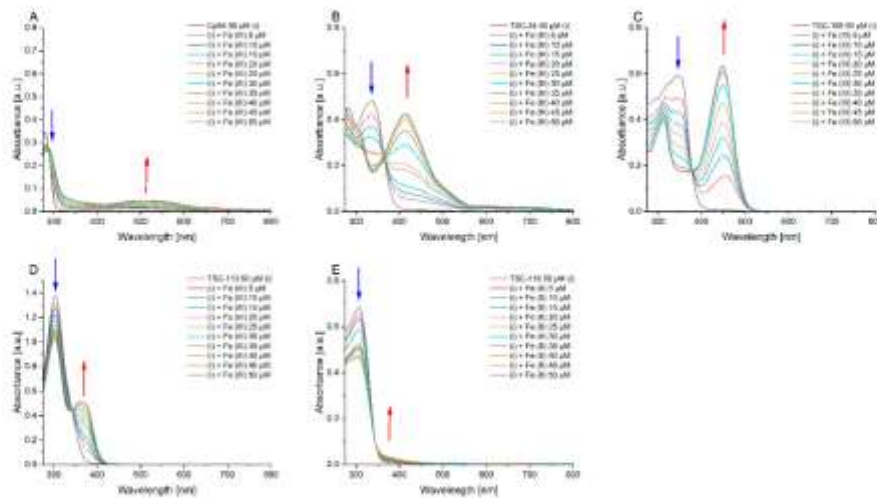


**Figure 4.** Absorption titration spectra of selected compounds (50  $\mu\text{M}$ ) with iron (III) ions in water: (A)—Cp-94; (B)—TSC-34; (C)—TSC-109; (D)—TSC-113; (E)—TSC-116. Blue arrows indicate a decrease in band intensity for the test compound, while red arrows highlight an increase in band intensity for the complex. Measurements were performed at room temperature 4 h after the samples had been prepared.

**Table 2.** Spectroscopic data for tested compounds dissolved in water with iron (III) ions ( $\text{Fe}^{3+}$ ).

Sample	Compound	Isosbestic Point [nm]	Complex with $\text{Fe}^{3+}$
	$\lambda_{\text{max}}$ [nm]		$\lambda_{\text{max}}$ [nm]
Cp-94	280	290	510
TSC-34	337	366	415
TSC-109	340	378	449
TSC-113	305	342	362
TSC-116	308	345	385

Compounds in the TSC group are widely studied, particularly for their anticancer activity. One of the most well-researched compounds is Dp44mT due to its ability to chelate iron ions. This compound has been examined in various environments. In our study, we observe the appearance of an isosbestic point, the emergence of a new band from the complex of the compound with iron, and the disappearance of a band associated with the free compound. These observations confirm that the TSCs studied also chelate iron ions in aqueous environments [32–34].

### 2.5. The Phototoxic Effect

After the accumulation experiments and confirming the selected compounds' chelating ability, the tested compounds' phototoxic effect in combination with 5-ALA was assessed. No significant decrease in cell viability was observed for any compound in any cell line without light (dark toxicity). However, after cell irradiation with red light, significant decreases in cell viability were observed for TSC-34 in combination with 5-ALA on the HCT116 and MCF-7 cell lines, with surviving fractions of 36.6% and 45.6%, respectively. Treatment with TSC-113 also significantly decreased the cell viability of the HCT116 and MCF-7 cell lines, with surviving fractions of 40.8% and 31.5%, respectively. In contrast, for

the Hs683 cell line, a decrease in viability was observed only after treatment with TSC-34 in combination with 5-ALA, resulting in a surviving fraction of 39.5% (Figure 5C). No decrease in cell viability was observed in any cell line tested after treatment with Cp94 in combination with 5-ALA.

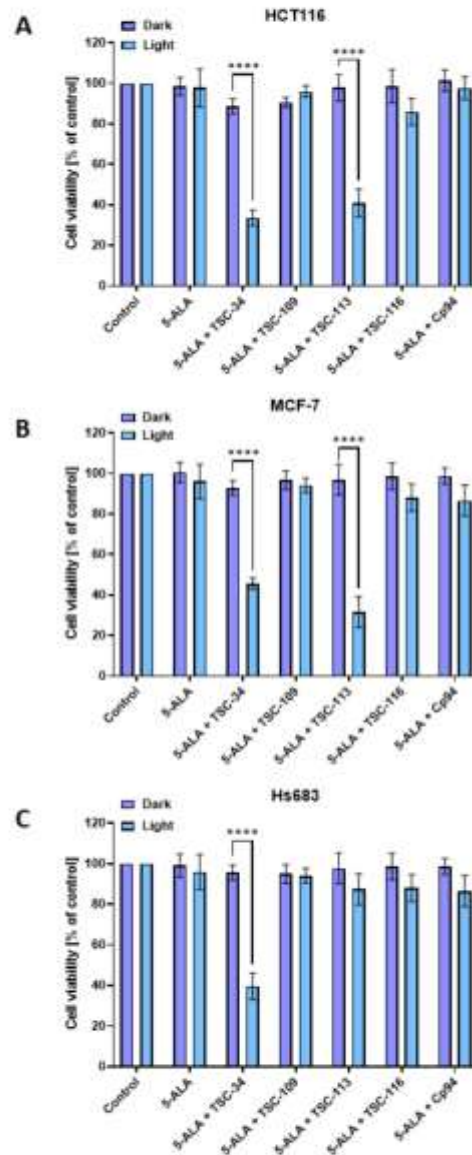


**Figure 5.** Phototoxic effect after treatment with 5-ALA, TSCs, Cp94, and their combinations on (A): HCT116, (B): MCF-7, and (C): Hs683 cell lines. The data are presented as means  $\pm$  standard deviation from three independent experiments and analyzed using one-way ANOVA with Tukey's post hoc test, indicating significance levels as follows: \*\*\*\*  $p < 0.0001$ .

These results demonstrate the efficacy of our compounds against cancer cells in ALA-PDT therapy. Despite using a relatively low concentration of TSCs (25  $\mu$ M), a therapeutic effect was still achieved. The tested TSCs effectively inhibited the growth of irradiated cells, in contrast to the Cp94 reference.

## 2.6. Iron Metabolism

An experiment in which FECH expression was measured demonstrated that for the HCT116 and MCF-7 cell lines, a decrease in FECH expression was observed after treatment with TSC-34 and TSC-113 (Figure 6A,B). This aligns with literature reports and may explain the significant photocytotoxic effect on these cell lines. In contrast, for the Hs683 cell line, we observed an increase in FECH expression after treatment with TSC-34 and TSC-113 (Figure 6C). Despite the expected absence of a phototoxic effect on this cell line, a strong cytotoxic effect was observed after treatment with TSC-34. Additionally, in the HCT116 and MCF-7 cell lines treated with Cp94, a decrease in FECH expression was also observed, yet no phototoxic effect was noted. As demonstrated, elevated expression of FECH correlates with reduced PPIX accumulation. Conversely, diminished FECH expression leads to increased PPIX accumulation induced by 5-ALA treatment in various cancer cell lines [10]. In another study where FECH expression was repressed, untreated cells exhibited heightened PPIX levels, while no significant changes in PPIX accumulation were observed after 5-ALA treatment [35]. This observation suggests that FECH expression is not the sole factor in effective ALA-PDT, indicating that other factors must influence ALA-PDT efficacy.

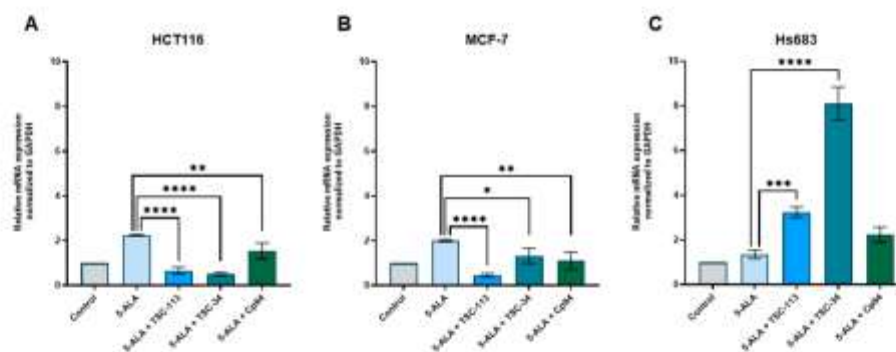


**Figure 6.** Expression of FECH in the (A): HCT116, (B): MCF-7, and (C): Hs683 cell lines. The data are presented as means  $\pm$  standard deviation from three independent experiments and analyzed using one-way ANOVA with Tukey's post hoc test, indicating significance levels as follows: \*  $p < 0.05$ , \*\*  $p < 0.01$ , \*\*\*  $p < 0.001$ , \*\*\*\*  $p < 0.0001$ .

The MCF-7 cell line exhibited a decrease in HO-1 expression after treatment with all TSC derivatives, as well as Cp94 (Figure 7B). For the HCT116 cell line, we observed a decrease in HO-1 expression only with TSC-34 treatment (Figure 7A). In the case of the Hs683 cell line (Figure 7C), our observations contrasted with literature findings. Increased levels of HO-1 are typically associated with low ALA-PDT efficiency [12], which may explain the lack of a phototoxic effect after TSC-113 treatment. However, this does not account for the strong phototoxic effect observed with TSC-34 treatment in this cell line. Combining the results obtained for FECH and HO-1, we can conclude that the reduced expression of FECH, leading to increased PPIX accumulation along with decreased protection against ROS due to reduced HO-1 expression, explains the strong phototoxic effects observed after TSC-34 treatment in the HCT116 and MCF-7 cell lines. However, the opposite results for the Hs683 line do not explain the effective response to TSC-34 treatment, although they may account for the lack of response after TSC-113 treatment.

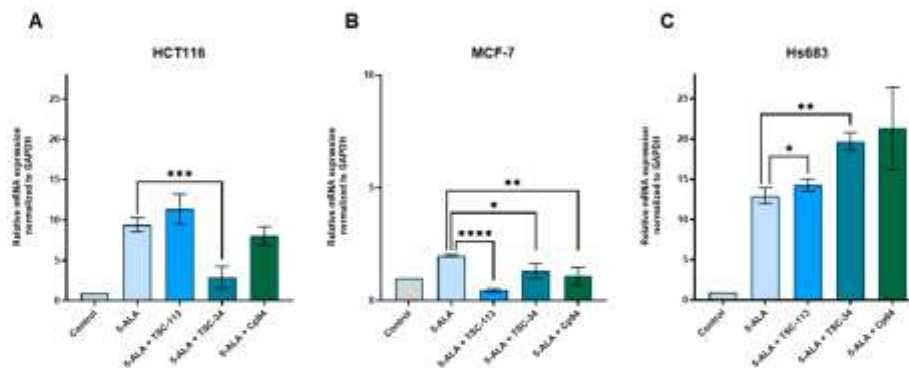


**Figure 7.** Expression of HO-1 in the (A): HCT116, (B): MCF-7, and (C): Hs683 cell lines. The data are presented as means  $\pm$  standard deviation from three independent experiments and analyzed using one-way ANOVA with Tukey's post hoc test, indicating significance levels as follows: \*  $p < 0.05$ , \*\*  $p < 0.01$ , \*\*\*  $p < 0.001$ , \*\*\*\*  $p < 0.0001$ .

A significant upregulation of FTMT expression in cells treated with the combination of TSC-34 and 5-ALA across all cell lines was observed (Figure 8). Notably, for the HCT116 cell line, increased expression of FTMT was also noted after treatment with Cp94 and 5-ALA. As demonstrated, disruption of iron availability using deferiprone causes an increase in FTMT expression [36]. Elevated levels of this protein induce mitochondrial damage and depolarization of the mitochondrial membrane, consequently triggering mitophagy. Additionally, knockdown of FTMT, as well as deferiprone treatment, reduces ROS levels. In our study, after treatment with TSC-34, we observed a significant increase in FTMT expression, which can lead to changes in mitochondrial membrane polarity, resulting in mitochondrial damage and increased ROS production. These changes can disrupt mitochondrial morphology [37]. One of the main factors maintaining mitochondrial architecture is the mitochondrial contact site and cristae organizing system (MICOS) complex, which physically interacts with FECH. Disruption of MICOS function leads to PPIX accumulation and reduced FECH activity [38]. The interplay between FTMT and FECH may explain the effectiveness of ALA-PDT after TSC-34 treatment in the HCT116 and MCF-7 cell lines. In the case of Hs683 cells, despite the increase in FTMT expression, we did not observe a decrease in FECH expression. However, the described mechanism may influence the strong phototoxic effect observed in this cell line.

Our findings indicate a notable reduction in FXN expression (Figure 9A,B) when HCT116 and MCF-7 cell lines are treated with a combination of TSC-113 and Cp94 alongside 5-ALA. However, TSC-34 treatment did not result in significant changes. In contrast, no statistically significant alterations in gene expression were observed in the Hs683 cell line (Figure 9C). While FXN does not directly impact the heme biosynthetic pathway, studies conducted on human embryonic kidney cells indicate that diminished FXN expression leads to a gradual reduction in FECH levels over an extended period [39]. Primary symptoms associated with reduced FXN expression, such as decreased iron-sulfur cluster concentrations and indications of oxidative stress, manifest at an early stage. It has been proposed that the inhibition of FECH activity in these cells is attributed to a decline in the concentration of [2Fe-2S] clusters, crucial for the proper functioning of FECH [40]. Explaining the impact of alterations in FXN expression on ALA-PDT efficiency proves challenging due to the incomplete understanding of FXN's role in cellular iron metabolism. Nonetheless, the reduced expression observed after treatment with TSC-113 in combination with 5-ALA in the HCT116 and MCF-7 cell lines suggests a potential connection between ALA-PDT efficiency and decreased FXN expression, possibly through an indirect modulation of FECH activity. Conversely, in cells treated with Cp94 in combination with 5-ALA,



despite a decrease in FXN expression, this effect is not evident. Meanwhile, the absence of significant changes in the Hs683 cell line and the pronounced phototoxic effect following treatment with TSC-113 and TSC-34 indicate the involvement of other mechanisms independent of FXN in influencing the efficacy of treatment with these chelators. Interestingly, studies have demonstrated that in conditions of iron deficiency, FECH can dissociate an iron ion from heme, resulting in the formation of PPIX [41,42].

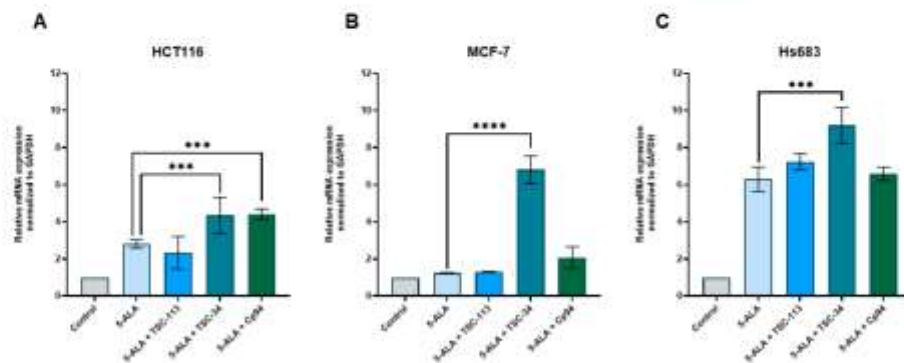


**Figure 8.** Expression of FTMT in the (A): HCT116, (B): MCF-7, and (C): Hs683 cell lines. The data are presented as means  $\pm$  standard deviation from three independent experiments and analyzed using one-way ANOVA with Tukey's post hoc test, indicating significance levels as follows: \*\*\*  $p < 0.001$ , \*\*\*\*  $p < 0.0001$ .

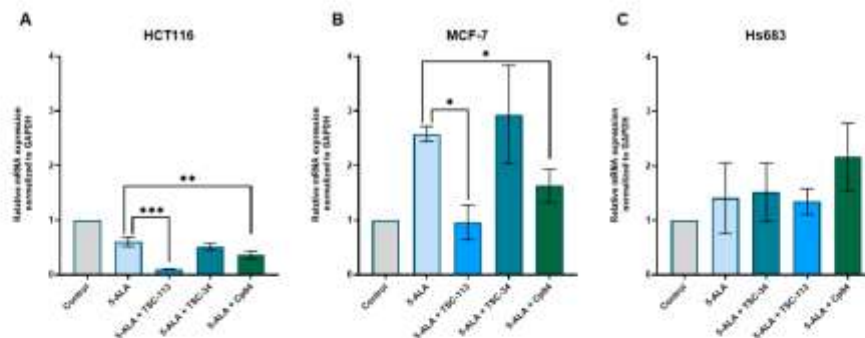


**Figure 9.** Expression of FXN in the (A): HCT116, (B): MCF-7, and (C): Hs683 cell lines. The data are presented as means  $\pm$  standard deviation from three independent experiments and analyzed using one-way ANOVA with Tukey's post hoc test, indicating significance levels as follows: \*  $p < 0.05$ , \*\*  $p < 0.01$ , \*\*\*  $p < 0.001$ .

The conducted research indicates that treatment with TSC-113 and 5-ALA results in a decrease in the expression of both forms of MFRNs on the HCT116 cell line (Figure 10A,D) and the MCF-7 cell line for MFRN2 (Figure 10E), while no significant changes in MRFN1 expression were observed. Treating the HCT116 cell line with the combination of TSC-34 and 5-ALA led to a slight increase in MFRN2 expression (Figure 10D). However, a notable increase in MFRN1 expression was observed after Cp94 treatment on the HCT116 and MCF7 cell lines (Figure 10A,B), while no changes were detected in MFRN2 expression (Figure 10D,E). In the Hs683 cell line, only TSC-34 treatment increased the expression of both MFRN1 and 2 (Figure 10C,F); in other cases, no significant changes were observed.

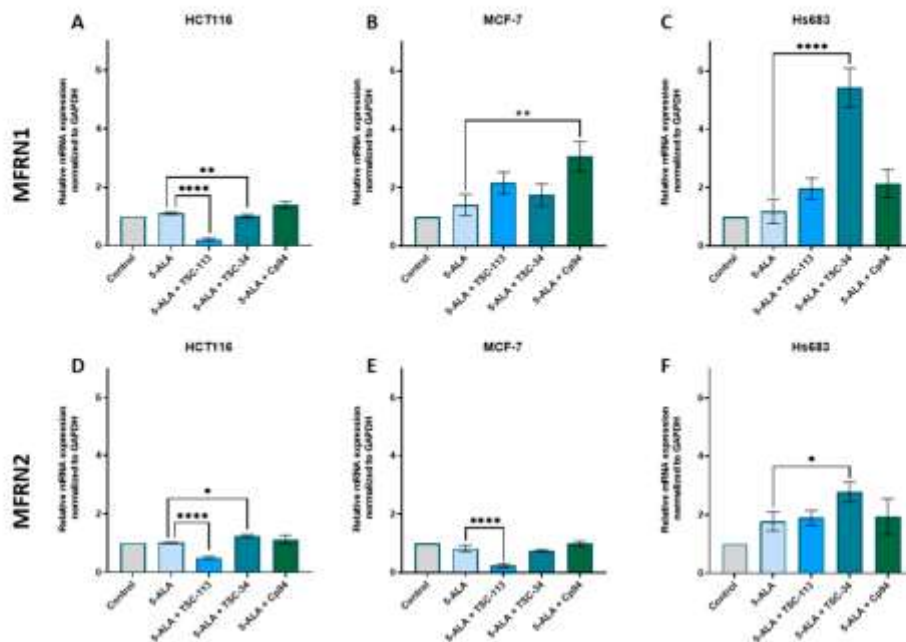


**Figure 10.** Expression of MFRN 1 and 2 genes on the (A,D): HCT116, (B,E): MCF-7 and (C,F): Hs683 cell lines. The data are presented as means  $\pm$  standard deviation from three independent experiments and analyzed using one-way ANOVA with Tukey's post hoc test, indicating significance levels as follows: \*  $p < 0.05$ , \*\*  $p < 0.01$ , \*\*\*\*  $p < 0.0001$ .

As mentioned above, MFRN is thought to form a complex with FECH and likely transfers an iron ion directly to the active center of FECH. Our observed decrease in the expression of both forms after treatment with TSC-113 in the HCT116 cell line and isoform 2 in the MCF-7 cell line may explain the efficacy of this derivative in ALA-PDT. The reduction in MFRN expression leads to a lack of iron transport necessary for heme biosynthesis, resulting in increased PPIX accumulation. This is consistent with the observation that the MCF-7 cell line, which has reduced MFRN1/2 expression, shows increased PPIX accumulation and a stronger phototoxic effect compared to healthy cells with higher MFRN1/2 expression [43]. Additionally, they showed that treating these cells with iron does not diminish the accumulation of PPIX, which proves that the expression of enzymes involved in heme biosynthesis is crucial. Another study demonstrated that cells overexpressing MFRN1 also exhibited increased glutathione levels, which promotes cell survival [44]. In our study, we observed an increased expression of MFRN1/2 in the Hs683 cell line following TSC-34 treatment, which should result in a weakened photodynamic effect. However, we did not observe this effect in our study. Nonetheless, it is important to note that this increase in MFRN1/2 expression could potentially be a response to the demand for iron ions and may not directly impact the efficacy of ALA-PDT.

Our findings revealed a significant increase in DMT1 expression following 5-ALA-only treatment across all tested cell lines compared to control groups (Figure 11). The observed increase in DMT1 expression after treatment with 5-ALA alone indicates an enhanced demand for iron ions. In our previous studies, we showed that cell lines treated with 5-ALA alone exhibited increased levels of free heme compared to control groups. This observation was considered a potential explanation for the absence of phototoxic effects in cells treated with 5-ALA alone [23] and is seemingly supported by DMT1 expression.



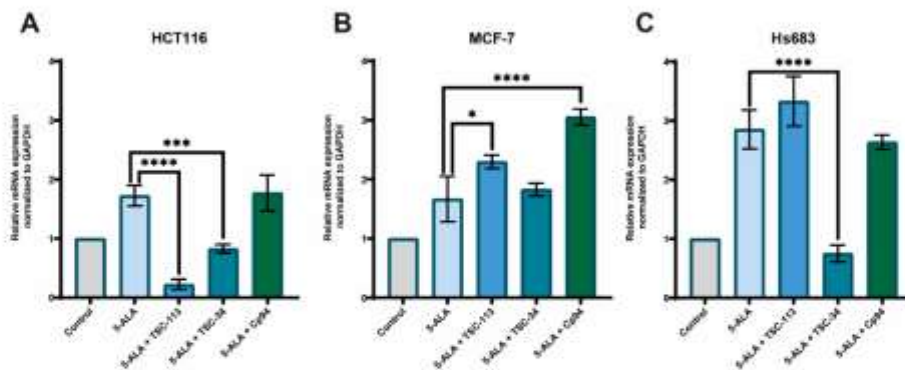


**Figure 11.** Expression of DMT1 in the (A): HCT116, (B): MCF-7, and (C): Hs683 cell lines. The data are presented as means  $\pm$  standard deviation from three independent experiments and analyzed using one-way ANOVA with Tukey's post hoc test, indicating significance levels as follows: \*  $p < 0.05$ , \*\*\*  $p < 0.001$ , \*\*\*\*  $p < 0.0001$ .

When chelators are combined with 5-ALA, a distinct pattern of DMT1 expression emerges. Specifically, in the HCT116 cell line, there is a significant decrease in DMT1 expression following treatment with TSC-34 and TSC-113 (Figure 11A). Conversely, treatment with Cp94 maintains DMT1 expression at a level comparable to that observed in cells treated with only 5-ALA. In the MCF-7 cell line, a significant increase in DMT1 expression is noted when treated with a combination of TSC-113 and Cp94 alongside 5-ALA (Figure 11B). Interestingly, no significant changes are observed for cells treated with TSC-34, although its expression remains comparable to that induced by 5-ALA alone. On the other hand, the Hs683 cell line exhibits a significant decrease in DMT1 expression when treated with TSC-34, while its expression level is otherwise similar to that of cells treated only with 5-ALA (Figure 11C). While the findings presented above may initially seem contradictory, existing literature highlights that different chelators can elicit distinct effects on DMT1 expression. For instance, studies demonstrate that treating rat lung cancer cells with quercetin leads to a decrease in DMT1 expression [18], whereas breast cancer cells subjected to DFO treatment exhibit the opposite effect, resulting in an increase in DMT1 expression [45]. Additionally, there is limited information on the regulation of DMT1 expression, particularly during disruptions of the iron availability in the cells, posing a challenge in correlating the obtained results with the efficiency of ALA-PDT. Nevertheless, a diminished expression of DMT1 may potentially enhance its efficiency by reducing iron uptake.

The results suggest that treatment with 5-ALA or the combination of TSC-113 and TSC-34 with 5-ALA does not significantly alter ABCB8 transcript levels in HCT116 and MCF-7 cell lines (Figure 12A,B). Notably, only the co-administration of Cp94 with 5-ALA induces a substantial increase in ABCB8 expression across all tested cell lines. However, in the Hs683 cell line, a significant increase in ABCB8 expression is observed not only following Cp94 and 5-ALA treatment but also with TSC-34 (Figure 12C). The impact of ABCB8 expression on the efficacy of ALA-PDT remains unexplored in existing literature, to the best of our knowledge. However, previous studies indicate that downregulation of the ABCB8 gene in renal cell carcinoma lines results in diminished cell survival, as evidenced by mitochondrial damage and heightened accumulation of ROS within mitochondria [21]. A comparable scenario was observed in mouse cardiomyocytes with reduced ABCB8 expression, leading to cardiomyopathy and mitochondrial iron accumulation [46]. This would elucidate the absence of a phototoxic effect following treatment with the combination of Cp94 and 5-ALA, positing that heightened expression of this transporter is linked to increased cell survival. However, in the case of TSC-34, despite an increase in ABCB8 expression, we still observed a phototoxic effect. This is consistent with our previous results for another transporter

responsible for iron ejection from the cell, ABCG2. These results demonstrate the high efficacy and versatility of our compounds, particularly TSC-34, in enhancing the efficacy of ALA-PDT.

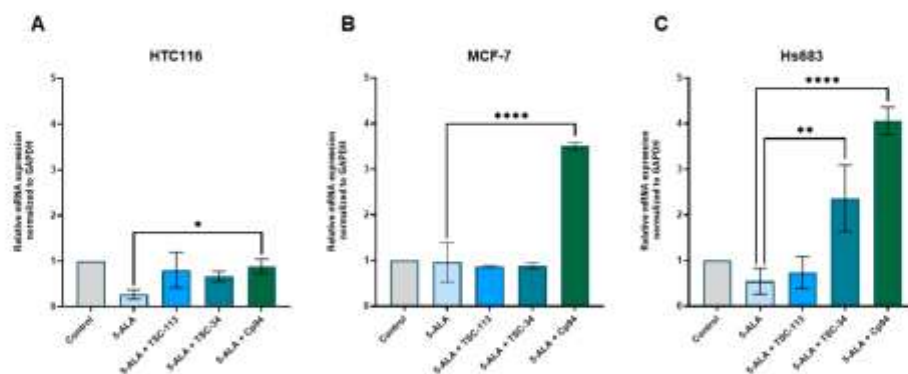


**Figure 12.** Expression of ABCB8 in the (A): HCT116, (B): MCF-7, and (C): Hs683 cell lines. The data are presented as means  $\pm$  standard deviation from three independent experiments and analyzed using one-way ANOVA with Tukey's post hoc test, indicating significance levels as follows: \*  $p < 0.05$ , \*\*  $p < 0.01$ , \*\*\*\*  $p < 0.0001$ .

### 3. Materials and Methods

#### 3.1. Synthesis—Reagents and Equipment

The chemical reagents employed in this study were acquired from Sigma-Aldrich (Burlington, MA, USA) and ACROS Organics (Thermo Fisher Scientific, Waltham, MA, USA). Thin layer chromatography (TLC) was conducted on alumina-coated silica gel 40 F254 plates (Merck, Darmstadt, Germany). Visualization of the chromatographic plates was achieved using ultraviolet light (254 nm) and subsequent exposure to iodine vapor for detection. Melting points were ascertained using an Optimelt MPA100 (Stanford Research Systems, Sunnyvale, CA, USA). Nuclear magnetic resonance (NMR) spectroscopy was used for the characterization of all synthesized compounds and was performed on a Bruker AM-400 spectrometer (399.95 MHz for  $^1\text{H}$ ; 99.99 MHz for  $^{13}\text{C}$ ; BrukerBioSpin Corp., Coventry, UK). Chemical shifts are delineated in parts per million (ppm), referenced to the internal standard tetramethylsilane- $\text{Si}(\text{CH}_3)_4$ . Signals susceptible to rapid exchange were excluded when broad or indistinct. The syntheses of the studied compounds were performed on a CEM-DISCOVERY microwave reactor (CEM Corporation, Matthews, NC, USA) with temperature and pressure control. The mass spectrometry characterizations of synthesized TSCs were collected using an electrospray single-quad Agilent Infinity Lab LC/MSDXT mass spectrometer, equipped with an Agilent HPLC 1260 Infinity II system (Agilent Technologies, Santa Clara, CA, USA) and SB C18 column (1.8  $\mu\text{m}$ , 2.1  $\times$  50 mm). Logarithmic partition coefficients (cLogP) were computationally determined by employing ChemDraw version 21 (Perkin-Elmer, Waltham, MA, USA).

#### 3.2. General Synthetic Protocol for the Creation of Aromatic TSCs

In brief, in a 25 mL sealed tube equipped with a magnetic stirrer, equimolar amounts of (1,1'-thiocarbonyl)bis-1*H*-imidazole (1 eq) and an appropriate *N*-alkyl or *N*-aryl derivatives of piperazine or thiomorpholine (1 eq) were added, followed by the addition of 12 mL of methylene chloride. The system was then tightly sealed with a septum cap and stirred at room temperature for 24 h. The resulting intermediate was extracted three times with distilled water. The organic phase obtained was dried over anhydrous calcium chloride and then evaporated under reduced pressure using a rotary evaporator. To the resulting imidazolylthio ketone derivative (1 eq), an equimolar amount of hydrazine hydrate and

25 mL of ethanol were added. The reaction mixture was heated for 2 h under reflux. Then, the reaction mixture was stored in a laboratory refrigerator at  $-20\text{ }^{\circ}\text{C}$ , resulting in the formation of a crystalline solid, which was subsequently crystallized from anhydrous methanol to form the desired TSC (Figure S1 in Supporting Information).

In a 10 mL glass vessel equipped with a magnetic stirrer, equimolar amounts of TSC and the corresponding aldehyde were added. Subsequently, 5 mL of dry ethanol and three drops of ice-cold acetic acid were added. The vessel was hermetically sealed with a cap and positioned within a CEM microwave reactor at  $83\text{ }^{\circ}\text{C}$  for 20 min (the power of the reactor did not exceed 100 W). The resultant product was crystallized using methanol. The spectral characterization of all synthesized aromatic TSCs is presented in the Supporting Information.

### 3.3. Cell Lines and Cell Culture

The HCT116 (colorectal cancer) and MCF-7 (breast cancer) cell lines were procured from the American Type Culture Collection (ATCC; Manassas, VA, USA), while the Hs683 cell line was generously provided by Prof. Gabriela Kramer-Marek from the Institute of Cancer Research (London, UK). These cell lines were cultured in Dulbecco's Modified Eagle's Medium (DMEM; Sigma-Aldrich; St. Louis, MO, USA) supplemented with 10% fetal bovine serum (FBS; Sigma-Aldrich; St. Louis, MO, USA) and 1% antibiotic mixture (penicillin and streptomycin; Gibco; Grand Island, NY, USA). Culturing was conducted in 75 cm<sup>2</sup> flasks (Nunc, Sigma-Aldrich; St. Louis, MO, USA) at  $37\text{ }^{\circ}\text{C}$  in a humidified atmosphere containing 5% CO<sub>2</sub>. Before experimentation, all cell lines underwent mycoplasma contamination via PCR.

### 3.4. Cytotoxicity Studies

Cells were seeded at a density of 5000 cells per well in a 96-well plate and incubated for 24 h under standard conditions. Subsequently, the tested compounds were added at a concentration of 50  $\mu\text{M}$  and incubated for 72 h. Following this incubation period, the medium containing the test compounds was aspirated, and phenol red-free medium supplemented with CellTiter 96<sup>®</sup> Aqueous One Solution (MTS, Promega, Madison, WI, USA) was added. After approximately 1 h, the absorbance at a wavelength of 490 nm was measured using a multi-well plate reader (Synergy 4, BioTek, Winooski, VT, USA). The obtained absorbance values were utilized to calculate the antiproliferative activity of the tested compounds.

### 3.5. Chelating Abilities

The compounds, along with iron (III) ions, were initially dissolved in dimethylsulfoxide (DMSO) to yield a stock solution of 8.358 mM. Subsequently, all samples were diluted with ultrapure water to obtain a concentration of 100  $\mu\text{M}$ . Solutions containing the tested compounds and iron ions were then prepared by transferring appropriate volumes into a 96-well black plate with a transparent bottom (Nunc, Sigma-Aldrich; St. Louis, MO, USA). Each well was loaded with 200  $\mu\text{L}$  of solution, comprising the tested compound at a concentration of 50  $\mu\text{M}$  and increasing concentrations of iron ions from 0 to 50  $\mu\text{M}$ . Absorption spectra were recorded following a 4 h incubation at room temperature using a Varioskan LUX (Thermo Fisher Scientific, Waltham, MA, USA) multi-well plate reader in the 275–800 nm range with a 5 nm step.

### 3.6. Accumulation of PPIX

Cells were seeded into a 96-well black plate with a transparent bottom (Nunc, Sigma-Aldrich; St. Louis, MO, USA) at a density of  $1.1 \times 10^4$  cells per well and cultured under standard conditions for 24 h. After incubation, the cells were treated with TSC and Cp94 at a concentration of 25  $\mu\text{M}$ , 1 mM of freshly prepared 5-ALA, and their combination in a phenol red-free medium. After 24 h of incubation with the compounds, PPIX fluorescence was measured using a multi-well plate reader (Synergy 4, BioTek, VT, USA) at an



excitation wavelength of 407 nm and an emission wavelength of 638 nm. The obtained fluorescence values were then used to calculate the relative fluorescence intensity of PPIX as a percentage of 5-ALA. All experiments were conducted under reduced illumination to prevent photobleaching of PPIX and were repeated four times.

### 3.7. Phototoxic Effect

Cells were seeded and treated following the same procedure as described for measuring PPIX accumulation. Following a 24 h incubation with the compounds, the cells underwent three washes with phenol red-free medium and were then exposed to red light (634 nm  $\pm$  5 nm) at a dose of 12 J/cm<sup>2</sup>. Following irradiation, fresh medium was replenished, and the cells were further incubated under standard conditions for an additional 24 h. Simultaneously, a control experiment was conducted without irradiation. Cell viability was assessed using the MTS assay, following the same protocol as for cytotoxicity evaluation. All experiments were carried out in the absence of light. The results are presented as the mean  $\pm$  standard deviation of three independent experiments, and cell viability was calculated using GraphPad Prism 8 software (GraphPad Software Inc.; San Diego, CA, USA).

### 3.8. Genes Expression

Cells were seeded at a density of  $4 \times 10^5$  cells per dish (3 cm plastic Petri dishes; Nunc, Sigma-Aldrich; St. Louis, MO, USA) and incubated for 24 h at 37 °C. Subsequently, the old medium was aspirated, and solutions of 5-ALA (1 mM), TSC, and Cp94 (25  $\mu$ M) were added. After an additional 24 h of incubation, total RNA was extracted from the cells using TRIzol reagent (Invitrogen; Carlsbad, CA, USA) following the manufacturer's protocol.

For reverse transcription, 2  $\mu$ g of total RNA was utilized with the GoScript™ Reverse Transcriptase kit (Promega; Madison, WI, USA) and Oligo(dT)23 Primers (Sigma-Aldrich; St. Louis, MO, USA). Quantitative RT-PCR was performed using a CFX96 Touch™ Real-Time PCR Detection System (Biorad; Hercules, CA, USA), SYBR® Green Master Mix (Biorad; Hercules, CA, USA), the appropriate primer pairs, and cDNA template. Primer sequences were designed using Primer3 online software, <https://www.ncbi.nlm.nih.gov/tools/primer-blast/> accessed on 20 March 2023 (Table 3) and synthesized and provided by Sigma-Aldrich (Sigma-Aldrich; St. Louis, MO, USA). Data analysis involved comparing the expression of the target gene to a reference gene, GAPDH, using the 2<sup>- $\Delta\Delta$ CT</sup> method (Livak and Schmittgen method). The experiments were conducted with a minimum of three repetitions in triplicate.

**Table 3.** Primers designed and used in this study.

Gene Name	Sequence 5'→3' (F—Forward, R—Reverse)	
DMT1	F	GGTCACGCTTGCCCGA
	R	CAATCCGCCAGCCTAGTCC
MFRN1	F	ACTCGGTGAAGACACGAATGC
	R	CAGCTATCCCGTTGGCTAGG
MFRN2	F	CACTGCGTGATGTACCCAT
	R	CAACACATTGCGATAGCGGG
ABC8	F	TATTCGGGTCGGGATTCGG
	R	TCCAGTTTCCCATIACGCCA
FNX	F	TGGACCTAAGCGTTATGACTGG
	R	TCTTCCCGTGTGAGTTGCTT
FTMT	F	CCATCAACCGCCAGATCAAC
	R	GTGCAATCCAGCAACGACT

Table 3. Cont.

Gene Name	Sequence 5'→3' (F—Forward, R—Reverse)	
	FECH	F
R		GCTTCCGTCCCACTTGATTA
HO-1	F	CATCCCCTACACACCAGCCA
	R	ATGTTGGGGAAGGTGAAGAAGG

### 3.9. Statistical Analysis

All experiments were repeated at least three times independently, with the results presented as the mean  $\pm$  standard deviation. Data analysis was performed using GraphPad Prism 8 software (GraphPad Software Inc., San Diego, CA, USA). Statistical significance between groups was assessed using one-way or two-way ANOVA followed by Tukey's post hoc test. A two-tailed  $p$ -value of 0.05 or less was considered statistically significant, with significance levels indicated as follows: \*  $p < 0.05$ , \*\*  $p < 0.01$ , \*\*\*  $p < 0.001$ , \*\*\*\*  $p < 0.0001$ .

### 4. Conclusions

This paper presents an analysis of the effects of selected derivatives from the TSC group on iron metabolism in ALA-PDT. The compounds were selected based on our previous studies, taking into account their ability to increase PPIX levels after incubation with 5-ALA while maintaining the absence of dark toxicity. The effectiveness of our novel TSC derivatives in increasing PPIX concentrations is greater than commonly used iron chelators. The main mechanism of the observed effect is related to the formation of iron complexes. Therefore, this ability was confirmed by the spectroscopic studies in which isosbestic points indicative of the generation of complexes with iron were measured.

It is also worth mentioning that our compounds inhibit the proliferation of cancer cells under red light irradiation. This shows that the concentration used has a therapeutic effect, which is extremely important from a practical application point of view. Low doses are desirable to minimize side effects. In contrast to our TSC derivatives, the Cp94 reference used was not effective at the concentration tested.

An expression analysis of genes involved in iron metabolism included both common targets and those for which there is little information. The standard gene studied in the context of PPIX accumulation is FECH. Our study confirmed the widely held opinion that a reduction in FECH expression has a positive effect on PPIX accumulation for the HCT116 and MCF-7 cell lines. However, our study of the Hs683 line, which exhibits non-standard behavior, once again overturned the widely held trend. Namely, for the TSC-34 derivative, despite an increase in FECH, we registered both an increase in PPIX and a marked decrease in cell viability after irradiation. We observed a similar trend for HO-1, which was consistent with the literature for the HCT116 and MCF-7 cell lines and a break from this trend for Hs683 cells. The increase in HO-1 expression is a non-standard phenomenon in the context of increased PPIX accumulation and phototoxic effects after incubation with TSC-34. In the case of FTMT, the expression of which was increased in the majority of cases, we observed an interesting correlation with FECH. Namely, we hypothesize that an increase in FTMT expression results in the destruction of MICOS through the production of ROS, which has a positive effect on increasing the concentration of PPIX and the effect of PDT. We also recorded interaction with FECH for downregulated FXN but in a less direct way; in this case, it is related to the decrease in iron-sulfur cluster concentrations affecting the concentration of FECH. MFRN, as the main supplier of iron ions to FECH, also showed a correlation; namely, its decrease was the explanation for the induced photocytotoxic effect for TSC-113. An explanation for this effect could also be the downregulation of the iron ion transporter, DMT1, and expression for the HCT116 and Hs683 cell lines. The last gene analyzed was ABCG8, which is responsible for iron efflux from the cell. Therefore, in our study, we traced the fate of iron from entry to exit of the cell.

The results indicate that, despite overexpression of this gene occurring in the Hs683 cell line, TSC-34 increased the concentration of PPIX to the extent that it was able to induce an effect after irradiation. These results demonstrate the great potential of our compounds, in particular the TSC-34 derivative, in increasing the efficacy of ALA-PDT.

**Supplementary Materials:** The following supporting information can be downloaded at: <https://www.mdpi.com/article/10.3390/ijms251910468/s1>.

**Author Contributions:** R.G. created the research hypothesis, planned the experiments, performed the biological assays, analyzed the data, and wrote the manuscript; P.R. and R.G. performed and analyzed the chelation studies; M.R. performed the synthesis; M.S. described the synthetic part and analyzed the structural data; and A.M.-W. supervised R.G., analyzed the data, and wrote the manuscript. All authors have read and agreed to the published version of the manuscript.

**Funding:** This research was funded by the National Science Centre grants 2019/35/N/NZ7/02780 (RG) and 2020/39/O/NZ5/02342 (AMW).

**Institutional Review Board Statement:** Not applicable.

**Informed Consent Statement:** Not applicable.

**Data Availability Statement:** The data presented in this study are available on request from the corresponding author ([anna.mrozek-wilczkiewicz@us.edu.pl](mailto:anna.mrozek-wilczkiewicz@us.edu.pl) or [anna.mrozek-wilczkiewicz@polsl.pl](mailto:anna.mrozek-wilczkiewicz@polsl.pl)).

**Conflicts of Interest:** The authors declare no conflict of interest.

## References

- Nomoto, T.; Komoto, K.; Nagano, T.; Ishii, T.; Guo, H.; Honda, Y.; Ogura, S.I.; Ishizuka, M.; Nishiyama, N. Polymeric iron chelators for enhancing 5-aminolevulinic acid-induced photodynamic therapy. *Cancer Sci.* **2023**, *114*, 1086–1094. [\[CrossRef\]](#)
- Qin, J.; Zhou, C.; Zhu, M.; Shi, S.; Zhang, L.; Zhao, Y.; Li, C.; Wang, Y.; Wang, Y. Iron chelation promotes 5-aminolevulinic acid-based photodynamic therapy against oral tongue squamous cell carcinoma. *Photodiagn. Photodyn. Ther.* **2020**, *31*, 101907. [\[CrossRef\]](#)
- Peng, Q.; Warloe, T.; Berg, K.; Moan, J.; Kongshaug, M.; Giercksky, K.E.; Nesland, J.M. 5-Aminolevulinic acid-based photodynamic therapy. Clinical research and future challenges. *Cancer* **1997**, *79*, 2282–2308. [\[CrossRef\]](#)
- Curnow, A.; Pye, A. The importance of iron chelation and iron availability during PpIX-induced photodynamic therapy. *Photonics Lasers Med.* **2015**, *4*, 39–58. [\[CrossRef\]](#)
- Uehlinger, P.; Ballini, J.P.; van den Bergh, H.; Wagnieres, G. On the role of iron and one of its chelating agents in the production of protoporphyrin IX generated by 5-aminolevulinic acid and its hexyl ester derivative tested on an epidermal equivalent of human skin. *Photochem. Photobiol.* **2006**, *82*, 1069–1076. [\[CrossRef\]](#) [\[PubMed\]](#)
- Li, A.; Liang, C.; Xu, L.; Wang, Y.; Liu, W.; Zhang, K.; Liu, J.; Shi, J. Boosting 5-ALA-based photodynamic therapy by a liposomal nanomedicine through intracellular iron ion regulation. *Acta Pharm. Sin. B* **2021**, *11*, 1329–1340. [\[CrossRef\]](#) [\[PubMed\]](#)
- De Rosa, F.S.; Marchetti, J.M.; Thomazini, J.A.; Tedesco, A.C.; Bentley, M.V. A vehicle for photodynamic therapy of skin cancer: Influence of dimethylsulphoxide on 5-aminolevulinic acid in vitro cutaneous permeation and in vivo protoporphyrin IX accumulation determined by confocal microscopy. *J. Control. Release* **2000**, *65*, 359–366. [\[CrossRef\]](#)
- Magnussen, A.; Reburn, C.; Perry, A.; Wood, M.; Curnow, A. Experimental investigation of a combinational iron chelating protoporphyrin IX prodrug for fluorescence detection and photodynamic therapy. *Lasers Med. Sci.* **2022**, *37*, 1155–1166. [\[CrossRef\]](#) [\[PubMed\]](#)
- Chang, S.C.; MacRobert, A.J.; Porter, J.B.; Bown, S.G. The efficacy of an iron chelator (CP94) in increasing cellular protoporphyrin IX following intravesical 5-aminolevulinic acid administration: An in vivo study. *J. Photochem. Photobiol. B* **1997**, *38*, 114–122. [\[CrossRef\]](#)
- Feuerstein, T.; Berkovitch-Luria, G.; Nudelman, A.; Rephaeli, A.; Malik, Z. Modulating ALA-PDT efficacy of multidrug resistant MCF-7 breast cancer cells using ALA prodrug. *Photochem. Photobiol. Sci.* **2011**, *10*, 1926–1933. [\[CrossRef\]](#)
- Fukuhara, H.; Inoue, K.; Kurabayashi, A.; Furihata, M.; Fujita, H.; Utsumi, K.; Sasaki, J.; Shuin, T. The inhibition of ferrochelatase enhances 5-aminolevulinic acid-based photodynamic action for prostate cancer. *Photodiagn. Photodyn. Ther.* **2013**, *10*, 399–409. [\[CrossRef\]](#) [\[PubMed\]](#)
- Mastrangelopoulou, M.; Grigalavicius, M.; Raabe, T.H.; Skarpen, E.; Juzenas, P.; Peng, Q.; Berg, K.; Theodossiou, T.A. Predictive biomarkers for 5-ALA-PDT can lead to personalized treatments and overcome tumor-specific resistances. *Cancer Rep.* **2022**, *5*, e1278. [\[CrossRef\]](#) [\[PubMed\]](#)
- Levi, S.; Ripamonti, M.; Dardi, M.; Cozzi, A.; Santambrogio, P. Mitochondrial Ferritin: Its Role in Physiological and Pathological Conditions. *Cells* **2021**, *10*, 1969. [\[CrossRef\]](#)



14. Martelli, A.; Wattenhofer-Donze, M.; Schmucker, S.; Bouvet, S.; Reutenauer, L.; Puccio, H. Frataxin is essential for extramitochondrial Fe-S cluster proteins in mammalian tissues. *Hum. Mol. Genet.* **2007**, *16*, 2651–2658. [\[CrossRef\]](#) [\[PubMed\]](#)
15. Schmucker, S.; Martelli, A.; Colin, F.; Page, A.; Wattenhofer-Donze, M.; Reutenauer, L.; Puccio, H. Mammalian frataxin: An essential function for cellular viability through an interaction with a preformed ISCU/NFS1/ISD11 iron-sulfur assembly complex. *PLoS ONE* **2011**, *6*, e16199. [\[CrossRef\]](#) [\[PubMed\]](#)
16. Ali, M.Y.; Oliva, C.R.; Flor, S.; Griguer, C.E. Mitoferrin, Cellular and Mitochondrial Iron Homeostasis. *Cells* **2022**, *11*, 3464. [\[CrossRef\]](#)
17. Yien, Y.Y.; Perfetto, M. Regulation of Heme Synthesis by Mitochondrial Homeostasis Proteins. *Front. Cell Dev. Biol.* **2022**, *10*, 895521. [\[CrossRef\]](#)
18. Barra, J.; Crosbourn, I.; Roberge, C.L.; Bossardi-Ramos, R.; Warren, J.S.A.; Matteson, K.; Wang, L.; Jourdeheuil, F.; Borisov, S.M.; Bresnahan, E. DMT1-dependent endosome-mitochondria interactions regulate mitochondrial iron translocation and metastatic outgrowth. *Oncogene* **2024**, *43*, 650–667. [\[CrossRef\]](#)
19. Tan, Q.; Zhang, X.; Li, S.; Liu, W.; Yan, J.; Wang, S.; Cui, F.; Li, D.; Li, J. DMT1 differentially regulates mitochondrial complex activities to reduce glutathione loss and mitigate ferroptosis. *Free Radic. Biol. Med.* **2023**, *207*, 32–44. [\[CrossRef\]](#)
20. Wolff, N.A.; Garrick, M.D.; Zhao, L.; Garrick, L.M.; Ghio, A.J.; Thevenod, F. A role for divalent metal transporter (DMT1) in mitochondrial uptake of iron and manganese. *Sci. Rep.* **2018**, *8*, 211. [\[CrossRef\]](#)
21. Ichikawa, Y.; Bayeva, M.; Ghanefar, M.; Potini, V.; Sun, L.; Mutharasan, R.K.; Wu, R.; Khechaduri, A.; Jairaj Naik, T.; Ardehali, H. Disruption of ATP-binding cassette B8 in mice leads to cardiomyopathy through a decrease in mitochondrial iron export. *Proc. Natl. Acad. Sci. USA* **2012**, *109*, 4152–4157. [\[CrossRef\]](#) [\[PubMed\]](#)
22. Gawecki, R.; Malarz, K.; Rejmund, M.; Polanski, J.; Mrozek-Wilczkiewicz, A. Impact of thiosemicarbazones on the accumulation of PpIX and the expression of the associated genes. *J. Photochem. Photobiol. B* **2019**, *199*, 111585. [\[CrossRef\]](#)
23. Gawecki, R.; Polanski, J.; Mrozek-Wilczkiewicz, A. A Thiosemicarbazone Derivative as a Booster in Photodynamic Therapy—A Way to Improve the Therapeutic Effect. *Int. J. Mol. Sci.* **2022**, *23*, 15370. [\[CrossRef\]](#)
24. Serda, M.; Kalinowski, D.S.; Rasko, N.; Potuckova, E.; Mrozek-Wilczkiewicz, A.; Musiol, R.; Malecki, J.G.; Sajewicz, M.; Ratuszna, A.; Muchowicz, A. Exploring the anti-cancer activity of novel thiosemicarbazones generated through the combination of retro-fragments: Dissection of critical structure-activity relationships. *PLoS ONE* **2014**, *9*, e110291. [\[CrossRef\]](#) [\[PubMed\]](#)
25. Rzycka-Korzec, R.; Malarz, K.; Gawecki, R.; Mrozek-Wilczkiewicz, A.; Malecki, J.G.; Schab-Balcerzak, E.; Korzec, M.; Polanski, J. Effect of the complex-formation ability of thiosemicarbazones containing (aza)benzene or 3-nitro-1,8-naphthalimide unit towards Cu(II) and Fe(III) ions on their anticancer activity. *J. Photochem. Photobiol. A Chem.* **2021**, *415*, 113314. [\[CrossRef\]](#)
26. Hashmi, K.; Satya; Gupta, S.; Siddique, A.; Khan, T.; Joshi, S. Medicinal applications of vanadium complexes with Schiff bases. *J. Trace Elem. Med. Biol.* **2023**, *79*, 127245. [\[CrossRef\]](#) [\[PubMed\]](#)
27. Lewis, N.A.; Liu, F.; Seymour, L.; Magnusen, A.; Erves, T.R.; Arca, J.F.; Beckford, F.A.; Venkatraman, R.; Gonzalez-Sarrias, A.; Fronczek, F.R. Synthesis, characterization, and preliminary in vitro studies of vanadium(IV) complexes with a Schiff base and thiosemicarbazones as mixed-ligands. *Eur. J. Inorg. Chem.* **2012**, *2012*, 664–677. [\[CrossRef\]](#)
28. Mrozek-Wilczkiewicz, A.; Serda, M.; Musiol, R.; Malecki, G.; Szurko, A.; Malecki, J.G.; Sajewicz, M.; Ratuszna, A.; Polanski, J. Iron chelators in photodynamic therapy revisited: Synergistic effect by novel highly active thiosemicarbazones. *ACS Med. Chem. Lett.* **2014**, *5*, 336–339. [\[CrossRef\]](#)
29. Curnow, A.; McIlroy, B.W.; Postle-Hacon, M.J.; Porter, J.B.; MacRobert, A.J.; Bown, S.G. Enhancement of 5-aminolaevulinic acid-induced photodynamic therapy in normal rat colon using hydroxypyridinone iron-chelating agents. *Br. J. Cancer* **1998**, *78*, 1278–1282. [\[CrossRef\]](#)
30. Palasuberniam, P.; Kraus, D.; Mansi, M.; Braun, A.; Howley, R.; Myers, K.A.; Chen, B. Ferrochelatase Deficiency Abrogated the Enhancement of Aminolevulinic Acid-mediated Protoporphyrin IX by Iron Chelator Deferoxamine. *Photochem. Photobiol.* **2019**, *95*, 1052–1059. [\[CrossRef\]](#)
31. Blake, E.; Curnow, A. The hydroxypyridinone iron chelator CP94 can enhance PpIX-induced PDT of cultured human glioma cells. *Photochem. Photobiol.* **2010**, *86*, 1154–1160. [\[CrossRef\]](#) [\[PubMed\]](#)
32. Hasinoff, B.B.; Patel, D. The iron chelator Dp44mT does not protect myocytes against doxorubicin. *J. Inorg. Biochem.* **2009**, *103*, 1093–1101. [\[CrossRef\]](#)
33. Santoro, A.; Vileno, B.; Palacios, O.; Peris-Diaz, M.D.; Riegel, G.; Gaiddon, C.; Krezel, A.; Faller, P. Reactivity of Cu(II)-, Zn(II)- and Fe(II)-thiosemicarbazone complexes with glutathione and metallothionein: From stability to dissociation to transmetallation. *Metallomics* **2019**, *11*, 994–1004. [\[CrossRef\]](#)
34. Serda, M.; Kalinowski, D.S.; Mrozek-Wilczkiewicz, A.; Musiol, R.; Szurko, A.; Ratuszna, A.; Pantarat, N.; Kovacevic, Z.; Merlot, A.M.; Richardson, D.R. Synthesis and characterization of quinoline-based thiosemicarbazones and correlation of cellular iron-binding efficacy to anti-tumor efficacy. *Bioorg. Med. Chem. Lett.* **2012**, *22*, 5527–5531. [\[CrossRef\]](#) [\[PubMed\]](#)
35. Yang, X.; Li, W.; Palasuberniam, P.; Myers, K.A.; Wang, C.; Chen, B. Effects of Silencing Heme Biosynthesis Enzymes on 5-Aminolevulinic Acid-mediated Protoporphyrin IX Fluorescence and Photodynamic Therapy. *Photochem. Photobiol.* **2015**, *91*, 923–930. [\[CrossRef\]](#)
36. Hara, Y.; Yanatori, I.; Tanaka, A.; Kishi, F.; Lemasters, J.J.; Nishina, S.; Sasaki, K.; Hino, K. Iron loss triggers mitophagy through induction of mitochondrial ferritin. *EMBO Rep.* **2020**, *21*, e50202. [\[CrossRef\]](#) [\[PubMed\]](#)

37. Zhao, H.; Yin, R.; Wang, Y.; Lee, Y.H.; Luo, T.; Zhang, J.; Qiu, H.; Ambrose, S.; Wang, L.; Ren, J. Modulating mitochondrial morphology enhances antitumor effect of 5-ALA-mediated photodynamic therapy both in vitro and in vivo. *J. Photochem. Photobiol. B* **2017**, *176*, 81–91. [[CrossRef](#)]
38. Dietz, J.V.; Willoughby, M.M.; Piel, R.B., 3rd; Ross, T.A.; Bohovych, I.; Addis, H.G.; Fox, J.L.; Lanzilotta, W.N.; Dailey, H.A.; Wohlschlegel, J.A. Mitochondrial contact site and cristae organizing system (MICOS) machinery supports heme biosynthesis by enabling optimal performance of ferrochelatase. *Redox Biol.* **2021**, *46*, 102125. [[CrossRef](#)]
39. Lu, C.; Cortopassi, G. Frataxin knockdown causes loss of cytoplasmic iron-sulfur cluster functions, redox alterations and induction of heme transcripts. *Arch. Biochem. Biophys.* **2007**, *457*, 111–122. [[CrossRef](#)]
40. Weerth, R.S.; Medlock, A.E.; Dailey, H.A. Ironing out the distribution of [2Fe-2S] motifs in ferrochelatases. *J. Biol. Chem.* **2021**, *297*, 101017. [[CrossRef](#)]
41. Crooks, D.R.; Ghosh, M.C.; Haller, R.G.; Tong, W.H.; Rouault, T.A. Posttranslational stability of the heme biosynthetic enzyme ferrochelatase is dependent on iron availability and intact iron-sulfur cluster assembly machinery. *Blood* **2010**, *115*, 860–869. [[CrossRef](#)] [[PubMed](#)]
42. Chau, T.T.; Ishigaki, M.; Kataoka, T.; Taketani, S. Porcine ferrochelatase: The relationship between iron-removal reaction and the conversion of heme to Zn-protoporphyrin. *Biosci. Biotechnol. Biochem.* **2010**, *74*, 1415–1420. [[CrossRef](#)]
43. Hayashi, M.; Fukuhara, H.; Inoue, K.; Shuin, T.; Hagiya, Y.; Nakajima, M.; Tanaka, T.; Ogura, S. The effect of iron ion on the specificity of photodynamic therapy with 5-aminolevulinic acid. *PLoS ONE* **2015**, *10*, e0122351. [[CrossRef](#)] [[PubMed](#)]
44. Ali, M.Y.; Griguer, C.E.; Flor, S.; Oliva, C.R. Mitoferrin-1 Promotes Proliferation and Abrogates Protein Oxidation via the Glutathione Pathway in Glioblastoma. *Antioxidants* **2023**, *12*, 349. [[CrossRef](#)]
45. Chen, C.; Wang, S.; Liu, P. Deferoxamine Enhanced Mitochondrial Iron Accumulation and Promoted Cell Migration in Triple-Negative MDA-MB-231 Breast Cancer Cells Via a ROS-Dependent Mechanism. *Int. J. Mol. Sci.* **2019**, *20*, 4952. [[CrossRef](#)] [[PubMed](#)]
46. Blajan, I.; Miersch, H.; Schmidt, D.; Kristiansen, G.; Perner, S.; Ritter, M.; Ellinger, J.; Klumper, N. Comprehensive Analysis of the ATP-binding Cassette Subfamily B Across Renal Cancers Identifies ABCB8 Overexpression in Phenotypically Aggressive Clear Cell Renal Cell Carcinoma. *Eur. Urol. Focus* **2021**, *7*, 1121–1129. [[CrossRef](#)]

**Disclaimer/Publisher's Note:** The statements, opinions and data contained in all publications are solely those of the individual author(s) and contributor(s) and not of MDPI and/or the editor(s). MDPI and/or the editor(s) disclaim responsibility for any injury to people or property resulting from any ideas, methods, instructions or products referred to in the content.

## Iron Metabolism in Aminolevulinic Acid-Photodynamic Therapy with Iron Chelators from the Thiosemicarbazone Group

Robert Gawecki <sup>1,2</sup>, Patrycja Rawicka <sup>1</sup>, Marta Rogalska <sup>3</sup>, Maciej Serda <sup>3</sup> and Anna Mrozek-Wilczkiewicz <sup>1,4,\*</sup>

<sup>1</sup> Institute of Physics, University of Silesia in Katowice, 75 Pułku Piechoty 1A, 41-500 Chorzow, Poland;

robert.gawecki@us.edu.pl (R.G.); patrycja.rawicka@us.edu.pl (P.R.)

<sup>2</sup> SPIN-Lab Centre for Microscopic Research of Matter, University of Silesia in Katowice, 75 Pułku Piechoty

1A, 41-500 Chorzow, Poland

<sup>3</sup> Institute of Chemistry, University of Silesia in Katowice, Szkolna 9, 40-006 Katowice, Poland;

rejmund.m@gmail.com (M.R.); maciej.serda@us.edu.pl (M.S.)

<sup>4</sup> Department of Systems Biology and Engineering, Silesian University of Technology, Akademicka 16,

44-100 Gliwice, Poland

\* Correspondence: anna.mrozek-wilczkiewicz@us.edu.pl or anna.mrozek-wilczkiewicz@polsl.pl

### SUPPORTING INFORMATION

1. <sup>1</sup>H- and <sup>13</sup>C-NMR spectral characterization of synthesized thiosemicarbazides and thiosemicarbazones.
2. Absorption spectrum obtained for the solvent used in titration measurements (sample blank).

1.

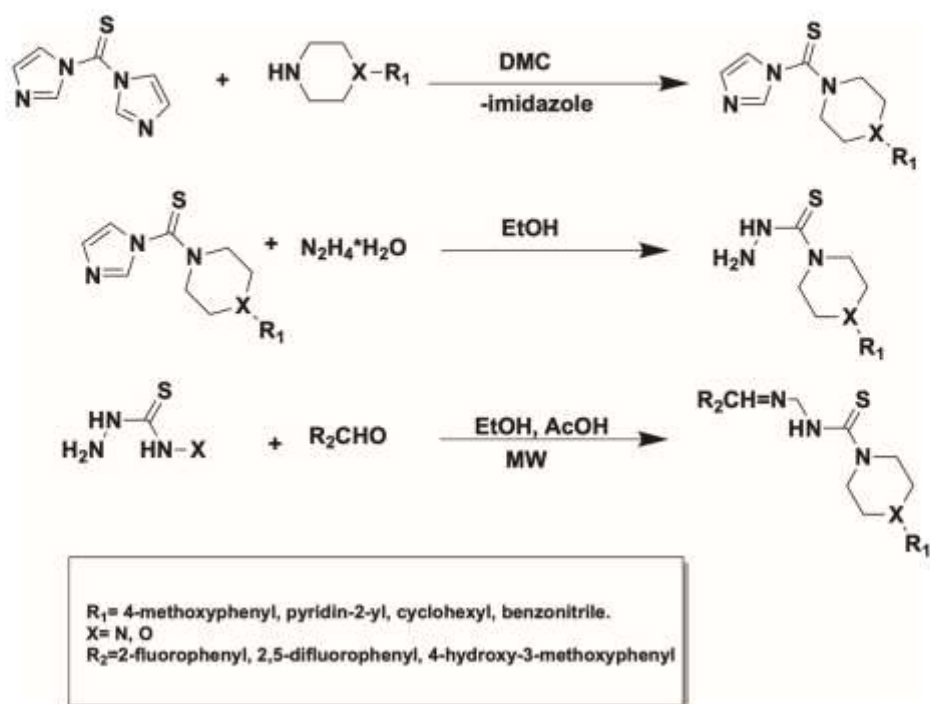
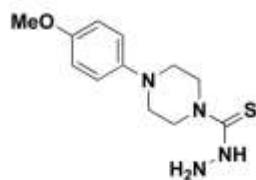


Figure S1. The synthetic protocol used for obtaining selected thiosemicarbazones.



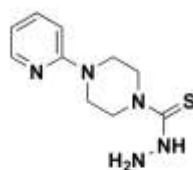
*4-(4-methoxyphenyl)piperazine-1-carbothiohydrazide*

$^1\text{H-NMR}$  (400 MHz,  $d_6$ -DMSO, ppm):  $\delta$  3.00 (m, 3H, CH<sub>3</sub>), 3.86 (m, 4H, CH<sub>2</sub>), 4.11 (m, 4H, CH<sub>2</sub>), 4.77 (s, 2H, NH<sub>2</sub>), 6.83 (d, 2H,  $J = 9.0$  Hz), 6.90 (m, 2H, ArH), 9.17 (s, 1H, NH).

$^{13}\text{C-NMR}$  (101 MHz,  $d_6$ -DMSO, ppm):  $\delta$  19.0; 49.9; 56.5; 114.8; 118.2; 145.4; 153.7; 183.1.

LogP: 0.71

Yield: 81%.



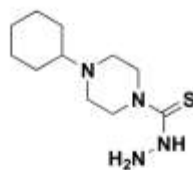
*4-(pyridin-2-yl)piperazine-1-carbothiohydrazide*

**<sup>1</sup>H-NMR (400 MHz, *d*<sub>6</sub>-DMSO, ppm):** δ 3.18 (s, 4H, CH<sub>2</sub>), 3.85 (m, 4H, CH<sub>2</sub>), 4.77 (s, 2H, NH<sub>2</sub>), 6.67 (m, 1H, Ar-H), 6.83 (m, 1H, Ar-H), 7.56 (m, 1H, Ar-H), 8.13 (m, 1H, Ar-H), 9.13 (s, 1H, NH).

**<sup>13</sup>C-NMR (101 MHz, *d*<sub>6</sub>-DMSO, ppm):** δ 44.4; 47.2; 107.6; 113.7; 138.0; 148.0; 159.1; 183.0.

**LogP:** -0.02

**Yield:** 98 %.



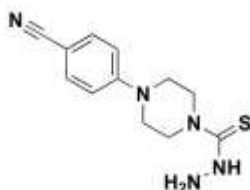
*4-cyclohexylpiperazine-1-carbothiohydrazide*

**<sup>1</sup>H-NMR (400 MHz, *d*<sub>6</sub>-DMSO, ppm):** δ 1.19 (m, 6H, CH<sub>2</sub>), 1.73 (d, 5H, *J* = 8.4 Hz), 3.36 (m, 4H, CH<sub>2</sub>), 3.66 (s, 4H, CH<sub>2</sub>), 4.73 (s, 2H, NH<sub>2</sub>), 9.02 (s, 1H, NH).

**<sup>13</sup>C-NMR (101 MHz, *d*<sub>6</sub>-DMSO, ppm):** δ 25.7; 26.3; 28.7; 48.3; 48.7; 62.9; 182.9.

**LogP:** 1.65

**Yield:** 59 %.



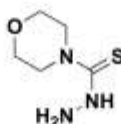
***4-(4-cyanophenyl)piperazine-1-carbothiohydrazide***

**<sup>1</sup>H-NMR (400 MHz, *d*<sub>6</sub>-DMSO, ppm):** δ 3.42 (m, 4H, CH<sub>2</sub>), 3.89 (m, 4H, CH<sub>2</sub>), 4.78 (s, 2H, NH<sub>2</sub>), 7.05 (s, 2H, Ar-H), 7.60 (m, 2H, Ar-H), 9.15 (s, 1H, NH).

**<sup>13</sup>C-NMR (101 MHz, *d*<sub>6</sub>-DMSO, ppm):** δ 45.9; 48.9; 98.6; 114.3; 120.5; 133.8; 153.0; 182.9.

**LogP:** 0.78

**Yield:** 70 %.



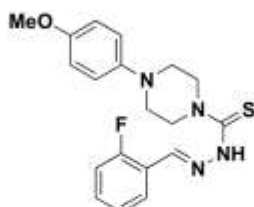
***morpholine-4-carbothiohydrazide***

**<sup>1</sup>H-NMR (400 MHz, *d*<sub>6</sub>-DMSO, ppm):** δ 3.59 (m, 4H, CH<sub>2</sub>), 3.68 (m, 4H, CH<sub>2</sub>), 4.79 (s, 2H, NH<sub>2</sub>), 9.12 (s, 1H, NH).

**LogP:** -0.84

**Yield:** 74 %.



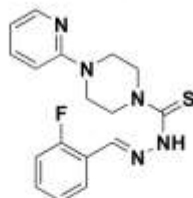
**TSC-82****(*E*)-*N'*-(2-fluorobenzylidene)-4-(4-methoxyphenyl)piperazine-1-carbothiohydrazide**

**<sup>1</sup>H-NMR (400 MHz, *d*<sub>6</sub>-DMSO, ppm):** δ 3.13 (bs, 4H, CH<sub>2</sub>), 3.70 (s, 3H, -OCH<sub>3</sub>), 4.07 (bs, 4H, CH<sub>2</sub>), 6.85 (d, 2H, *J* = 8.9 Hz), 6.95 (d, 2H, *J* = 9.0 Hz), 7.29 (dd, *J*<sub>1</sub> = 13.1 Hz, *J*<sub>2</sub> = 5.3 Hz, 2H), 7.46 (dd, *J*<sub>1</sub> = 13.6 Hz, *J*<sub>2</sub> = 6.1 Hz, 1H), 7.85 (t, 1H, *J* = 7.5 Hz), 8.40 (s, 1H, CH), 11.38 (s, 1H, NH).

**<sup>13</sup>C-NMR (126 MHz, *d*<sub>6</sub>-DMSO, ppm):** δ 181.0, 162.1, 160.1, 153.7, 145.4, 137.07 (d, *J* = 4.5 Hz), 132.1, 132.0, 126.67, 126.65, 125.4 (d, *J* = 3.3 Hz), 122.4 (d, *J* = 9.9 Hz), 118.2, 116.6, 116.4, 114.8, 55.64, 50.35, 50.17.

**LogP:** 2.67

**Yield:** 30%.

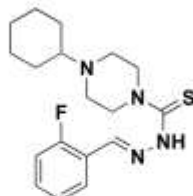
**TSC-102****(*E*)-*N'*-(2-fluorobenzylidene)-4-(pyridin-2-yl)piperazine-1-carbothiohydrazide**

**<sup>1</sup>H-NMR (400 MHz, *d*<sub>6</sub>-DMSO, ppm):** δ 3.65 (bs, 4H, CH<sub>2</sub>), 4.07 (bs, 4H, CH<sub>2</sub>), 6.68 (t, 1H, *J* = 5.5 Hz), 6.85 (d, 1H, *J* = 8.5 Hz), 7.28 (t, 2H, *J* = 9.2 Hz), 7.46 (d, 1H, *J* = 6.3 Hz), 7.57 (t, 1H, *J* = 7.7 Hz), 7.86 (t, 1H, *J* = 7.4 Hz), 8.15 (s, 1H, ArH), 8.41 (s, 1H, CH), 11.39 (bs, 1H, NH).

**<sup>13</sup>C-NMR (126 MHz, *d*<sub>6</sub>-DMSO, ppm):** 181.0, 162.1, 160.1, 159.0, 148.0, 138.1, 137.1 (d, *J* = 4.3 Hz), 132.1, 132.0, 126.7, 125.4 (d, *J* = 3.2 Hz), 122.4 (d, *J* = 9.9 Hz), 116.6, 116.4, 113.7, 107.5, 50.0, 44.6.

**LogP:** 1.94

**Yield:** 62%

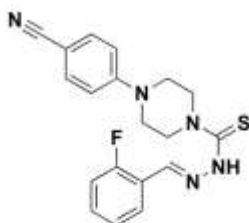
**TSC-109****(E)-4-cyclohexyl-N'-(2-fluorobenzylidene)piperazine-1-carbothiohydrazide**

**<sup>1</sup>H-NMR (400 MHz, *d*<sub>6</sub>-DMSO, ppm):** δ 1.20 (t, 4H, *J* = 9.8 Hz), 1.58 (d, 1H, *J* = 11.6 Hz), 1.71-1.81 (m, 4H, CH<sub>2</sub>), 2.27 (s, 1H, CH<sub>2</sub>), 2.58 (s, 4H, CH<sub>2</sub>), 3.89 (s, 4H, CH<sub>2</sub>), 4.09 (m, 1H, CH<sub>2</sub>), 7.27 (t, 2H, *J* = 8.6 Hz), 7.45 (dd, 1H, *J*<sub>1</sub> = 13.6 Hz, *J*<sub>2</sub> = 6.0 Hz), 7.83 (t, 1H, *J* = 7.3 Hz), 8.37 (s, 1H, CH), 11.25 (bs, 1H, NH).

**<sup>13</sup>C-NMR (126 MHz, *d*<sub>6</sub>-DMSO, ppm):** δ 180.7, 162.0, 160.0, 136.8, 132.0 (d, *J* = 8.4 Hz), 126.6, 125.4 (d, *J* = 3.1 Hz), 122.4 (d, *J* = 9.9 Hz), 116.6, 116.4, 62.9, 50.8, 49.0, 31.2, 28.7, 26.3, 25.7.

**LogP:** 3.61

**Yield:** 19 %

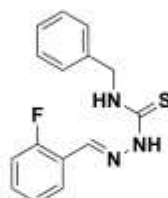
**TSC-113****(E)-4-(4-cyanophenyl)-N'-(2-fluorobenzylidene)piperazine-1-carbothiohydrazide**

**<sup>1</sup>H-NMR (400 MHz, *d*<sub>6</sub>-DMSO, ppm):** δ 3.54 (m, 4H, CH<sub>2</sub>), 4.09 (m, 4H, CH<sub>2</sub>), 7.01 (d, 2H, *J* = 8.8 Hz), 7.28 (dd, *J*<sub>1</sub> = 13.2 Hz, *J*<sub>2</sub> = 6.9 Hz, 2H), 7.46 (dd, 1H, *J*<sub>1</sub> = 13.3 Hz, *J*<sub>2</sub> = 6.4 Hz), 7.61 (d, 2H, *J* = 8.8 Hz), 7.87 (t, 1H, *J* = 7.4 Hz), 8.41 (s, 1H, CH), 11.41 (bs, 1H, NH).

**<sup>13</sup>C-NMR (126 MHz, *d*<sub>6</sub>-DMSO, ppm):** δ 180.9, 162.1, 160.1, 153.1, 153.0, 137.2, 137.1, 133.8, 132.1 (d, *J* = 8.5 Hz), 126.7, 126.7, 125.4 (d, *J* = 3.1 Hz), 122.3 (d, *J* = 10 Hz), 120.5, 116.5, 116.4, 114.2, 98.5, 49.56, 49.07, 46.1

**LogP:** 2.74

**Yield:** 56 %

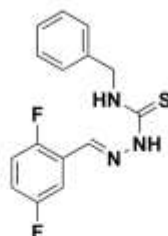
**TSC142****(E)-N-benzyl-2-(2-fluorobenzylidene)hydrazine-1-carbothioamide**

**<sup>1</sup>H-NMR (400 MHz, *d*<sub>6</sub>-DMSO, ppm):** δ 11.74 (bs, 1H, NH), 9.17 (t, *J* = 6.3 Hz, 1H, NH), 8.33 (s, 1H, CH), 8.26 (td, *J*<sub>1</sub> = 7.7, *J*<sub>2</sub> = 1.7 Hz, 1H, ArH), 7.51 – 7.40 (m, 1H, ArH), 7.40–7.30 (m, 4H, ArH), 7.30 – 7.20 (m, 3H, ArH), 4.86 (d, *J* = 6.2 Hz, 2H, CH<sub>2</sub>).

**<sup>13</sup>C-NMR (126 MHz, *d*<sub>6</sub>-DMSO, ppm):** δ 178.2, 162.3, 160.3, 139.8, 135.1 (d, *J* = 5.2 Hz), 132.2 (d, *J* = 8.4 Hz), 128.6, 127.6, 127.3 (m), 125.1 (d, *J* = 3.1 Hz), 122.30 (d, *J* = 9.7 Hz), 116.4, 116.2, 47.1.

**LogP:** 4.25

**Yield:** 64%

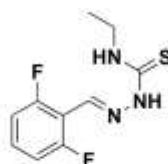
**TSC-145****(E)-N-benzyl-2-(2,5-difluorobenzylidene)hydrazine-1-carbothioamide**

**<sup>1</sup>H-NMR (400 MHz, *d*<sub>6</sub>-DMSO, ppm):** δ 11.81 (bs, 1H, NH), 9.32 (t, *J* = 6.4 Hz, 1H, NH), 8.27 (s, 1H, CH), 8.17 (dt, *J*<sub>1</sub> = 9.3 Hz, *J*<sub>2</sub> = 4.1 Hz, 1H, ArH), 7.35 (m, 6H, ArH), 7.25 (s, 1H, ArH), 4.87 (d, *J* = 6.2 Hz, 2H, CH<sub>2</sub>).

**<sup>13</sup>C-NMR (126 MHz, *d*<sub>6</sub>-DMSO, ppm):** δ 178.3, 160.0 (d, *J* = 1.8 Hz), 158.2 (d, *J* = 48.5 Hz), 139.7, 133.9 (t, *J* = 3.4 Hz), 128.6, 127.5, 127.2, 118.6 (dd, *J*<sub>1</sub> = 25.2 Hz, *J*<sub>2</sub> = 8.8 Hz), 118.1 (dd, *J*<sub>1</sub> = 24.1 Hz, 8.9 Hz), 112.9 (d, *J* = 3.0 Hz), 112.7 (d, *J* = 3.0 Hz), 47.0.

**LogP:** 4.41

**Yield:** 24%

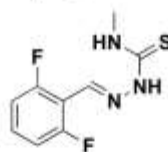
**TSC-146****(*E*)-2-(2,6-difluorobenzylidene)-*N*-ethylhydrazine-1-carbothioamide**

**<sup>1</sup>H-NMR (400 MHz, *d*<sub>6</sub>-DMSO, ppm):** δ 11.67 (bs, 1H, NH), 8.21 (s, 1H, CH), 7.99 (s, 1H, NH), 7.54 – 7.44 (m, 1H, ArH), 7.19 (t, *J* = 8.6 Hz, 2H, ArH), 3.63 – 3.53 (m, 2H, -CH<sub>2</sub>), 1.14 (t, *J* = 7.1 Hz, 3H, CH<sub>3</sub>).

**<sup>13</sup>C-NMR (126 MHz, *d*<sub>6</sub>-DMSO, ppm):** δ 177.4, 162.0 (d, *J* = 6.8 Hz), 159.5 (d, *J* = 6.5 Hz), 132.6, 132.0 (t, *J* = 10.6 Hz), 112.8 (d, *J* = 5.3 Hz), 112.7 (dd, *J*<sub>1</sub> = 19.2 Hz, *J*<sub>2</sub> = 5.3 Hz), 112.6 (d, *J* = 5.3 Hz), 111.9 (t, *J* = 14.0 Hz), 38.9, 14.8.

**LogP:** 2.87

**Yield:** 58 %

**TSC-147****(*E*)-2-(2,6-difluorobenzylidene)-*N*-methylhydrazine-1-carbothioamide**

**<sup>1</sup>H-NMR (400 MHz, *d*<sub>6</sub>-DMSO, ppm):** δ 11.69 (bs, 1H, NH), 8.21 (s, 1H, CH), 8.03 (m, 1H, NH), 7.53–7.45 (m, 1H, ArH), 7.19 (t, *J* = 8.6 Hz, 2H, ArH), 3.02 (d, *J* = 4.3 Hz, 3H, CH<sub>3</sub>).

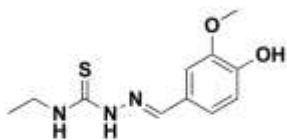
**<sup>13</sup>C-NMR (126 MHz, *d*<sub>6</sub>-DMSO, ppm):** δ 178.3, 161.7 (d, *J* = 6.6 Hz), 159.7 (d, *J* = 6.7 Hz), 132.5, 132.0 (t, *J* = 10.6 Hz), 112.8 (d, *J* = 4.6 Hz), 112.6 (d, *J* = 4.5 Hz), 111.9 (t, *J* = 14.0 Hz), 31.5.

**LogP:** 2.53

**Yield:** 43 %

TSC-197

(*E*)-*N*-ethyl-2-(4-hydroxy-3-methoxybenzylidene)hydrazine-1-carbothioamide

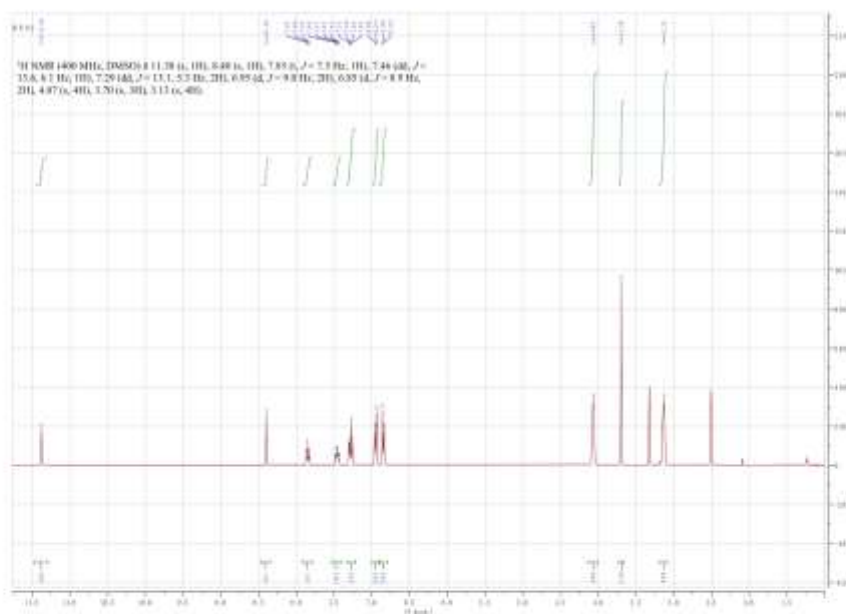


**<sup>1</sup>H-NMR (400 MHz, *d*<sub>6</sub>-DMSO, ppm):**  $\delta$  11.26 (s, 1H, NH), 9.46 (s, 1H, OH), 8.38 (t,  $J$ = 6.0 Hz, 1H, NH), 7.95 (s, 1H, CH), 7.38 (d,  $J$ = 1.9 Hz, 1H, ArH), 7.14 (dd,  $J_1$ = 8.2 Hz,  $J_2$ =1.9 Hz, 1H, ArH), 6.80 (d,  $J$ = 8.2 Hz, 1H, ArH), 3.84 (s, 3H, -OCH<sub>3</sub>), 3.66 – 3.55 (m, 2H, CH<sub>2</sub>), 1.16 (t,  $J$ = 7.1 Hz, 3H, CH<sub>3</sub>).

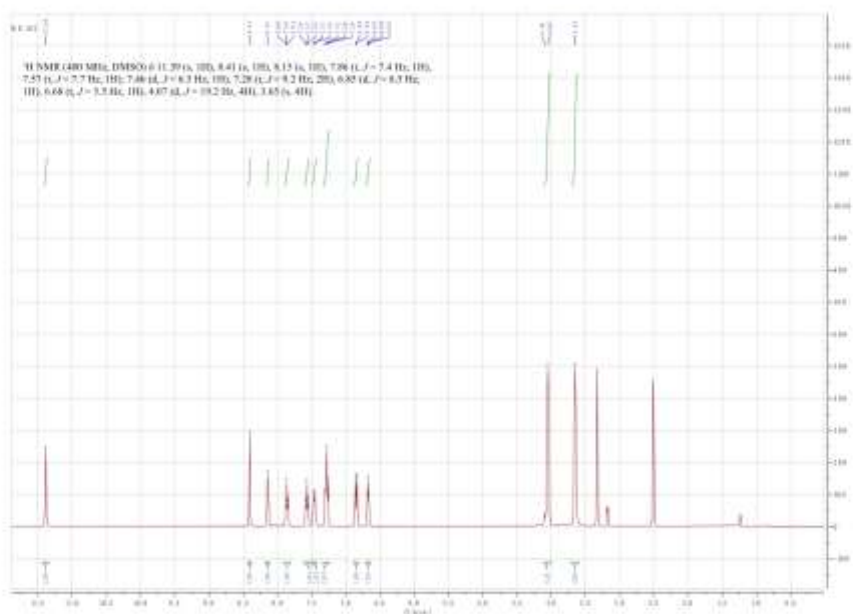
**<sup>13</sup>C-NMR (126 MHz, *d*<sub>6</sub>-DMSO, ppm):**  $\delta$  176.8, 149.2, 148.4, 143.1, 126.0, 122.3, 115.9, 110.6, 56.3, 38.7, 15.2.

**LogP:** 2.04

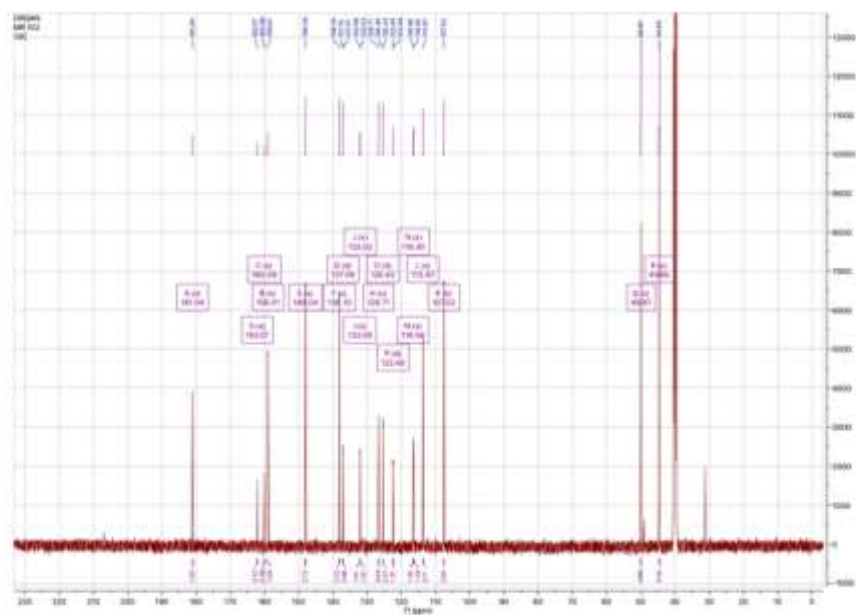
**Yield:** 68 %



<sup>1</sup>H-NMR spectrum of thiosemicarbazone TSC-82.

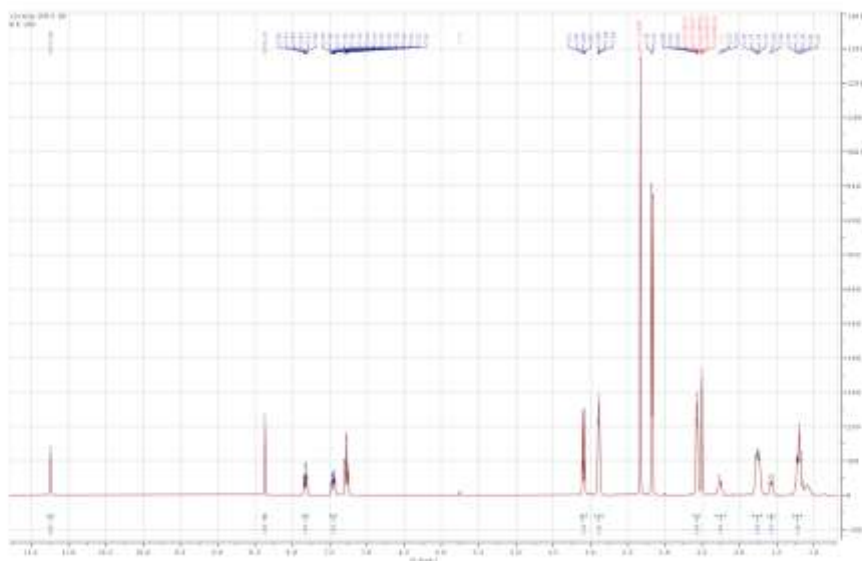


$^1\text{H-NMR}$  spectrum of thiosemicarbazone TSC-102.

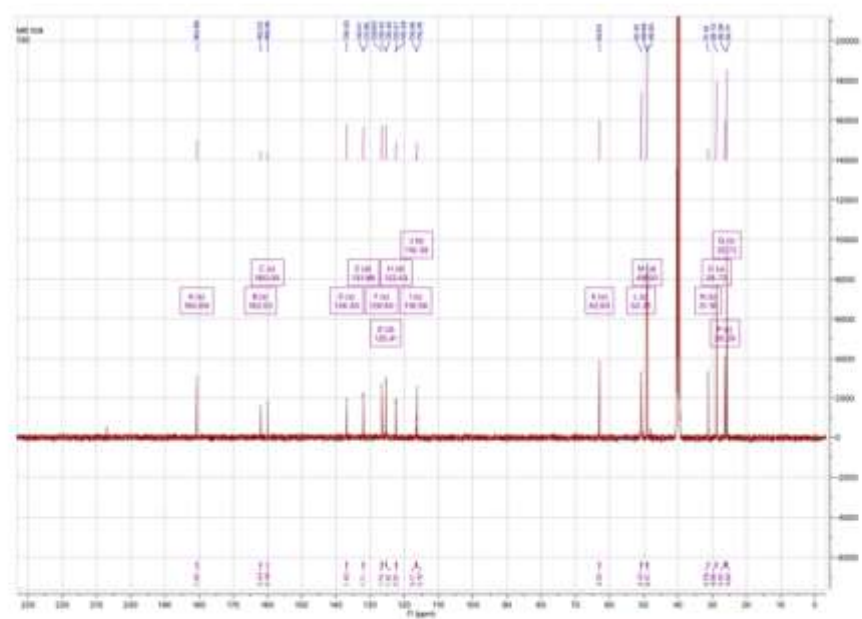


$^{13}\text{C-NMR}$  spectrum of thiosemicarbazone TSC-102.

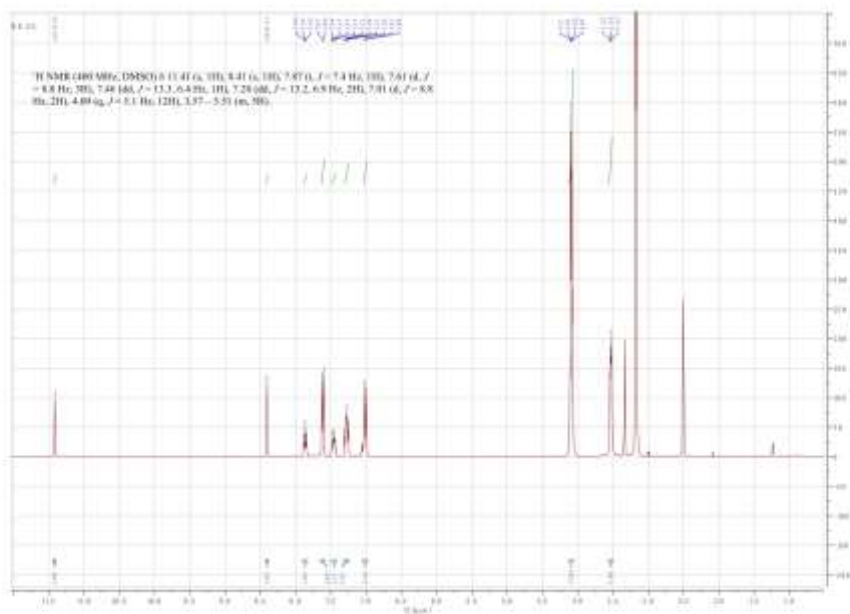




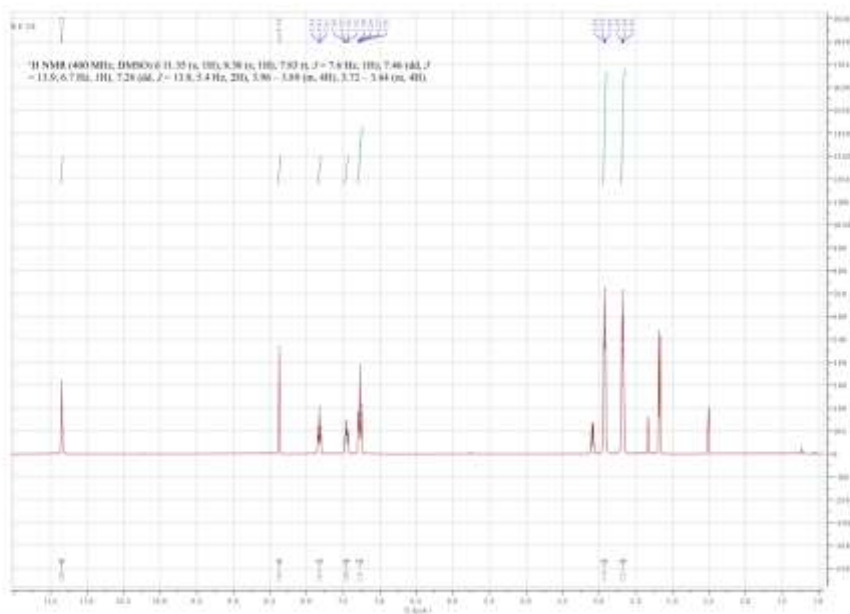
<sup>1</sup>H-NMR spectrum of thiosemicarbazone TSC-109.



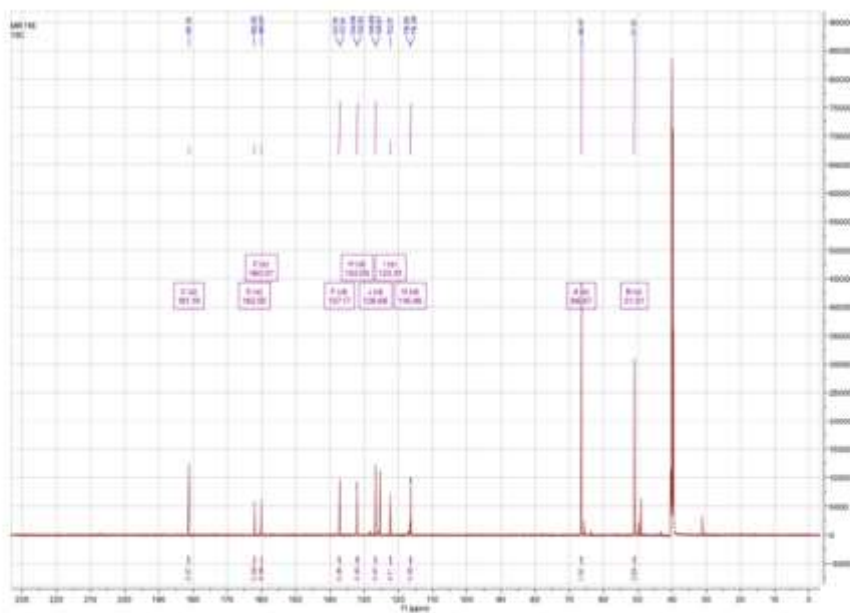
<sup>13</sup>C-NMR spectrum of thiosemicarbazone TSC-109.



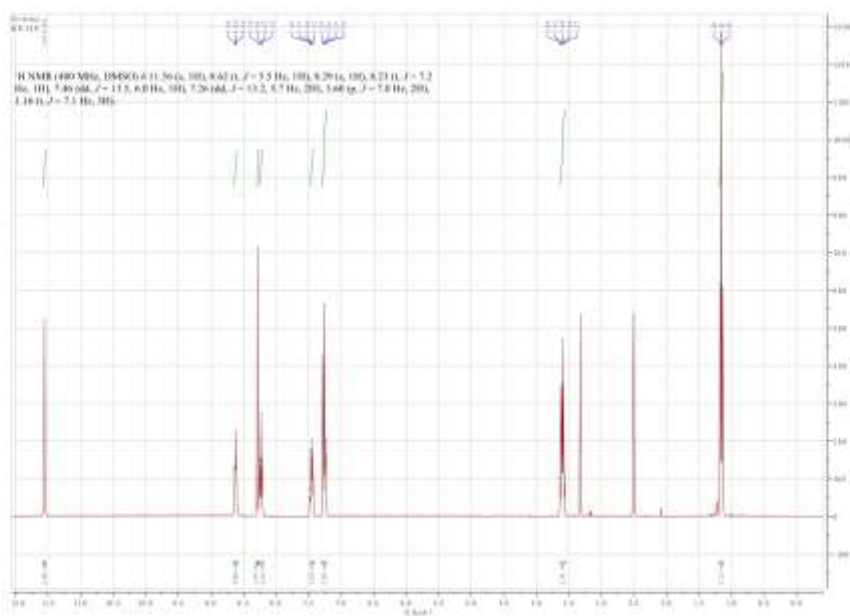
<sup>1</sup>H-NMR spectrum of thiosemicarbazone TSC-113.



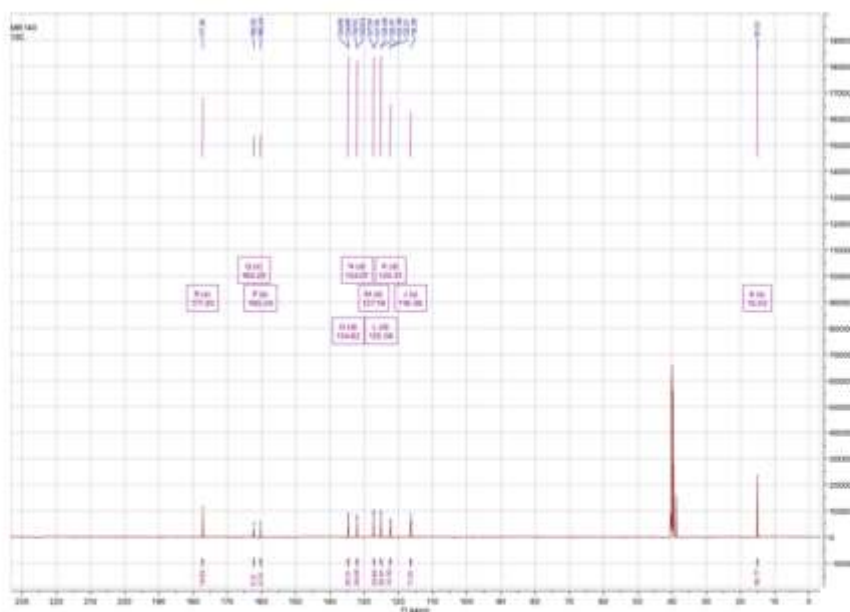
<sup>1</sup>H-NMR spectrum of thiosemicarbazone TSC-116.



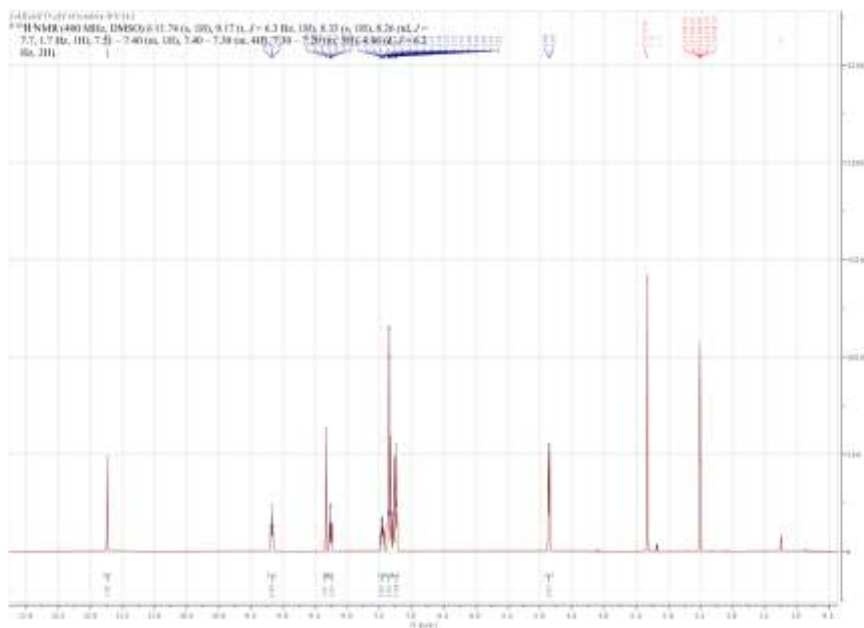
<sup>13</sup>C-NMR spectrum of thiosemicarbazone TSC-116.



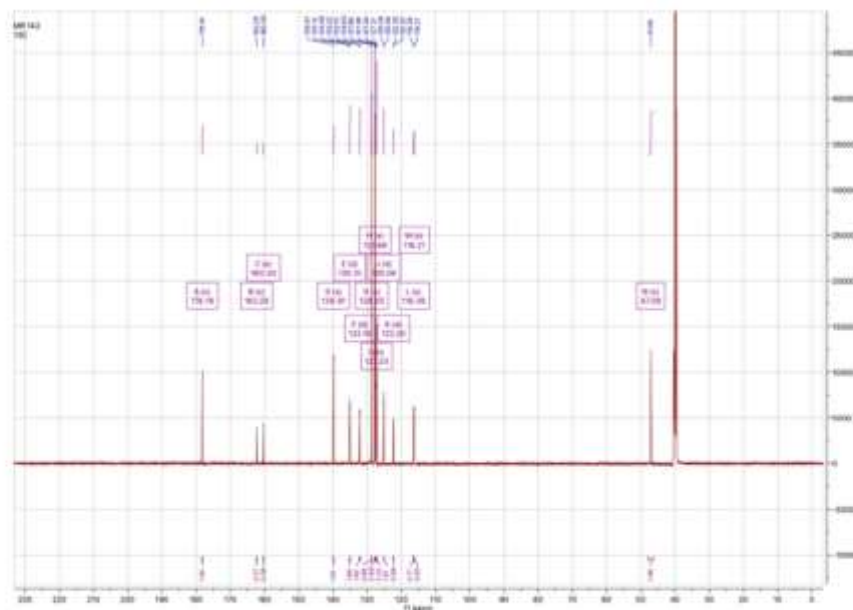
<sup>1</sup>H-NMR spectrum of thiosemicarbazone TSC-140.



<sup>13</sup>C-NMR spectrum of thiosemicarbazone TSC-140.

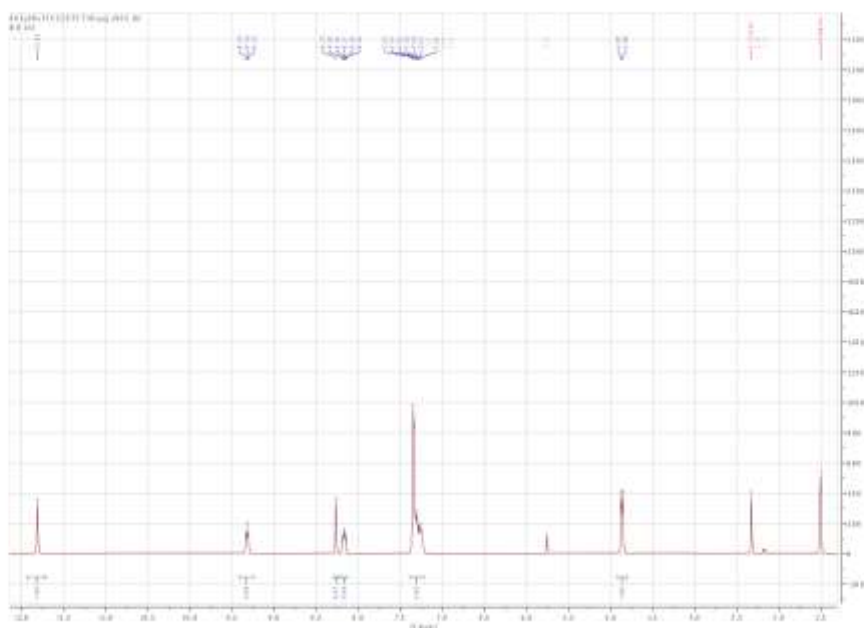


<sup>1</sup>H-NMR spectrum of thiosemicarbazone TSC-142.

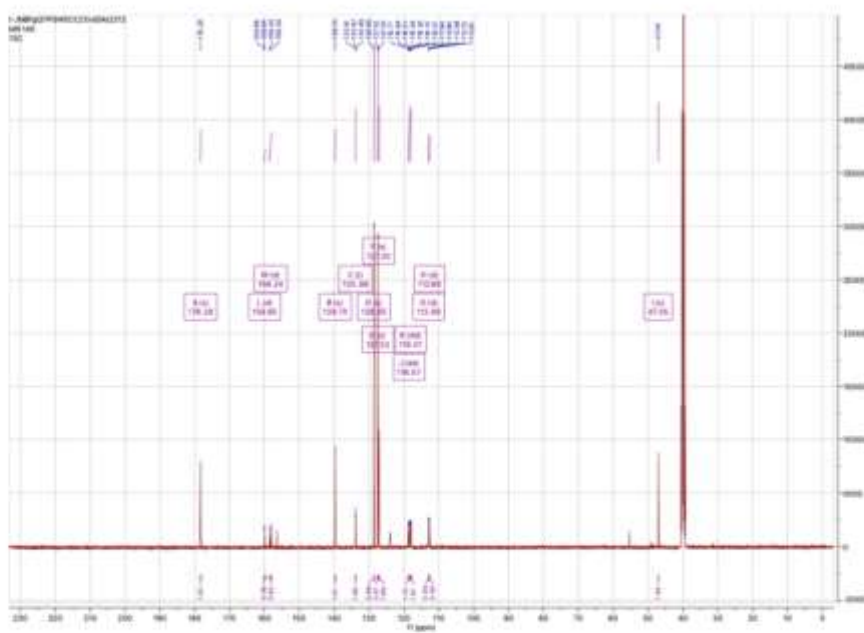


<sup>13</sup>C-NMR spectrum of thiosemicarbazone TSC-142.





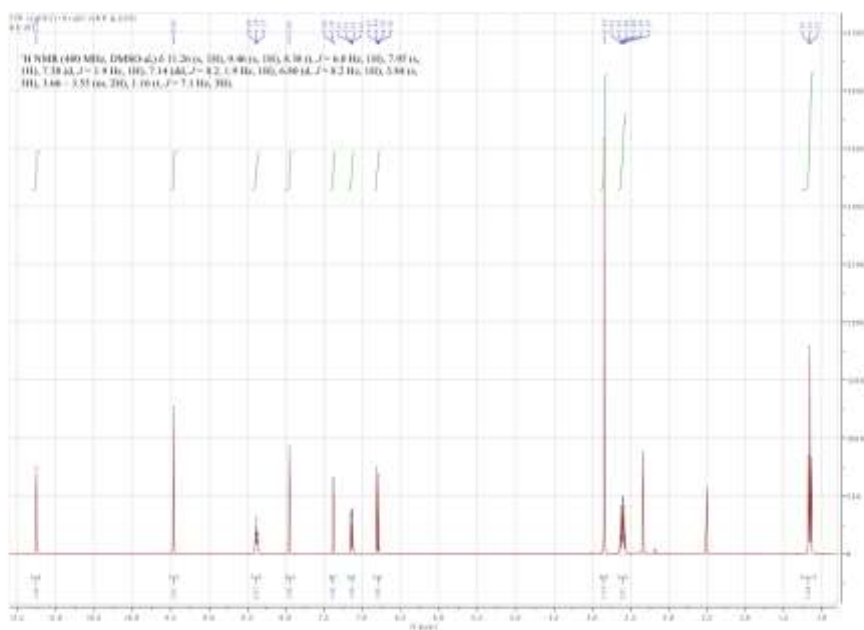
<sup>1</sup>H-NMR spectrum of thiosemicarbazone TSC-145.



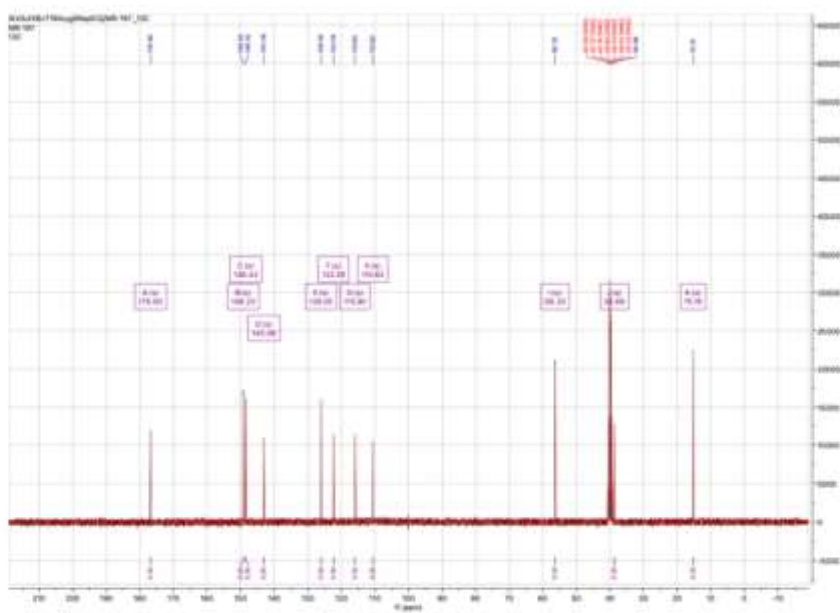
<sup>13</sup>C-NMR spectrum of thiosemicarbazone TSC-145





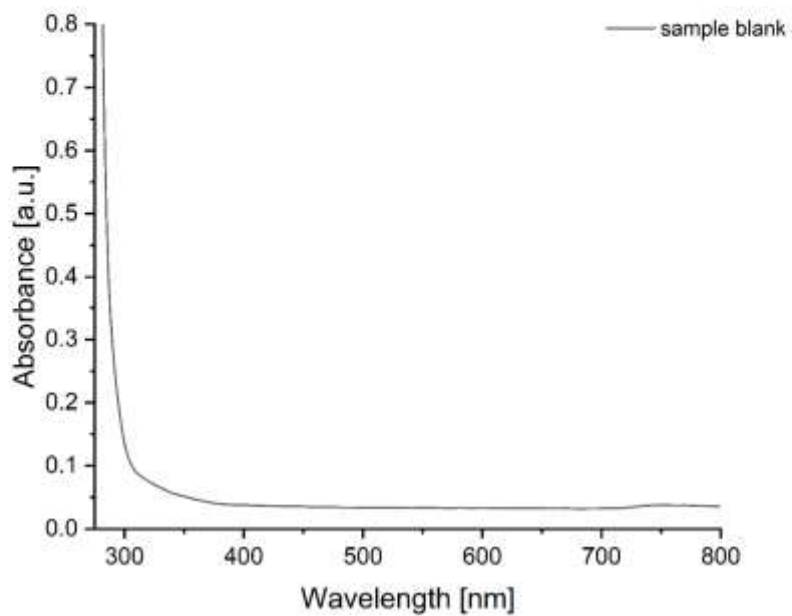


<sup>1</sup>H-NMR spectrum of thiosemicarbazone TSC-197.



<sup>13</sup>C-NMR spectrum of thiosemicarbazone TSC-197.

2.



Absorption spectrum obtained for the solvent used in titration measurements (sample blank). Measurements were performed at room temperature.



## 5. OŚWIADCZENIA WSPÓŁAUTORÓW



Chorzów, 10.09.2024

dr hab. Ann Mrozek-Wilczkiewicz, prof. UŚ

Instytut Fizyki im. Augusta Chełkowskiego

Wydział Nauk Ścisłych i Technicznych

Uniwersytet Śląski w Katowicach

Ul. 75 Pułku Piechoty 1A

41-500, Chorzów

### OŚWIADCZENIE

Oświadczam, że w pracy:

**P1.** Gawecki R., Malarz K., Rejmund M., Polanski J., Mrozek-Wilczkiewicz A. **Impact of thiosemicarbazones on the accumulation of PpIX and the expression of the associated genes.** *Journal of Photochemistry and Photobiology B: Biology*, 2019, 199, 111585.

Mój udział polegał na zaplanowaniu i nadzorze przeprowadzonych badań oraz pisaniu manuskryptu.

**P2.** Gawecki R., Polanski J., Mrozek-Wilczkiewicz A. **A Thiosemicarbazone Derivative as a Booster in Photodynamic Therapy—A Way to Improve the Therapeutic Effect.** *International Journal of Molecular Sciences*, 2022, 23(23), 15370.

Mój udział polegał na zaplanowaniu i nadzorze przeprowadzonych badań oraz pisaniu manuskryptu.

Uniwersytet Śląski w Katowicach  
Nazwa jednostki / Działu / Wydziału  
ul. Bankowa 12, 40-007 Katowice  
tel.: 32 123 45 67, fax: 32 123 45 67, e-mail: adres@us.edu.pl  
www.us.edu.pl





UNIWERSYTET ŚLĄSKI  
W KATOWICACH

**P3. Gawecki R., Rawicka P., Rogalska M., Serda M., Mrozek-Wilczkiewicz A. Iron Metabolism in Aminolevulinic Acid-Photodynamic Therapy with Iron Chelators from the Thiosemicarbazone Group.** *International Journal of Molecular Sciences*, 2024, 25(19), 10468.

Mój udział polegał na nadzorze merytorycznym przeprowadzonych badań oraz pisaniu manuskryptu.

Podpis współautora publikacji

Uniwersytet Śląski w Katowicach  
Nazwa jednostki / Działu / Wydziału  
ul. Bankowa 12, 40-007 Katowice  
tel.: 32 123 45 67, fax: 32 123 45 67, e-mail: adres@us.edu.pl  
[www.us.edu.pl](http://www.us.edu.pl)



Nicea, 10.09.2024

prof. dr hab. Jarosław Polański  
Instytut Chemii  
Wydział Nauk Ścisłych i Technicznych  
Uniwersytet Śląski w Katowicach  
Ul. 75 Pułku Piechoty 1A  
41-500, Chorzów

### OŚWIADCZENIE

Oświadczam, że w pracy:

**P1. Gawecki R., Malarz K., Rejmund M., Polanski J., Mrozek-Wilczkiewicz A. Impact of thiosemicarbazones on the accumulation of PpIX and the expression of the associated genes. *Journal of Photochemistry and Photobiology B: Biology*, 2019, 199, 111585.**

Mój udział polegał na nadzorowaniu syntezy i wsparciu merytorycznym dr Marty Rogalskiej (Rejmund)

**P2. Gawecki R., Polanski J., Mrozek-Wilczkiewicz A. A Thiosemicarbazone Derivative as a Booster in Photodynamic Therapy—A Way to Improve the Therapeutic Effect. *International Journal of Molecular Sciences*, 2022, 23(23), 15370.**

Mój udział polegał na dostarczeniu badanej pochodnej tiosemikarbazonu oraz korekcji manuskryptu.



Signed by /  
Podpisano przez:  
Jarosław Polański  
Uniwersytet Śląski  
Autor publikacji  
2024-09-11 17:52

dr Marta Rogalska (Rejmund)

Instytut Chemii

Wydział Nauk Ścisłych i Technicznych

Uniwersytet Śląski w Katowicach

Ul. 75 Pułku Piechoty 1A

41-500, Chorzów

### OŚWIADCZENIE

Oświadczam, że w pracy:

**P1.** Gawecki R., Malarz K., Rejmund M., Polanski J., Mrozek-Wilczkiewicz A. **Impact of thiosemicarbazones on the accumulation of PpIX and the expression of the associated genes.** *Journal of Photochemistry and Photobiology B: Biology*, 2019, 199, 111585.

Mój udział polegał na syntezie badanych tiosemikarbazonów.

**P3.** Gawecki R., Rawicka P., Rogalska M., Serda M., Mrozek-Wilczkiewicz A. **Iron Metabolism in Aminolevulinic Acid-Photodynamic Therapy with Iron Chelators from the Thiosemicarbazone Group.** *International Journal of Molecular Sciences*, 2024, 25(19), 10468.

Mój udział polegał na syntezie badanych tiosemikarbazonów.



Podpis współautora publikacji

Chorzów. 08.09.2024

dr Katarzyna Malarz, prof. UŚ  
Instytut Fizyki im. Augusta Chełkowskiego  
Wydział Nauk Ścisłych i Technicznych  
Uniwersytet Śląski w Katowicach  
Ul. 75 Pułku Piechoty 1A  
41-500, Chorzów

#### OŚWIADCZENIE

Oświadczam, że w pracy:

**PI. Gawrecki R., Malarz K., Rejmund M., Polanski J., Mrozek-Wilczkiewicz A. Impact of thiosemicarbazones on the accumulation of PpIX and the expression of the associated genes. *Journal of Photochemistry and Photobiology B: Biology*, 2019, 199, 111585.**

mój udział polegał na współudziale w badaniach ekspresji genów oraz w pisaniu manuskryptu.



Podpis współautora publikacji

Chorzów, 10.09.2024

dr hab. inż. Maciej Serda, prof. UŚ

Instytut Chemii

Wydział Nauk Ścisłych i Technicznych

Uniwersytet Śląski w Katowicach

Ul. 75 Pułku Piechoty 1A

41-500, Chorzów

### OŚWIADCZENIE

Oświadczam, że w pracy:

**P3. Gawecki R., Rawicka P., Rogalska M., Serda M., Mrozek-Wileczkiewicz A. Iron Metabolism in Aminolevulinic Acid-Photodynamic Therapy with Iron Chelators from the Thiosemicarbazone Group.** *International Journal of Molecular Sciences*, 2024, 25(19), 10468.

Mój udział polegał na opisie widm NMR oraz syntezy badanych tiosemikarbazonów.

.....  
Podpis współautora publikacji



Digitally signed  
by Maciej Serda  
Date:  
2024.09.30  
08:58:59 CEST



Chorzów, 10.09.2024

dr Patrycja Rawicka

Instytut Fizyki im. Augusta Chełkowskiego

Wydział Nauk Ścisłych i Technicznych

Uniwersytet Śląski w Katowicach

Ul. 75 Pułku Piechoty 1A

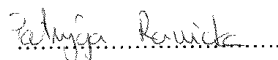
41-500, Chorzów

### OŚWIADCZENIE

Oświadczam, że w pracy:

**P3. Gawrecki R., Rawicka P., Rogalska M., Serda M., Mrozek-Wilczkiewicz A. Iron Metabolism in Aminolevulinic Acid-Photodynamic Therapy with Iron Chelators from the Thiosemicarbazone Group. *International Journal of Molecular Sciences*, 2024, 25(19), 10468.**

Mój udział polegał na współwykonaniu, analizie i opisanie widm absorpcyjnych badanych tiosemikarbazonów w kontekście ich zdolności do chelatowania jonów żelaza.



Podpis współautora publikacji

## 6. LITERATURA

- [1] N. Jokhadze, A. Das, D.S. Dizon, Global cancer statistics: A healthy population relies on population health, *CA Cancer J Clin* 74 (2024) 224–226. <https://doi.org/10.3322/CAAC.21838>.
- [2] N. Vasan, J. Baselga, D.M. Hyman, A view on drug resistance in cancer, *Nature* 2019 575:7782 575 (2019) 299–309. <https://doi.org/10.1038/s41586-019-1730-1>.
- [3] V. Schirrmacher, From chemotherapy to biological therapy: A review of novel concepts to reduce the side effects of systemic cancer treatment (Review), *Int J Oncol* 54 (2019) 407–419. <https://doi.org/10.3892/IJO.2018.4661/HTML>.
- [4] S. Ebrahimi, M. Khaleghi Ghadiri, W. Stummer, A. Gorji, Enhancing 5-ALA-PDT efficacy against resistant tumor cells: Strategies and advances, *Life Sci* 351 (2024) 122808. <https://doi.org/10.1016/J.LFS.2024.122808>.
- [5] K. Plaetzer, B. Krammer, J. Berlanda, F. Berr, T. Kiesslich, Photophysics and photochemistry of photodynamic therapy: Fundamental aspects, *Lasers Med Sci* 24 (2009) 259–268. <https://doi.org/10.1007/S10103-008-0539-1/FIGURES/5>.
- [6] C.S. Foote, Definition of type i and type ii photosensitized oxidation, *Photochem Photobiol* 54 (1991) 659–659. <https://doi.org/10.1111/J.1751-1097.1991.TB02071.X>.
- [7] W.M. Sharman, C.M. Allen, J.E. Van Lier, [35] Role of activated oxygen species in photodynamic therapy, *Methods Enzymol* 319 (2000) 376–400. [https://doi.org/10.1016/S0076-6879\(00\)19037-8](https://doi.org/10.1016/S0076-6879(00)19037-8).
- [8] B. Halliwell, J.M.C. Gutteridge, [4] Role of iron in oxygen radical reactions, *Methods Enzymol* 105 (1984) 47–56. [https://doi.org/10.1016/S0076-6879\(84\)05007-2](https://doi.org/10.1016/S0076-6879(84)05007-2).
- [9] T. Schneider, M. Gugliotti, M.J. Politi, M.S. Baptista, Quantitative Determination of Singlet Oxygen By Laser Deflection Calorimetry, <https://doi.org/10.1080/00032710008543053> 33 (2008) 297–305. <https://doi.org/10.1080/00032710008543053>.
- [10] A. Juzeniene, K.P. Nielsen, J. Moan, Biophysical Aspects of Photodynamic Therapy, *Journal of Environmental Pathology, Toxicology and Oncology* 25 (2006) 7–28. <https://doi.org/10.1615/JENVIRONPATHOLTOXICOLONCOL.V25.I1-2.20>.
- [11] M. Ochsner, Photophysical and photobiological processes in the photodynamic therapy of tumours, *J Photochem Photobiol B* 39 (1997) 1–18. [https://doi.org/10.1016/S1011-1344\(96\)07428-3](https://doi.org/10.1016/S1011-1344(96)07428-3).
- [12] Z. Malik, H. Lugaci, Destruction of erythroleukaemic cells by photoactivation of endogenous porphyrins., *Br J Cancer* 56 (1987) 589. <https://doi.org/10.1038/BJC.1987.246>.
- [13] J.C. Kennedy, R.H. Pottier, New trends in photobiology: Endogenous protoporphyrin IX, a clinically useful photosensitizer for photodynamic therapy, *J Photochem Photobiol B* 14 (1992) 275–292. [https://doi.org/10.1016/1011-1344\(92\)85108-7](https://doi.org/10.1016/1011-1344(92)85108-7).
- [14] H.A. Dailey, T.A. Dailey, C.K. Wu, A.E. Medlock, J.P. Rose, K.F. Wang, Ferrochelatase at the millennium: Structures, mechanisms and [2Fe-2S] clusters, *Cellular and Molecular Life Sciences* 57 (2000) 1909–1926. <https://doi.org/10.1007/PL00000672/METRICS>.

- [15] S.A. Swenson, C.M. Moore, J.R. Marcero, A.E. Medlock, A.R. Reddi, O. Khalimonchuk, From Synthesis to Utilization: The Ins and Outs of Mitochondrial Heme, *Cells* 2020, Vol. 9, Page 579 9 (2020) 579. <https://doi.org/10.3390/CELLS9030579>.
- [16] M. Bayeva, A. Khechaduri, R. Wu, M.A. Burke, J.A. Wasserstrom, N. Singh, M. Liesa, O.S. Shirihai, N.B. Langer, B.H. Paw, H. Ardehali, ATP-binding cassette B10 regulates early steps of heme synthesis, *Circ Res* 113 (2013) 279–287. <https://doi.org/10.1161/CIRCRESAHA.113.301552>.
- [17] N.J. Nordmann, A.P. Michael, 5-Aminolevulinic acid radiodynamic therapy for treatment of high-grade gliomas: A systematic review, *Clin Neurol Neurosurg* 201 (2021) 106430. <https://doi.org/10.1016/J.CLINEURO.2020.106430>.
- [18] S.W. Cramer, C.C. Chen, Photodynamic Therapy for the Treatment of Glioblastoma, *Front Surg* 6 (2020) 81. <https://doi.org/10.3389/FSURG.2019.00081/BIBTEX>.
- [19] K. Mahmoudi, K.L. Garvey, A. Bouras, G. Cramer, H. Stepp, J.G. Jesu Raj, D. Bozec, T.M. Busch, C.G. Hadjipanayis, 5-aminolevulinic acid photodynamic therapy for the treatment of high-grade gliomas, *Journal of Neuro-Oncology* 2019 141:3 141 (2019) 595–607. <https://doi.org/10.1007/S11060-019-03103-4>.
- [20] A.E. Medlock, M.T. Shiferaw, J.R. Marcero, A.A. Vashisht, J.A. Wohlschlegel, J.D. Phillips, H.A. Dailey, Identification of the Mitochondrial Heme Metabolism Complex, *PLoS One* 10 (2015). <https://doi.org/10.1371/JOURNAL.PONE.0135896>.
- [21] R.B. Piel, M.T. Shiferaw, A.A. Vashisht, J.R. Marcero, J.L. Praissman, J.D. Phillips, J.A. Wohlschlegel, A.E. Medlock, A Novel Role for Progesterone Receptor Membrane Component 1 (PGRMC1): A Partner and Regulator of Ferrochelatase, *Biochemistry* 55 (2016) 5204. <https://doi.org/10.1021/ACS.BIOCHEM.6B00756>.
- [22] C.A. Clough, J. Pangallo, M. Sarchi, J.O. Ilagan, K. North, R. Bergantinos, M.C. Stolla, J. Naru, P. Nugent, E. Kim, D.L. Stirewalt, A.R. Subramaniam, O. Abdel-Wahab, J.L. Abkowitz, R.K. Bradley, S. Doulatov, Coordinated missplicing of TMEM14C and ABCB7 causes ring sideroblast formation in SF3B1-mutant myelodysplastic syndrome, *Blood* 139 (2022) 2038–2049. <https://doi.org/10.1182/BLOOD.2021012652>.
- [23] A. Belot, H. Puy, I. Hamza, H.L. Bonkovsky, Update on heme biosynthesis, tissue-specific regulation, heme transport, relation to iron metabolism and cellular energy, *Liver International* 00 (2024) 1–16. <https://doi.org/10.1111/LIV.15965>.
- [24] T. Jansen, M. Hortmann, M. Oelze, B. Opitz, S. Steven, R. Schell, M. Knorr, S. Karbach, S. Schuhmacher, P. Wenzel, T. Münzel, A. Daiber, Conversion of biliverdin to bilirubin by biliverdin reductase contributes to endothelial cell protection by heme oxygenase-1-evidence for direct and indirect antioxidant actions of bilirubin, *J Mol Cell Cardiol* 49 (2010) 186–195. <https://doi.org/10.1016/J.YJMCC.2010.04.011>.
- [25] S.Y. Kim, S.C. Park, Physiological antioxidative network of the bilirubin system in aging and age-related diseases, *Front Pharmacol* 3 MAR (2012) 45. <https://doi.org/10.3389/FPHAR.2012.00045/BIBTEX>.
- [26] L.E. Otterbein, F.H. Bach, J. Alam, M. Soares, H.T. Lu, M. Wysk, R.J. Davis, R.A. Flavell, A.M.K. Choi, Carbon monoxide has anti-inflammatory effects involving the mitogen-activated protein kinase pathway, *Nat Med* 6 (2000) 422–428. <https://doi.org/10.1038/74680>.

- [27] S. Brouard, L.E. Otterbein, J. Anrather, E. Tobiasch, F.H. Bach, A.M.K. Choi, M.P. Soares, Carbon monoxide generated by heme oxygenase 1 suppresses endothelial cell apoptosis, *J Exp Med* 192 (2000) 1015–1025. <https://doi.org/10.1084/JEM.192.7.1015>.
- [28] M. Kiening, N. Lange, A Recap of Heme Metabolism towards Understanding Protoporphyrin IX Selectivity in Cancer Cells, *International Journal of Molecular Sciences* 2022, Vol. 23, Page 7974 23 (2022) 7974. <https://doi.org/10.3390/IJMS23147974>.
- [29] Y.Y. Yien, M. Perfetto, Regulation of Heme Synthesis by Mitochondrial Homeostasis Proteins, *Front Cell Dev Biol* 10 (2022) 1167. <https://doi.org/10.3389/FCELL.2022.895521/BIBTEX>.
- [30] Y. Ren, H. Liu, X. Liu, Y. Zheng, Z. Li, C. Li, K.W.K. Yeung, S. Zhu, Y. Liang, Z. Cui, S. Wu, Photoresponsive Materials for Antibacterial Applications, *Cell Rep Phys Sci* 1 (2020) 100245. <https://doi.org/10.1016/J.XCRP.2020.100245>.
- [31] X. Yang, W. Li, P. Palasuberniam, K.A. Myers, C. Wang, B. Chen, Effects of Silencing Heme Biosynthesis Enzymes on 5-Aminolevulinic Acid-mediated Protoporphyrin IX Fluorescence and Photodynamic Therapy, *Photochem Photobiol* 91 (2015) 923–930. <https://doi.org/10.1111/PHP.12454>.
- [32] R.C. Krieg, H. Messmann, J. Rauch, S. Seeger, R. Knuechel, Metabolic Characterization of Tumor Cell-specific Protoporphyrin IX Accumulation After Exposure to 5-Aminolevulinic Acid in Human Colonic Cells, *Photochem Photobiol* 76 (2002) 518–525. [https://doi.org/10.1562/0031-8655\(2002\)0760518MCOTCS2.0.CO2](https://doi.org/10.1562/0031-8655(2002)0760518MCOTCS2.0.CO2).
- [33] S. Bazzocco, H. Dopeso, F. Carton-Garcia, I. Macaya, E. Andretta, F. Chionh, P. Rodrigues, M. Garrido, H. Alazzouzi, R. Nieto, A. Sanchez, S. Schwartz, J. Bilic, J.M. Mariadason, D. Arango, Highly expressed genes in rapidly proliferating tumor cells as new targets for colorectal cancer treatment, *Clinical Cancer Research* 21 (2015) 3695–3704. <https://doi.org/10.1158/1078-0432.CCR-14-2457/175398/AM/HIGHLY-EXPRESSED-GENES-IN-RAPIDLY-PROLIFERATING>.
- [34] N.G. Abraham, J.M. Camadro, S.T. Hoffstein, R.D. Levere, Effects of iron deficiency and chronic iron overloading on mitochondrial heme biosynthetic enzymes in rat liver, *Biochimica et Biophysica Acta (BBA) - Protein Structure and Molecular Enzymology* 870 (1986) 339–349. [https://doi.org/10.1016/0167-4838\(86\)90238-4](https://doi.org/10.1016/0167-4838(86)90238-4).
- [35] D.R. Crooks, M.C. Ghosh, R.G. Haller, W.H. Tong, T.A. Rouault, Posttranslational stability of the heme biosynthetic enzyme ferrochelatase is dependent on iron availability and intact iron-sulfur cluster assembly machinery, *Blood* 115 (2010) 860–869. <https://doi.org/10.1182/BLOOD-2009-09-243105>.
- [36] T.T. Chau, M. Ishigaki, T. Kataoka, S. Taketani, Porcine Ferrochelatase: The Relationship between Iron-Removal Reaction and the Conversion of Heme to Zn-Protoporphyrin, *Biosci Biotechnol Biochem* 74 (2010) 1415–1420. <https://doi.org/10.1271/BBB.100078>.
- [37] S. Taketani, M. Ishigaki, A. Mizutani, M. Uebayashi, M. Numata, Y. Ohgari, S. Kitajima, Heme synthase (Ferrochelatase) catalyzes the removal of iron from heme and demetalation of metalloporphyrins, *Biochemistry* 46 (2007) 15054–15061. <https://doi.org/10.1021/BI701460X/ASSET/IMAGES/LARGE/BI701460XF00006.JPEG>.
- [38] S.-K. Chiang, S.-E. Chen, L.-C. Chang, E.E. Schmidt, H. Motohashi, A. Kipp, The Role of HO-1 and Its Crosstalk with Oxidative Stress in Cancer Cell Survival, *Cells* 2021, Vol. 10, Page 2401 10 (2021) 2401. <https://doi.org/10.3390/CELLS10092401>.

- [39] C.D. Ferris, S.R. Jaffrey, A. Sawa, M. Takahashi, S.D. Brady, R.K. Barrow, S.A. Tysoe, H. Wolosker, D.E. Barañano, S. Doré, K.D. Poss, S.H. Snyder, Haem oxygenase-1 prevents cell death by regulating cellular iron, *Nature Cell Biology* 1999 1:3 1 (1999) 152–157. <https://doi.org/10.1038/11072>.
- [40] D.E. Barañano, H. Wolosker, B. Byoung-II, R.K. Barrow, S.H. Snyder, C.D. Ferrist, A mammalian iron ATPase induced by iron, *Journal of Biological Chemistry* 275 (2000) 15166–15173. <https://doi.org/10.1074/jbc.275.20.15166>.
- [41] S. Sansaloni-Pastor, E. Varesio, N. Lange, Modulation and proteomic changes on the heme pathway following treatment with 5-aminolevulinic acid, *J Photochem Photobiol B* 233 (2022) 112484. <https://doi.org/10.1016/J.JPHOTOBIOB.2022.112484>.
- [42] V.S. Chelakkot, K. Liu, E. Yoshioka, S. Saha, D. Xu, M. Licursi, A. Dorward, K. Hirasawa, MEK reduces cancer-specific PpIX accumulation through the RSK-ABCB1 and HIF-1 $\alpha$ -FECH axes, *Sci Rep* 10 (2020). <https://doi.org/10.1038/S41598-020-79144-X>.
- [43] H. Kobuchi, K. Moriya, T. Ogino, H. Fujita, K. Inoue, T. Shuin, T. Yasuda, K. Utsumi, T. Utsumi, Mitochondrial Localization of ABC Transporter ABCG2 and Its Function in 5-Aminolevulinic Acid-Mediated Protoporphyrin IX Accumulation, *PLoS One* 7 (2012) e50082. <https://doi.org/10.1371/JOURNAL.PONE.0050082>.
- [44] Y. Hagiya, H. Fukuhara, K. Matsumoto, Y. Endo, M. Nakajima, T. Tanaka, I. Okura, A. Kurabayashi, M. Furihata, K. Inoue, T. Shuin, S. ichiro Ogura, Expression levels of PEPT1 and ABCG2 play key roles in 5-aminolevulinic acid (ALA)-induced tumor-specific protoporphyrin IX (PpIX) accumulation in bladder cancer, *Photodiagnosis Photodyn Ther* 10 (2013) 288–295. <https://doi.org/10.1016/J.PDPDT.2013.02.001>.
- [45] Y. Hagiya, Y. Endo, Y. Yonemura, K. Takahashi, M. Ishizuka, F. Abe, T. Tanaka, I. Okura, M. Nakajima, T. Ishikawa, S. ichiro Ogura, Pivotal roles of peptide transporter PEPT1 and ATP-binding cassette (ABC) transporter ABCG2 in 5-aminolevulinic acid (ALA)-based photocytotoxicity of gastric cancer cells in vitro, *Photodiagnosis Photodyn Ther* 9 (2012) 204–214. <https://doi.org/10.1016/J.PDPDT.2011.12.004>.
- [46] M. Morita, H. Tanaka, Y. Kumamoto, A. Nakamura, Y. Harada, T. Ogata, K. Sakaguchi, T. Taguchi, T. Takamatsu, Fluorescence-based discrimination of breast cancer cells by direct exposure to 5-aminolevulinic acid, *Cancer Med* 8 (2019) 5524–5533. <https://doi.org/10.1002/CAM4.2466>.
- [47] S.A. Adibi, E.L. Morse, The Number of Glycine Residues Which Limits Intact Absorption of Glycine Oligopeptides in Human Jejunum, *J Clin Invest* 60 (1977) 1008–1016. <https://doi.org/10.1172/JCI108851>.
- [48] F. Döring, J. Walter, J. Will, M. Föcking, M. Boll, S. Amasheh, W. Clauss, H. Daniel, Delta-aminolevulinic acid transport by intestinal and renal peptide transporters and its physiological and clinical implications., *J Clin Invest* 101 (1998) 2761–2767. <https://doi.org/10.1172/JCI1909>.
- [49] L. Rodriguez, A. Batlle, G. Di Venosa, A.J. MacRobert, S. Battah, H. Daniel, A. Casas, Study of the mechanisms of uptake of 5-aminolevulinic acid derivatives by PEPT1 and PEPT2 transporters as a tool to improve photodynamic therapy of tumours, *Int J Biochem Cell Biol* 38 (2006) 1530–1539. <https://doi.org/10.1016/J.BIOCEL.2006.03.002>.
- [50] C.M.H. Anderson, M. Jevons, M. Thangaraju, N. Edwards, N.J. Conlon, S. Woods, V. Ganapathy, D.T. Thwaites, Transport of the Photodynamic Therapy Agent 5-Aminolevulinic Acid by Distinct H $^{+}$ -

Coupled Nutrient Carriers Coexpressed in the Small Intestine, *Journal of Pharmacology and Experimental Therapeutics* 332 (2010) 220–228. <https://doi.org/10.1124/JPET.109.159822>.

- [51] Y. Xie, Y. Hu, D.E. Smith, The proton-coupled oligopeptide transporter 1 plays a major role in the intestinal permeability and absorption of 5-aminolevulinic acid, *Br J Pharmacol* 173 (2016) 167. <https://doi.org/10.1111/BPH.13356>.
- [52] D. Meredith, C.S. Temple, N. Guha, C.J. Sword, C.A.R. Boyd, I.D. Collier, K.M. Morgan, P.D. Bailey, Modified amino acids and peptides as substrates for the intestinal peptide transporter PepT1, *Eur J Biochem* 267 (2000) 3723–3728. <https://doi.org/10.1046/J.1432-1327.2000.01405.X>.
- [53] Y. Ma, T. Zhou, X. Kong, R. C. Hider, Chelating Agents for the Treatment of Systemic Iron Overload, *Curr Med Chem* 19 (2012) 2816–2827. <https://doi.org/10.2174/092986712800609724>.
- [54] S. Sassa, S. Schwartz, G. Ruth, Accumulation of protoporphyrin IX from delta-aminolevulinic acid in bovine skin fibroblasts with hereditary erythropoietic protoporphyria. A gene-dosage effect, *J Exp Med* 153 (1981) 1094. <https://doi.org/10.1084/JEM.153.5.1094>.
- [55] Z. Malik, G. Kostenich, L. Roitman, B. Ehrenberg, A. Orenstein, Topical application of 5-aminolevulinic acid, DMSO and EDTA: protoporphyrin IX accumulation in skin and tumours of mice, *J Photochem Photobiol B* 28 (1995) 213–218. [https://doi.org/10.1016/1011-1344\(95\)07117-K](https://doi.org/10.1016/1011-1344(95)07117-K).
- [56] Y. Ma, T. Zhou, X. Kong, R.C. Hider, Chelating Agents for the Treatment of Systemic Iron Overload, *Curr Med Chem* 19 (2012) 2816–2827. <https://doi.org/10.2174/092986712800609724>.
- [57] T. Kurz, B. Gustafsson, U.T. Brunk, Intralysosomal iron chelation protects against oxidative stress-induced cellular damage, *FEBS J* 273 (2006) 3106–3117. <https://doi.org/10.1111/J.1742-4658.2006.05321.X>.
- [58] K. Choudry, R.C.C. Brooke, W. Farrar, L.E. Rhodes, The effect of an iron chelating agent on protoporphyrin IX levels and phototoxicity in topical 5-aminolaevulinic acid photodynamic therapy, *British Journal of Dermatology* 149 (2003) 124–130. <https://doi.org/10.1046/J.1365-2133.2003.05351.X>.
- [59] A.L.R. De Souza, K. Marra, J. Gunn, K.S. Samkoe, S.C. Kanick, S.C. Davis, M.S. Chapman, E. V. Maytin, T. Hasan, B.W. Pogue, Comparing desferrioxamine and light fractionation enhancement of ALA-PpIX photodynamic therapy in skin cancer, *British Journal of Cancer* 2016 115:7 115 (2016) 805–813. <https://doi.org/10.1038/bjc.2016.267>.
- [60] J.L. Buss, B.B. Hasinoff, Ferrous Ion Strongly Promotes the Ring Opening of the Hydrolysis Intermediates of the Antioxidant Cardioprotective Agent Dexrazoxane (ICRF-187), *Arch Biochem Biophys* 317 (1995) 121–127. <https://doi.org/10.1006/ABBI.1995.1143>.
- [61] E. Blake, J. Allen, A. Curnow, An In Vitro Comparison of the Effects of the Iron-Chelating Agents, CP94 and Dexrazoxane, on Protoporphyrin IX Accumulation for Photodynamic Therapy and/or Fluorescence Guided Resection, *Photochem Photobiol* 87 (2011) 1419–1426. <https://doi.org/10.1111/J.1751-1097.2011.00985.X>.
- [62] S. Battah, R.C. Hider, A.J. MacRobert, P.S. Dobbin, T. Zhou, Hydroxypyridinone and 5-Aminolaevulinic Acid Conjugates for Photodynamic Therapy, *J Med Chem* 60 (2017) 3498–3510. [https://doi.org/10.1021/ACS.JMEDCHEM.7B00346/SUPPL\\_FILE/JM7B00346\\_SI\\_001.CSV](https://doi.org/10.1021/ACS.JMEDCHEM.7B00346/SUPPL_FILE/JM7B00346_SI_001.CSV).



- [63] E. Blake, A. Curnow, The Hydroxypyridinone Iron Chelator CP94 Can Enhance PpIX-induced PDT of Cultured Human Glioma Cells, *Photochem Photobiol* 86 (2010) 1154–1160. <https://doi.org/10.1111/J.1751-1097.2010.00770.X>.
- [64] S.M. Campbell, C.A. Morton, R. Alyahya, S. Horton, A. Pye, A. Curnow, Clinical investigation of the novel iron-chelating agent, CP94, to enhance topical photodynamic therapy of nodular basal cell carcinoma, *British Journal of Dermatology* 159 (2008) 387–393. <https://doi.org/10.1111/J.1365-2133.2008.08668.X>.
- [65] S. Anand, T. Hasan, E. V. Maytin, Treatment of nonmelanoma skin cancer with pro-differentiation agents and photodynamic therapy: Preclinical and clinical studies (Review), *Photochem Photobiol* (2024). <https://doi.org/10.1111/PHP.13914>.
- [66] S. Gupta, N. Singh, T. Khan, S. Joshi, Thiosemicarbazone derivatives of transition metals as multi-target drugs: A review, *Results Chem* 4 (2022) 100459. <https://doi.org/10.1016/J.RECHEM.2022.100459>.
- [67] K. Bajaj, R.M. Buchanan, C.A. Grapperhaus, Antifungal activity of thiosemicarbazones, bis(thiosemicarbazones), and their metal complexes, *J Inorg Biochem* 225 (2021) 111620. <https://doi.org/10.1016/J.JINORGBIO.2021.111620>.
- [68] P. Heffeter, V.F.S. Pape, É.A. Enyedy, B.K. Keppler, G. Szakacs, C.R. Kowol, Anticancer Thiosemicarbazones: Chemical Properties, Interaction with Iron Metabolism, and Resistance Development, <https://Home.Liebertpub.Com/Ars> 30 (2019) 1062–1082. <https://doi.org/10.1089/ARS.2017.7487>.
- [69] A. Mrozek-Wilczkiewicz, M. Serda, R. Musiol, G. Malecki, A. Szurko, A. Muchowicz, J. Golab, A. Ratuszna, J. Polanski, Iron chelators in photodynamic therapy revisited: Synergistic effect by novel highly active thiosemicarbazones, *ACS Med Chem Lett* 5 (2014) 336–339. [https://doi.org/10.1021/ML400422A/SUPPL\\_FILE/ML400422A\\_SI\\_001.PDF](https://doi.org/10.1021/ML400422A/SUPPL_FILE/ML400422A_SI_001.PDF).

## 7. AKTYWNOŚĆ NAUKOWA

*Publikacje nie wchodzące w skład rozprawy doktorskiej:*

1. Husak Y., Ma J., Wala-Kapica M., Leśniak K., Babilas D., Blacha-Grzechnik A., Dulski M., **Gawecki R.**, Matuła I., Dercz G., Pogorielov M., Lu X., Simka W. Antibacterial coatings on magnesium formed via plasma electrolytic oxidation in CuO suspension. *Materials Chemistry and Physics*. 2024, 323, 129627, <https://doi.org/10.1016/j.matchemphys.2024.129627>  
(pkt. MNiSW<sub>2024</sub>= 70; IF<sub>2023</sub>=4,3)
2. Serda M., **Gawecki R.**, Dulski M., Sajewicz M., Talik E., Szubka M., Zubko M., Malarz K., Mrozek-Wilczkiewicz A., Musioł R. Synthesis and applications of [60]fullerene nanoconjugate with 5-aminolevulinic acid and its glycoconjugate as drug delivery vehicles. *RSC Advances*. 2022, 12, 6377-6388, <https://doi.org/10.1039/D1RA08499B>  
(pkt. MNiSW<sub>2022</sub>= 100; IF<sub>2022</sub>=3,9)
3. Bielas R., Maksym P., Erfurt K., Hachuła B., **Gawecki R.**, Tarnacka M., Waśkiewicz S., Mielańczyk Ł., Mrozek-Wilczkiewicz A., Chrobok A., Paluch M., Kamiński K. Sugar decorated star-shaped (co)polymers with resveratrol-based core – physicochemical and biological properties. *Journal of Materials Science*. 2022, 57, 2257–2276, <https://doi.org/10.1007/s10853-021-06755-8>  
(pkt. MNiSW<sub>2022</sub>= 100; IF<sub>2022</sub>=4,5)
4. Korzec M., Kotowicz S., **Gawecki R.**, Malarz K., Mrozek-Wilczkiewicz A., Siwy M., Schab-Balcerzak E., Grzelak J., Maćkowski S. 1, 8-Naphthalimides 3-substituted with imine or  $\beta$ -ketoenamine unit evaluated as compounds for organic electronics and cel imaging. *Dyes and Pigments*. 2021, 193, 109508, <https://doi.org/10.1016/j.dyepig.2021.109508>  
(pkt. MNiSW<sub>2021</sub>= 100; IF<sub>2021</sub>= 5,122)
5. Rzycka-Korzec R., Malarz K., **Gawecki R.**, Mrozek-Wilczkiewicz A., Małecki J.G., Schab-Balcerzak E., Korzec M., Polanski J. Effect of the complex-formation ability of thiosemicarbazones containing (aza)benzene or 3-nitro-1,8-naphthalimide unit towards Cu(II) and Fe(III) ions on their anticancer activity. *Journal of Photochemistry and Photobiology A: Chemistry*. 2021, 415, 113314, <https://doi.org/10.1016/j.jphotochem.2021.113314>  
(pkt. MNiSW<sub>2021</sub>= 70; IF<sub>2021</sub>= 5,141)
6. Malarz K., Zych D., **Gawecki R.**, Kuczak M., Musioł R., Mrozek-Wilczkiewicz A. New derivatives of 4'-phenyl-2,2':6',2''-terpyridine as promising anticancer agents. *European Journal of Medicinal Chemistry*. 2021, 212, 113032, <https://doi.org/10.1016/j.ejmech.2020.113032>  
(pkt. MNiSW<sub>2021</sub>= 140; IF<sub>2021</sub>= 7,088)

7. Dulski M., **Gawecki R.**, Sułowicz S., Cichomski M., Kazek-Kęsik A., Wala M., Leśniak-Ziółkowska K., Simka W., Mrozek-Wilczkiewicz A., Gawęda M., Sitarz M., Dudek K. Key Properties of a Bioactive Ag-SiO<sub>2</sub>/TiO<sub>2</sub> Coating on NiTi Shape Memory Alloy as Necessary at the Development of a New Class of Biomedical Materials. *International Journal of Molecular Sciences*. 2021; 22(2):507 <https://doi.org/10.3390/ijms22020507>  
(pkt. MNiSW<sub>2021</sub>= 140; IF<sub>2021</sub>= 6,208)
8. Nalepa P., **Gawecki R.**, Szewczyk G., Balin K., Dulski M., Sajewicz M., Mrozek Wilczkiewicz A., Musioł R., Polanski J., Serda M. A [60]fullerene nanoconjugate with gemcitabine: synthesis, biophysical properties and biological evaluation for treating pancreatic cancer. *Cancer Nanotechnology*. 2020, 11:2, <https://doi.org/10.1186/s12645-020-00058-4>  
(pkt. MNiSW<sub>2020</sub>= 100; IF<sub>2020</sub>= 5,095)
9. Slodeka A., Zycha D., Maroń A., **Gawecki R.**, Mrozek-Wilczkiewicz A., Malarz K., Musioł R. Phenothiazine derivatives - synthesis, characterization, and theoretical studies with an emphasis on the solvatochromic properties. *Journal of Molecular Liquids*. 2019, 285, 515-525, <https://doi.org/10.1016/j.molliq.2019.04.102>  
(pkt. MNiSW<sub>2019</sub>= 100; IF<sub>2019</sub>= 5,065)
10. Spaczyńska E., Mrozek-Wilczkiewicz A., Malarz K., Kos J., Gonec T., Oravec M., **Gawecki R.**, Bak A., Dohanosova J., Kapustikova I., Liptaj T., Jampilek J., Musiol R. Design and synthesis of anticancer 1-hydroxynaphthalene-2-carboxanilides with a p53 independent mechanism of action. *Scientific Reports*. 2019, 9(1), 6387, <https://doi.org/10.1038/s41598-019-42595-y>  
(pkt. MNiSW<sub>2019</sub>= 140; IF<sub>2019</sub>= 3,998)
11. Dulski M., Dudek K., Chalon D., Kubacki J., Sulowicz S., Piotrowska-Seget Z., Mrozek-Wilczkiewicz A., **Gawecki R.**, Nowak A. Towards the development of innovative implant: NiTi alloy functionalized by multifunctional β-TCP+Ag/SiO<sub>2</sub> coatings. *ACS Applied Bio Materials*. 2019, 2(3), 987-998, <https://doi.org/10.1021/acsabm.8b00510>  
(pkt. MNiSW<sub>2019</sub>= 20; IF<sub>2019</sub>= -)
12. **Gawecki R.**, Sala K., Kurczyńska E.U., Świątek P., Płachno B.J. Immunodetection of some pectic, arabinogalactan proteins and hemicellulose epitopes in the micropylar transmitting tissue of apomictic dandelions (*Taraxacum*, Asteraceae, Lactuceae). *Protoplasma*. 2017, 254, 657–668, <https://doi.org/10.1007/s00709-016-0980-0>  
(pkt. MNiSW<sub>2017</sub>= 30; IF<sub>2017</sub>= 2,457)
13. Milewska-Hendel A., Polak M., Sala K., Zieleźnik-Rusinowska P., **Gawecki R.**, Kurczyńska E. Morpho-histological analysis of tomato (*Solanum lycopersicum*L.) plants after treatment with

juglone. *Acta Agrobotanica*. 2017, 70(2), 1701, DOI:10.5586/aa.1701 (pkt. MNiSW<sub>2017</sub>= 14; IF<sub>2017</sub>= -)

14. Betekhtin A., Rojek M., Milewska-Hendel A., **Gawecki R.**, Karcz J., Kurczynska E., Hasterok R. Spatial Distribution of Selected Chemical Cell Wall Components in the Embryogenic Callus of *Brachypodium distachyon*. *PLoS One*. 2016, 11(11):e0167426, <https://doi.org/10.1371/journal.pone.0167426> (pkt. MNiSW<sub>2016</sub>= 35; IF<sub>2016</sub>= 2,806)
15. Milewska-Hendel A., **Gawecki R.**, Zubko M., Stróż D., Kurczyńska E. Diverse influence of nanoparticles on plant growth with a particular emphasis on crop plants. *Acta Agrobotanica*. 2016, 69(4), 1694, DOI: 10.5586/aa.1694 \ (pkt. MNiSW<sub>2016</sub>= 14; IF<sub>2016</sub>= -)

#### *Patenty i zgłoszenia:*

1. Nanokoniugat diglicynowej pochodnej [60]fullerenu z gemcytabiną, sposób jego otrzymywania oraz jego zastosowanie. Maciej Serda, Paweł Nalepa, **Robert Gawecki**, Anna Mrozek-Wilczkiewicz, Robert Musioł. Numer patentu: 240524
2. Nanomateriał fullerenowy funkcjonalizowany kwasem 5-aminolewulinowym, sposób jego otrzymywania oraz jego zastosowanie. Maciej Serda, Robert Musioł, Anna Mrozek-Wilczkiewicz, **Robert Gawecki**, Dominik Dreszer, Julia Korzuch, Mateusz Dulski. Numer zgłoszenia: P.437483

#### *Projekty:*

1. Mateusz Dulski, SONATA 13 (2017/26/D/ST8/01117). Opracowanie technologii wytwarzania oraz charakterystyka nieorganicznych materiałów kompozytowych i wielofunkcyjnych powłok złożonych na stopach NiTi – **wykonawca**
2. Robert Gawecki, PRELUDIUM 18 (2019/35/N/NZ7/02780). Nowe chelatory żelaza z grupy tiosemikarbazonu w terapii fotodynamicznej – **kierownik**